SRR-CWDA-2021-00066
Revision 0

Evaluation of the Combined Uncertainties Associated with the Long-Term Performance of Saltstone Disposal Facility Flow Barriers

August 2021

Prepared by: Savannah River Remediation LLC
Waste Disposal Authority
Aiken, SC 29808

Prepared for U.S. Department of Energy Under Contract No. DE-AC09-09SR22505

APPROVALS

Author:

Steven Hommel

Digitally signed by Steven Hommel
Date: 2021.08.03 07:27:46 -04'00'

Steven P. Hommel — Date
WDA Assessments
Savannah River Remediation, LLC

Technical Review per S4-ENG.51:

Bailey E. Arnett

Digitally signed by Bailey E. Arnett
Date: 2021.08.03 07:54:10 -04'00'

Bailey Arnett — Date
WDA Determinations
Savannah River Remediation, LLC

Management Review:

KENT H. ROSENBERGER

Digitally signed by KENT H. ROSENBERGER
Date: 2021.08.03 08:10:37 -04'00'

Kent H. Rosenberger — Date
WDA Assessments, Manager
Savannah River Remediation, LLC

This page intentionally left blank.

TABLE OF CONTENTS

LIST OF FIGURES

LIST OF TABLES

ACRONYMS/ABBREVIATIONS

DLL	Dynamic Link Library
DOE	U.S. Department of Energy
FY	Fiscal Year
GCL	Geosynthetic Clay Liner
GTG	GoldSim Technology Group LLC
HDPE	High Density Polyethylene
HFC	HDPE Failure Condition
IHI	Inadvertent Human Intruder
K_{sat}	Saturated Hydraulic Conductivity
LLDL	Lower Lateral Drainage Layer
MCC	Moisture Characteristic Curve
MOP	Member of the Public
NRC	U.S. Nuclear Regulatory Commission
PA	Performance Assessment
PRCC	Partially Ranked Correlation Coefficient
QA	Quality Assurance
RS	Random Seed
RSI	Request for Supplemental Information
SDF	Saltstone Disposal Facility
SDU	Saltstone Disposal Unit
SPF	Saltstone Production Facility
SQAP	Software Quality Assurance Plan
SRRC	Stepwise Ranked Regression Coefficient
SRS	Savannah River Site
TCCZ	Tan Clay Confining Zone
TI	Time Interval
UAZ	Upper Aquifer Zone
ULDL	Upper Lateral Drainage Layer
UTRA	Upper Three Runs Aquifer

This page intentionally left blank.

1.0 INTRODUCTION

Disposal of salt solution at the Savannah River Site (SRS) Saltstone Disposal Facility (SDF) began in June 1990 has continued until present day. Salt solution is sent to the Saltstone Production Facility (SPF) for use in producing a grout slurry, which is then pumped into Saltstone Disposal Units (SDUs) at the SDF where it cures (or hardens) into the final low-level wasteform called saltstone. The SDUs currently containing saltstone are SDUs 1, 2A, 2B, 3A, 4, 5A, 5B, and 6. [SRR-CWDA-2020-00081] Note that historically SDUs 1 and 4 have also been referred to as Vaults 1 and 4.

In support of continued waste disposal operations at the SDF, additional SDUs will be constructed and filled with saltstone. [SRR-LWP-2009-00001] Once disposal operations end, the facility will be prepared for permanent closure. [SRR-CWDA-2020-00005]

The *Performance Assessment for the Saltstone Disposal Facility at the Savannah River Site* (SRR-CWDA-2019-00001), hereafter referred to as the SDF PA, relies on cementitious materials to limit radionuclide and chemical waste releases to the environment to levels that will meet federal and state regulatory requirements. The saltstone wasteform is a grout composed of hydrated slag, fly ash, and (optionally) Portland cement (SRR-CWDA-2020-00064).

The long-term performance of saltstone was evaluated as part of the SDF PA (SRR-CWDA-2019-00001). After issuing the SDF PA, the United States Nuclear Regulatory Commission (NRC) issued a letter (ML20254A003), hereafter referred to as the NRC Letter, which includes Requests for Supplemental Information (RSIs) to support their review of the SDF PA. This report provides the response to "RSI-1: Combined Uncertainty of Flow Barriers."

1.1 Purpose

The NRC Letter (ML20254A003) indicated that in order to:

> "evaluate the risk significance of flow barriers, the NRC staff needs information about the uncertainty in SDF performance caused by the combined uncertainty in the performance of closure cap, engineered barriers above the disposal structures, and saltstone wasteform."

The NRC Letter also proposed the following as a path forward for RSI-1:

> "Provide an analysis that demonstrates the effects of the combined uncertainties of the sand drainage layers, HDPE [high density polyethylene], HDPE/GCL [geosynthetic clay layer] composite barriers, saltstone degradation, and MCCs [moisture characteristic curves]. One method for providing that information would be to include those features and variables in a probabilistic analysis of the SDF performance and to provide results similar to the results provided in Sections 5.7.3 through 5.7.5 of the PA. The input ranges used in an analysis should be consistent with the responses to NRC RSI Comments about the sand drainage layers (see RSI-2); HDPE, GCL, and HDPE/GCL composite barriers (see RSI-3); saltstone degradation (see RSI-4); and MCCs (see RSI-5)."

The other RSIs referenced in this path forward are:

- RSI-2: Sand Drainage Layers. This RSI requests an evaluation of uncertainties associated with the long-term performance of the sand drainage layers.

- RSI-3: HDPE / GCL Composite Barriers. This RSI requests an evaluation of uncertainties associated with the long-term performance of the HDPE/GCL composite barrier.
- RSI-4: Saltstone Degradation. This RSI requests an evaluation of uncertainties associated with the long-term performance of the saltstone wasteform.
- RSI-5: Moisture Characteristic Curves. This RSI requests an evaluation of the risk significance of the MCCs given the uncertainties associated with the other RSIs.

In addition to the previous RSIs mentioned, the evaluations within this report also reference RSI-7: *Erosion in Adjacent Area to the SDF*, which is a request by the NRC to evaluate long-term uncertainties associated with erosion (ML20254A003).

The purpose of this report is to address RSI-1 by providing a probabilistic model designed to provide insights into the potential influences of combined uncertainties in the various SDF flow barriers. This analysis does not represent expected long-term conditions at the SDF because many of the model parameters were deliberately designed to be overly pessimistic to provide additional risk insights relative to various uncertainties. The probabilistic model described herein is effectively a hybrid of an uncertainty analysis and a sensitivity analysis. As such, dose results provided in this report may be used to inform decisions related to risk reduction, but do not reflect long-term, expected compliance conditions. For dose results that support compliance decisions, readers should consult the SDF PA (SRR-CWDA-2019-00001).

The analyses within this report were developed based on multiple references that have been prepared to provide support for this RSI-1 response. The most recent reference was the *Evaluation of the Uncertainties Associated with Long-Term Saltstone Degradation* (SRR-CWDA-2021-00056). Using the results of the Probabilistic Saltstone Degradation Model, a set of 1,000 Vadose Zone Flow models were constructed in PORFLOW. These flow fields were generated and used to perform contaminant transport to complete the evaluation of the combined flow barrier uncertainties.

1.2 Overview

The analysis described within this report uses 1,000 realizations, wherein each realization uses a unique set of inputs including infiltration rates, saltstone degradation rates, flow fields, etc. This approach is similar to the probabilistic simulations described in Section 5.7 of the SDF PA. The key differences are that the new realizations created for this RSI-1 analysis incorporates multiple uncertainties based on recommendations developed from the other RSI response documents, whereas the SDF PA relied on a smaller set of variables such that 54 discrete sets of flow fields were developed and used.

Additionally, the SDF PA simulated the effects of the entire system (i.e., using all 15 SDUs), whereas this RSI-1 analysis limited the scope of modeling to a single SDU. SDU 9 was selected for this analysis because, as a larger SDU, it has the potential to hold the largest amount of inventory thus representing the greatest risk potential (SRR-CWDA-2021-00057) and because the SDF PA results indicate that within the Compliance Period (or the first 1,000 years after SDF closure), the highest peak doses were attributable to SDU 9 (Sections 5.7.3 and 5.7.4 of SRR-CWDA-2019-00001).

This report describes the development of the 1,000 realizations of SDU 9 doses and analyzes those dose results to provide insights with respect to the uncertainties that most influence the potential doses. It should be noted that many of the parameter ranges and modeling assumptions developed for this analysis were selected to highlight or exaggerate these uncertainties. If this modeling effort had bounded inputs based on reasonably expected conditions, different modeling decisions would have been made. As such, the results described herein should not be interpreted as representing long-term expected conditions. Instead, the model results represent a combination of multiple sensitivity analyses in which it is possible for multiple unrealistic conditions to exist simultaneously in order to provide in depth insights for informing potential risks. In other words, the dose results provided herein are for informational purposes only and are not intended to represent the conditions necessary for demonstrating compliance to performance objectives.

Section 2.0 discusses how this response document for RSI-1 is related to the other RSIs. Based on the development of these other RSI responses, a probabilistic model was developed to address RSI-1. The development of this probabilistic model is described in Section 3.0, followed by a presentation and analysis of the model results in Section 4.0.

This page is intentionally left blank.

2.0 ASSOCIATED RSI RESPONSES

Responding to RSI-1 relies heavily on the responses to other RSIs. Specifically, in the NRC's recommended Path Forward for addressing RSI-1, it is stated that the "input ranges used in an analysis should be consistent with the responses to NRC RSI Comments about the sand drainage layers (see RSI-2); HDPE, GCL, and HDPE/GCL composite barriers (see RSI-3); saltstone degradation (see RSI-4); and MCCs (see RSI-5)." As such, this section provides a roadmap for how the various RSIs have been addressed and how those responses have been rolled into this response document for RSI-1. Section 2.1 describes how RSI-2 was addressed and affects the RSI-1 response, Section 2.2 describes how RSI-3 was addressed and affects the RSI-1 response, Section 2.3 describes how RSI-4 was addressed and affects the RSI-1 response, and Section 2.4 describes how RSI-5 was addressed (also see Section 3.7 and Appendix A). Additionally, Section 2.5 describes how the response to RSI-7 also affects the RSI-1 response. Finally, Section 2.6 provides a summary of the other RSIs to provide completeness.

2.1 Relationship Between the Responses to RSI-1 and RSI-2

For RSI-2: Sand Drainage Layers (ML20254A003), the NRC stated:

> "To evaluate the risk significance and the projected performance of the sand drainage layers, the NRC staff needs supplemental information about the uncertainty associated with the [lower lateral drainage layer] LLDL and the upper lateral drainage layer (ULDL)."

The response to RSI-2 was documented in *Closure Cap Model Parameter Evaluation: Saturated Hydraulic Conductivity of Sand* (SRR-CWDA-2021-00031). In that response, a set of recommendations was developed for evaluating the long-term performance of the sand drainage layers for both the ULDL and the LLDL. These recommendations were applied to the closure cap and infiltration rate modeling described in *Evaluation of the Uncertainties Associated with the SDF Closure Cap and Long-Term Infiltration Rates* (SRR-CWDA-2021-00040) to develop probabilistic infiltration rates. Then those infiltration rates were applied to the advective decalcification of saltstone as described in Section 4.4 of *Evaluation of the Uncertainties Associated with Long-Term Saltstone Degradation* (SRR-CWDA-2021-00056) to estimate the evolution of saltstone.

Next, for the analyses described herein, the infiltration rates from SRR-CWDA-2021-00040 and the saltstone evolution from SRR-CWDA-2021-00056 were both applied to the Vadose Zone Flow Model to generate a set of probabilistic flow fields. These probabilistic flow fields also applied uniform silting-in of the LLDL based on recommendations described in the interoffice memorandum *Selected PORFLOW Modeling Configurations to Support RSI-4 Analysis* (SRR-CWDA-2021-00057). The evolution of the LLDL sand was generated via the closure cap and infiltration rate modeling (see Section 5.2 of SRR-CWDA-2021-00040).

The probabilistic flow fields generated with the Vadose Zone Flow Model have been applied to the probabilistic SDF GoldSim Model described in the SDF PA (Sections 4.5, 5.6, and 5.7 of SRR-CWDA-2019-00001). Section 3.0 describes the setup of the SDF GoldSim Model and Section 4.0 provides an analysis of the results to satisfy RSI-1.

2.2 Relationship Between the Responses to RSI-1 and RSI-3

For RSI-3: High Density Polyethylene / Geosynthetic Clay Liner Composite Barriers (ML20254A003), the NRC stated:

> "To evaluate the risk significance and the projected performance of flow barriers, the NRC staff needs supplemental information about the uncertainty associated with the HDPE, the GCL, and the combined HDPE/GCL composite barriers in the closure cap, above the disposal structure roofs, and between the mud mats."

The response to RSI-3 was documented in *Closure Cap Model Parameter Evaluation: High Density Polyethylene (HDPE) and Geosynthetic Clay Liner (GCL) Composite Barrier Performance* (SRR-CWDA-2021-00033). In that response, a set of recommendations was developed for evaluating the long-term performances of both the HDPE and the GCL used in the SDF system (for both in the closure cap as well as the flow barriers above the SDU roof and between the SDU mud mats). These recommendations were applied to the closure cap and infiltration rate modeling described in *Evaluation of the Uncertainties Associated with the SDF Closure Cap and Long-Term Infiltration Rates* (SRR-CWDA-2021-00040) to develop probabilistic infiltration rates. Then those infiltration rates were applied to the advective decalcification of saltstone as described in Section 4.4 of *Evaluation of the Uncertainties Associated with Long-Term Saltstone Degradation* (SRR-CWDA-2021-00056) to estimate the evolution of saltstone.

Next, for the analyses described herein, the infiltration rates from SRR-CWDA-2021-00040 and the saltstone evolution from SRR-CWDA-2021-00056 were both applied to the Vadose Zone Flow Model to generate a set of probabilistic flow fields. These probabilistic flow fields also applied instantaneous degradation of the HDPE and GCL flow barriers above the SDU roof and between the SDU mud mats based on recommendations described in the interoffice memorandum *Selected PORFLOW Modeling Configurations to Support RSI-4 Analysis* (SRR-CWDA-2021-00057). The evolutions for these HDPE and GCL flow barriers were generated via the closure cap and infiltration rate modeling (see Sections 5.3 and 5.4 of SRR-CWDA-2021-00040).

The probabilistic flow fields generated with the Vadose Zone Flow Model have been applied to the probabilistic SDF GoldSim Model described in the SDF PA (Sections 4.5, 5.6, and 5.7 of SRR-CWDA-2019-00001). Section 3.0 describes the setup of the SDF GoldSim Model and Section 4.0 provides an analysis of the results to satisfy RSI-1.

2.3 Relationship Between the Responses to RSI-1 and RSI-4

For RSI-4: Saltstone Degradation (ML20254A003), the NRC stated:

> "To evaluate the risk significance of the hydraulic performance of saltstone, the NRC staff needs information about how the following issues affect saltstone degradation: (1) additional and coupled saltstone degradation mechanisms; (2) arithmetic averaging of hydraulic conductivity for degraded and intact saltstone; and (3) uncertainty in flow through the closure cap and engineered barriers above the disposal structures."

The response to RSI-4 was documented in *Evaluation of the Uncertainties Associated with Long-Term Saltstone Degradation* (SRR-CWDA-2021-00056). In that response, a set of recommendations was developed for evaluating the long-term performance of the saltstone waste

form. The modeling described within this report provided a set of probabilistic saltstone degradation evolutions. This saltstone evolution accounted for initial damage to the saltstone, decalcification, and mechanical damage due to potential seismic events.

Next, for the analyses described herein, the saltstone evolution from SRR-CWDA-2021-00056 was applied to the Vadose Zone Flow Model to generate a set of probabilistic flow fields. The probabilistic flow fields generated with the Vadose Zone Flow Model have been applied to the probabilistic SDF GoldSim Model described in the SDF PA (Sections 4.5, 5.6, and 5.7 of SRR-CWDA-2019-00001). Section 3.0 describes the setup of the SDF GoldSim Model and Section 4.0 provides an analysis of the results to satisfy RSI-1.

2.4 Relationship Between the Responses to RSI-1 and RSI-5

For RSI-5: Moisture Characteristic Curves (ML20254A003), the NRC stated:

> "To evaluate the risk significance of MCCs for cementitious materials and the gravel for the fast flow paths, the NRC staff needs information about the effect of the MCCs on near-field flow when the closure cap and engineered barriers above the disposal structures do not perform as designed."

A second set of probabilistic flow fields was generated with the Vadose Zone Flow Model. This second set of flow fields uses all of the same settings and inputs as the RSI-1 flow fields (see Sections 2.1, 2.2, 2.3, and 2.5) except that a relative permeability of 1 was assumed to generate model results in response to RSI-5. This second set of probabilistic flow fields has been applied to a modified version of the probabilistic SDF GoldSim Model described in the SDF PA (Sections 4.5, 5.6, and 5.7 of SRR-CWDA-2019-00001).

For additional discussion of the RSI-5 response, see Section 3.7 and Appendix A.

2.5 Relationship Between the Responses to RSI-1 and RSI-7

For RSI-7: Erosion in Adjacent Area to the SDF (ML20254A003), the NRC stated:

> "To evaluate the stability of the SDF, the NRC staff needs information about potential future erosion in the adjacent area surrounding the SDF that may affect stability of the SDF."

The response to RSI-7 was documented in *Evaluation of the Potential for Erosion in the Vicinity of Z Area* (SRR-CWDA-2021-00036). In that response, a set of recommendations was developed for evaluating the long-term erosion of the SDF closure cap as well as the adjacent areas. These recommendations were applied to the closure cap and infiltration rate modeling described in *Evaluation of the Uncertainties Associated with the SDF Closure Cap and Long-Term Infiltration Rates* (SRR-CWDA-2021-00040) to develop probabilistic infiltration rates. Then those infiltration rates were applied to the advective decalcification of saltstone as described in Section 4.4 of *Evaluation of the Uncertainties Associated with Long-Term Saltstone Degradation* (SRR-CWDA-2021-00056) to estimate the evolution of saltstone.

Next, for the analyses described herein, the infiltration rates from SRR-CWDA-2021-00040 and the saltstone evolution from SRR-CWDA-2021-00056 were both applied to the Vadose Zone Flow Model to generate a set of probabilistic flow fields. The probabilistic flow fields generated with the Vadose Zone Flow Model have been applied to the probabilistic SDF GoldSim Model

described in the SDF PA (Sections 4.5, 5.6, and 5.7 of SRR-CWDA-2019-00001). Section 3.0 describes the setup of the SDF GoldSim Model and Section 4.0 provides an analysis of the results to satisfy RSI-1.

2.6 Consideration for the Other RSIs

The other two RSIs described in ML20254A003 are:

- RSI-6: Complete Water Budgets

  "To evaluate the implementation of the conceptual model for near-field flow, the NRC staff needs supplemental information about the internal flow components of the entire disposal system with in- and outflow- components having the same units of rate or flow."

- RSI-8: Upper Three Runs Aquifer-Upper Aquifer Zone Lateral Flow Analysis

  "To evaluate the effects of plausible alternative conceptual models, the NRC staff needs information about: (1) lateral flow in the Upper Three Runs Aquifer-Upper Aquifer Zone (UTRA-UAZ); (2) contaminant flow and transport in the UTRA-UAZ on top of the Tan Clay Confining Zone (TCCZ); and (3) the projected dose to a human receptor who uses water from the UTRA-UAZ."

The NRC's recommended Path Forward for addressing RSI-6 identified a number of specific modeling cases that they desired complete water budgets from. An initial set of water budgets was provided to the NRC in November 2020 (SRR-CWDA-2020-00077). The remaining modeling cases requested by the NRC are identified as "the three cases to be performed for RSI-1 that resulted in the greatest dose, and, if they are not the same, then the three cases that resulted in the greatest amount of water flowing through the saltstone" (ML20254A003). These modeling cases are identified in Section 4.4.3. The associated electronic data shall be provided to the NRC with this report.

For RSI-8, a separate response document will be prepared.

3.0 PROBABILISTIC RSI-1 MODEL

The probabilistic RSI-1 model was developed in three parts. The first part was the generation of the SDU 9 flow fields. (Note that Appendix B provides a basis for using SDU 9 only.) The flow fields were generated with the PORFLOW modeling code (Section 3.1). Specifically, PORFLOW was used to run a modified version of the Vadose Zone Flow Model based on Section 4.4.4 of the SDF PA (SRR-CWDA-2019-00001). Changes relative to the SDF PA are described in Section 3.2.

The next part of the probabilistic RSI-1 model was the simulation of the Tc-99 fluxes at the water table. As described in Section 4.5.2.1 of the SDF PA (SRR-CWDA-2019-00001), the SDF GoldSim Model uses Tc-99 fluxes from the PORFLOW Vadose Zone Transport Model (as opposed to simulating the release and transport of Tc-99 as is done for the other radionuclides). This Tc-99-specific approach was necessary to compute the complex behavior of the Tc-99 releases relative to the solubility conditions and the shrinking core of the simulated reducing environment. Consistent with this approach, PORFLOW was used to generate the Tc-99 fluxes from SDU 9 as described in Section 3.3.

The third part of the probabilistic RSI-1 model was developed using the GoldSim software described in Section 3.4. The SDF GoldSim Model from the SDF PA was modified to read in the new flow fields as well as new Tc-99 fluxes generated from those flow fields. The new model file was named: *SRS Saltstone RSI-1 v1.000.gsm*. Section 3.5 describes the model changes internal to the GoldSim (*.gsm) file. In addition, a number of external files which are read into the SDF GoldSim Model (via dynamic link libraries (DLLs)) were also developed and/or modified as described in Section 3.6. Section 3.7 describes the probabilistic RSI-5 model, *SRS Saltstone RSI-5 v1.000.gsm*, which is nearly identical to the RSI-1 model.

Finally, Section 3.8 provides additional information about key modeling decisions that should be considered when reviewing the results of these models.

3.1 PORFLOW Software Description

The Vadose Zone Flow Model and the Vadose Zone Transport Model both use PORFLOW modeling software. PORFLOW is a commercial computational fluid dynamics tool developed by Analytic & Computational Research, Inc. PORFLOW numerically solves problems involving transient or steady state fluid flow, heat, salinity, and mass transport in multi-phase, variably saturated, porous, or fractured media with dynamic phase change. PORFLOW was used in the SDF PA modeling to calculate fluid flow and contaminant transport in the vadose and saturated zones. PORFLOW transport results can be used in subsequent models to calculate radiological doses and perform human health and ecological risk evaluations. PORFLOW flow results were also used to conduct probabilistic simulations of contaminant transport via GoldSim (see Section 3.4).

PORFLOW accommodates alternate fluid and media property relations and complex and arbitrary boundary conditions. The geometry may be two dimensional or three dimensional, Cartesian, or cylindrical, and the mesh may be structured or unstructured, giving maximum flexibility to the user. As with the SDF PA, Version 6.42.9 of PORFLOW was used to accomplish the RSI simulations.

Quality Assurance (QA) testing and verification of the software is documented in SRNL-STI-2018-00275. Because this is the same software as used for developing the SDF PA (SRR-CWDA-2019-00001), the same software QA applies. Section 6.0 of the *Performance Assessment for the Saltstone Disposal Facility at the Savannah River Site: Quality Assurance Report* (SRR-CWDA-2018-00068) provides a summary of the software QA, which includes PORFLOW.

3.2 Probabilistic Vadose Zone Flow Modeling

The probabilistic Vadose Zone Flow Model used for generating the RSI-1 flow fields was developed based on the deterministic Vadose Zone Flow Model described in Section 4.4.4 of the SDF PA. The key difference is that rather than applying discrete sampling of selected parameters (as was provided in Table 4.4-82 of the SDF PA) to generate a representative set of flow fields, infiltration rates and saltstone degradation rates from probabilistic models were used as inputs to generate a fully probabilistic set of flow fields.

Decisions associated with the modeling configurations are documented in SRR-CWDA-2021-00057. Specifically, PORFLOW modeling performed in support of the RSI analyses should:

- Include the infiltration rates based on SRR-CWDA-2021-00040,
- Apply instantaneous degradation of the HDPE/GCL composite barrier at the SDU roof and between the SDU mud mats, and
- Apply a silting-in configuration that assumes uniform degradation of the LLDL (as opposed to a "bottom-up" silting-in approach or a no silting-in approach).

These modeling decisions were deliberate to maximize the potential releases of Tc-99 (a key dose contributor) per SRR-CWDA-2021-00057, but do not represent expected conditions. The purpose for these decisions is not to provide a realistic set of potential future conditions but to provide greater risk insights relative to the uncertainties associated with the various flow barriers that have been considered.

For example, the application of instantaneous degradation of the HDPE/GCL composite barrier (at the SDU roof and between the SDU mud mats) is equivalent to the complete failure condition of the HDPE (as described in SRR-CWDA-2021-00033). As such, the timing of the failure condition was selected based on the random sampling of the HDPE service life. However, the probabilistic closure cap and infiltration model described in SRR-CWDA-2021-00040 indicates that there are three plausible end state conditions for HDPE barriers: complete failure, partial failure, or no failure. Of these, the partial failure condition represents the most likely expected condition. By assuming only the complete failure condition instead of randomly sampling between the various conditions, waste releases are limited prior to the failure and then maximized after the failure occurs, resulting in larger-than-expected peak releases. In reality, if HDPE failure does occur, it is expected to fail more gradually (and the failures are likely to be localized allowing less volumetric flow) resulting in smaller peak releases.

Note that this approach of applying instantaneous degradation of the HDPE/GCL composite barriers at the SDU roof and between the SDU mud mats is not entirely consistent with modeling that was performed for the closure cap and infiltration rates. The closure cap model also includes an HDPE/GCL composite barrier beneath the ULDL. As described in Section 5.3 of SRR-CWDA-

2021-00040, the performance of the HDPE/GCL composite barrier in the closure cap was modeled by sampling between all three HDPE failure conditions (complete failure, partial failure, or no failure). As such, assuming complete failure of the HDPE/GCL at the SDU roof and between the SDU mud mats for every realization is not consistent with the approach in SRR-CWDA-2021-00040. Despite being inconsistent, the complete failure of the HDPE/GCL composite barriers at the SDU roof and between the SDU mud mats is appropriate given the intent of RSI-1, which is to provide greater risk insights.

Similarly, SRR-CWDA-2021-00057 considered three possible degradation scenarios for the LLDL sand. This drainage layer is designed to promote lateral drainage away from the SDUs. As such, the sand is considered to degrade via "silting-in" wherein clays or other fine particles are assumed to migrate from the overlying backfill into the sand, thus reducing the saturated hydraulic conductivity (K_{sat}) of the sand. While the Vadose Zone Flow Model for RSI-1 assumes that the sand will degrade in this way, there is little evidence of this process occurring in natural systems.

Given these considerations and the modeling approaches used, the inputs used to generate each of the probabilistic flow fields were:

- Infiltration rate based on the modeling described in SRR-CWDA-2021-00040,
- Saturated hydraulic conductivity (K_{sat}) of the sand in the LLDL (over time) based on sampling recommended in SRR-CWDA-2021-00031 and modeling described in SRR-CWDA-2021-00040,
- The HDPE service life based on sampling recommended in SRR-CWDA-2021-00033 and modeling described in SRR-CWDA-2021-00040,
- The degraded K_{sat} for the combined HDPE and GCL composite barrier based on the modeling described in SRR-CWDA-2021-00040,
- The initial K_{sat} of saltstone based on sampling recommended in SRR-CWDA-2021-00056 and modeling described in SRR-CWDA-2021-00056,
- The initial degradation fraction of saltstone based on sampling recommended in SRR-CWDA-2021-00056 and modeling described in SRR-CWDA-2021-00056,
- The final K_{sat} of saltstone based on sampling of backfill K_{sat} as recommended in SRR-CWDA-2021-00040 and modeling described in SRR-CWDA-2021-00056,
- The p-averaging term (used for blending intact saltstone properties with degraded properties of saltstone) based on sampling recommended in SRR-CWDA-2021-00052 and modeling described in SRR-CWDA-2021-00056,
- The time at which saltstone degradation would be complete if seismic events were not included based on modeling described in SRR-CWDA-2021-00056,
- The timing of each seismic event that is sampled to occur based on sampling recommended in SRR-CWDA-2021-00052 and modeling described in SRR-CWDA-2021-00056, and
- The magnitude of damage caused by each seismic event based on sampling recommended in SRR-CWDA-2021-00052 and modeling described in SRR-CWDA-2021-00056.

As indicated by this list, many variables have been considered herein, especially relative to the SDF PA.

Finally, because a large number of flow fields are being generated by the Vadose Zone Flow Model, the time intervals (TI) have been revised to reduce modeling run times. First, rather than modeling out to 20,000 or 100,000 years after SDF closure, the flow fields were only generated out to 10,000 years (i.e., the "Performance Period" in the SDF PA). Within this 10,000-year period, the flow fields were generated using 27 discrete time intervals (Table 3.2-1).

Table 3.2-1: Time Intervals Used for the Flow Fields Developed to Support RSI-1 Modeling

Time Interval (TI)	Start Year	End Year
TI01	0	50
TI02	50	92
TI03	92	150
TI04	150	200
TI05	200	250
TI06	250	300
TI07	300	350
TI08	350	400
TI09	400	450
TI10	450	500
TI11	500	600
TI12	600	700
TI13	700	800
TI14	800	900
TI15	900	1,075
TI16	1,075	1,229
TI17	1,229	1,496
TI18	1,496	1,552
TI19	1,552	1,767
TI20	1,767	2,000
TI21	2,000	2,300
TI22	2,300	2,800
TI23	2,800	3,500
TI24	3,500	4,500
TI25	4,500	6,000
TI26	6,000	8,000
TI27	8,000	10,000

Within each time interval, the flow fields are modeled as steady state flow conditions such that changes to flow conditions occur at the transitions from one time interval to the next. It is expected that using this fairly limited number of time intervals may introduce some modeling artifacts as the step changes in the flow conditions between time intervals can be significant.

3.3 Probabilistic Vadose Zone Transport Modeling for Tc-99

The probabilistic Vadose Zone Transport Model used for generating the Tc-99 fluxes for RSI-1 was developed based on the deterministic Vadose Zone Transport Model described in Section 4.4.5 of the SDF PA. The setup for the Vadose Zone Transport Model is identical to the Compliance Case of the SDF PA, except that the 1,000 probabilistic flow fields were used.

To support the SDF GoldSim Modeling, specific Tc solubility conditions were applied. The solubility condition assumed for each realization was based on the sampling in the SDF GoldSim Model *SRS Saltstone v5.053_RS1a.gsm*, which was the first of three 1,000-realization simulations that were performed as part of the SDF PA (see Section 5.7.2 of SRR-CWDA-2019-00001).

3.4 GoldSim Software Description

The probabilistic model *SRS Saltstone RSI-1 v1.000.gsm* was developed using GoldSim modeling software. GoldSim is a commercial program developed by GoldSim Technology Group LLC (GTG). It is a user-friendly, graphical, Windows-based program designed for carrying out dynamic probabilistic simulations of complex systems to support management and decision-making in engineering, science, and business. In addition to the probabilistic capabilities, it also has deterministic capabilities.

GoldSim was designed to facilitate the construction of large, complex models. The user can build a model of a system in a hierarchical, modular manner, such that the model can evolve and add detail as more knowledge regarding the system is obtained. Other features, such as the ability to manipulate arrays, the ability to "localize" parts of a model, and the ability to assign version numbers to a model that is constantly being modified and improved, further facilitate the construction and management of large models. GoldSim has an extensive internal database of units and conversion factors allowing the user to enter data and display results in any units and/or define customized units. GoldSim ensures dimensional consistency in models and carries out all the unit conversions internally, eliminating the need to carry out error-prone unit conversions.

GoldSim Version 12.1 was used for the probabilistic modeling described within this report. The GTG provides a user's guide (GTG-2018a). The Software Quality Assurance Plan (SQAP) for GoldSim is covered by B-SQP-C-00002.

Because this is the same software as used for developing the SDF PA (SRR-CWDA-2019-00001), the same software QA applies. Section 6.0 of the *Performance Assessment for the Saltstone Disposal Facility at the Savannah River Site: Quality Assurance Report* (SRR-CWDA-2018-00068) provides a summary of the software QA, which includes GoldSim.

3.5 Changes to the Model Files Relative to the SDF GoldSim Model File

Version v5.057 of the SDF GoldSim Model was selected as a starting model for the development of the RSI-1 model file: *SRS Saltstone RSI-5 v1.000.gsm*. This is the latest version of the SDF GoldSim Model as described in the *QA Addendum to* [Fiscal Year] *FY2019 SDF PA QA Report, SRR-CWDA-2018-00068* (SRR-CWDA-2019-00046).

To prepare the model file for using the probabilistic flow data, the model changes described in Table 3.5-1 were applied. The resulting model file was saved as: *SRS Saltstone RSI-1 v1.000.gsm.*

Table 3.5-1: Model Changes to Develop the RSI-1 Model from the SDF PA Model

Model Element	Path in Model File	Change Description
InventoryChooser_switch	\User_Input	Set to 2 to support probabilistic inventory.
SDU_Choice	\User_Input	Set to value to 10 to support running only SDU 9.
UseSpecifiedFlowField	\User_Input	Set to TRUE because model will be set to read in data based on realization values of 1 to 1,000, so the realization value must be used for data lookups.
SpecifiedFlowField	\User_Input	Set to be equal to the Realization value (1 to 1,000).
HumanUptakeChooser_switch	\User_Input	Set to 2 to support probabilistic uptake values.
IntruderInventorySwitch	\User_Input	Set to 3 to use inadvertent human intruder (IHI) drilling concentrations based on 1-meter concentrations.
PlusSDU1and4	\GlobalModel_Input\GeneralParameters	Set to False to ensure that contributions from SDUs 1 and 4 are not included in this model. This model was designed to only evaluate releases from SDU 9. The input parameters for the other SDUs have been revised.
SS_Degradation_Params	\SensitivityAnalysis_New	Added container to hold data from the previous RSI models.
SalstoneDegradationParams	\SensitivityAnalysis_New	Added lookup table to provide the sampled value from the previous RSI models.
SSDeg_FinalSaltstoneKsat	\SensitivityAnalysis_New\SS_Degradation_Params	Added data element to read sampled value from previous RSI model for specific realizations.
SSDeg_Precipitation	\SensitivityAnalysis_New\SS_Degradation_Params	Added data element to read sampled value from previous RSI model for specific realizations.
SSDeg_Evapotranspiration	\SensitivityAnalysis_New\SS_Degradation_Params	Added data element to read sampled value from previous RSI model for specific realizations.
SSDeg_Runoff	\SensitivityAnalysis_New\SS_Degradation_Params	Added data element to read sampled value from previous RSI model for specific realizations.
SSDeg_ClimateCondition	\SensitivityAnalysis_New\SS_Degradation_Params	Added data element to read sampled value from previous RSI model for specific realizations.
SSDeg_ClimateTransitionTime	\SensitivityAnalysis_New\SS_Degradation_Params	Added data element to read sampled value from previous RSI model for specific realizations.
SSDeg_Backfill_Ksat_Initial	\SensitivityAnalysis_New\SS_Degradation_Params	Added data element to read sampled value from previous RSI model for specific realizations.
SSDeg_K_Top	\SensitivityAnalysis_New\SS_Degradation_Params	Added data element to read sampled value from previous RSI model for specific realizations.
SSDeg_F_Cover	\SensitivityAnalysis_New\SS_Degradation_Params	Added data element to read sampled value from previous RSI model for specific realizations.
SSDeg_Soil_Bulk_Density	\SensitivityAnalysis_New\SS_Degradation_Params	Added data element to read sampled value from previous RSI model for specific realizations.
SSDeg_Sand_Ksat_Initial	\SensitivityAnalysis_New\SS_Degradation_Params	Added data element to read sampled value from previous RSI model for specific realizations.
SSDeg_Sand_Ksat_Final	\SensitivityAnalysis_New\SS_Degradation_Params	Added data element to read sampled value from previous RSI model for specific realizations.
SSDeg_Sand_Deg_Duration	\SensitivityAnalysis_New\SS_Degradation_Params	Added data element to read sampled value from previous RSI model for specific realizations.
SSDeg_Initial_HDPE_Defect_Diam	\SensitivityAnalysis_New\SS_Degradation_Params	Added data element to read sampled value from previous RSI model for specific realizations.

Table 3.5-1: Model Changes to Develop the RSI-1 Model from the SDF PA Model (Continued)

Model Element	Path in Model File	Change Description
SSDeg_HDPE_Service_Life	\SensitivityAnalysis_New\SS_Degradation_Params	Added data element to read sampled value from previous RSI model for specific realizations.
SSDeg_HDPE_Initial_Defect_Freq	\SensitivityAnalysis_New\SS_Degradation_Params	Added data element to read sampled value from previous RSI model for specific realizations.
SSDeg_HDPE_Failure_Condition	\SensitivityAnalysis_New\SS_Degradation_Params	Added data element to read sampled value from previous RSI model for specific realizations.
SSDeg_GCL_Thickness	\SensitivityAnalysis_New\SS_Degradation_Params	Added data element to read sampled value from previous RSI model for specific realizations.
SSDeg_GCL_Ksat_Initial	\SensitivityAnalysis_New\SS_Degradation_Params	Added data element to read sampled value from previous RSI model for specific realizations.
SSDeg_GCL_Deg_Multiplier	\SensitivityAnalysis_New\SS_Degradation_Params	Added data element to read sampled value from previous RSI model for specific realizations.
SSDeg_Saltstone_Ksat_Initial	\SensitivityAnalysis_New\SS_Degradation_Params	Added data element to read sampled value from previous RSI model for specific realizations.
SSDeg_Ca_Sol	\SensitivityAnalysis_New\SS_Degradation_Params	Added data element to read sampled value from previous RSI model for specific realizations.
SSDeg_Deff	\SensitivityAnalysis_New\SS_Degradation_Params	Added data element to read sampled value from previous RSI model for specific realizations.
SSDeg_Initial_Crack_Density	\SensitivityAnalysis_New\SS_Degradation_Params	Added data element to read sampled value from previous RSI model for specific realizations.
SSDeg_pAveragingPower	\SensitivityAnalysis_New\SS_Degradation_Params	Added data element to read sampled value from previous RSI model for specific realizations.
SSDeg_SeisDmgFrac	\SensitivityAnalysis_New\SS_Degradation_Params	Added data element to read sampled value from previous RSI model for specific realizations.
SSDeg_SeisEventCount	\SensitivityAnalysis_New\SS_Degradation_Params	Added data element to read sampled value from previous RSI model for specific realizations.
Endpoints_PA	\SensitivityAnalysis_New	Added results from the values sampled in previous RSI models. This allows the output from the Endpoints_PA element to fully support probabilistic sensitivity analyses.
SDU_TransportSubmodel	\DisposalUnits\SDUs\Outer Loop\InnerLoop	Added InventoryUncert_Tc99_SDU9 as an input interface.
Tc99FluxToUZ_SDU_a	Within the SDU Submodel: \InputData\SDUPORFLOW Data	Multiplied the Tc-99 flux by the Tc-99 inventory uncertainty, then changed it back because inventory is not expected to influence Tc-99 releases in a linear way due to the solubility controls. So no change.
SDU_TransportSubmodel	\DisposalUnits\SDUs\Outer Loop\InnerLoop	Changed duration from 20,000 years to 10,000 years.
Model Timing [Not an element, but a file setting]	Run → Model	Changed duration from 20,000 years to 10,000 years.
Model Timing [Not an element, but a file setting]	Run → Model [Monte Carlo tab]	Set to run probabilistically with 1,000 realizations.

3.6 Changes to External Files Used by the Probabilistic RSI-1 Model File

As described in Section 4.2.2.5 of the SDF PA (SRR-CWDA-2019-00001), a dynamic link library (DLL), ReadFlowFields.DLL, was developed for use in conjunction with the SDF GoldSim Model (B-SQP-C-00003). Functionally, this software is used to read data into the SDF GoldSim Model

file from an external input file. The SQAP for ReadFlowFields.DLL is covered by B-SQP-C-00003.

Because this is the same software used for developing the SDF PA (SRR-CWDA-2019-00001), the same software QA applies. Section 6.0 of the *Performance Assessment for the Saltstone Disposal Facility at the Savannah River Site: Quality Assurance Report* (SRR-CWDA-2018-00068) provides a summary of the software QA, which includes ReadFlowFields.DLL.

For the SDF GoldSim Model, the DLL is used to read in flow data from files generated using the Vadose Zone Flow Model and from the Vadose Zone Transport Model. Since this RSI-1 analysis generated a new set of flow data and a new set of Tc-99 flux data, the input files for the DLL had to be modified to ensure that appropriate values will be used.

Because the only SDU being simulated as part of this modeling effort is SDU 9, the only input file that required modification was the one that provides instructions for reading SDU 9 data: *ReadPFData9.in*. Figure 3.6-1 shows the original *ReadPFData9.in* instructions as used for the SDF PA. Line 1 indicates how many files will be read in to the GoldSim file. Because there are 14 files identified, the next 14 lines (Lines 2 to 15) specify the directory and file name for each required file. Lines 16 and 17 each show 14 integer values (one value for each file); these are used to specify the number of lines or rows that are used as headers within each of the 14 files. Line 18 specifies how many rows of actual data may be read from each file. Finally, Lines 19 and 20 are used to identify the character positions (within Lines 2 to 15) which can be dynamically changed based on values from the GoldSim model file itself. These last two lines are critical because they enable the file to interact with GoldSim and to move through lists of multiple flow fields without having to explicitly list every file.

Figure 3.6-1: *ReadPFData9.in,* SDU 9 Read Flow Field Input Instructions for the SDF PA

Line	Text
1	14 ! number of data files to be read
2	C:\SDF_FY19Data01\V9\RLZ001\Flow\GoldSim.tab
3	C:\SDF_FY19Data01\V9\RLZ001\Transport\De_Tc-99.tab
4	C:\SDF_FY19Data01\V9\DET001\BE\Flow\GoldSim.tab
5	C:\SDF_FY19Data01\V9\DET001\BE\Transport\De_I-129.tab
6	C:\SDF_FY19Data01\V9\DET001\CV\Flow\GoldSim.tab
7	C:\SDF_FY19Data01\V9\DET001\CV\Transport\De_I-129.tab
8	C:\SDF_FY19Data01\V9\DET001\CE\Flow\GoldSim.tab
9	C:\SDF_FY19Data01\V9\DET001\CE\Transport\De_I-129.tab
10	C:\SDF_FY19Data01\V9\RLZ001\SDU9\Sol1\SDU10Release.txt
11	C:\SDF_FY19Data01\V9\RLZ001\SDU9\Sol2\SDU10Release.txt
12	C:\SDF_FY19Data01\V9\RLZ001\SDU9\Sol3\SDU10Release.txt
13	C:\SDF_FY19Data01\DET-Tc99\BE\SDUXXRelease.txt
14	C:\SDF_FY19Data01\DET-Tc99\CV\SDUXXRelease.txt
15	C:\SDF_FY19Data01\DET-Tc99\CE\SDUXXRelease.txt
16	0 0 0 0 0 0 0 0 2 2 2 2 2 2 ! # of lines in the TOF header
17	1 1 1 1 1 1 1 1 0 0 0 0 0 0 ! # of rows in the header for each table
18	200 200 200 200 200 200 200 200 50001 50001 50001 50001 50001 50001
19	20 20 20 20 20 20 20 20 20 20 20 34 34 34
20	25 25 25 25 25 25 25 25 25 25 25 46 46 46

In support of the RSI-1 analysis, Lines 2, 3, 10, 11, and 12 of *ReadPFData9.in* were revised to point to a new file directory wherein the new flow fields and Tc-99 flux data from the Vadose Zone Flow Model (Section 3.2) and from the Vadose Zone Transport Model (Section 3.3) have been organized (see Figure 3.6-2). Specifically, the directory `C:\SDF_FY19Data01\` was replaced with `C:\SDF_RSI1Data01\` and an additional "00" was added to the values following "RLZ" to support reading in up to 1,000 possible realizations (because this will be replaced with integer values with up to four characters).

Figure 3.6-2: *ReadPFData9.in,* SDU 9 Read Flow Field Input Instructions for RSI-1

Line	Text
1	14 ! number of data files to be read
2	C:\SDF_RSI1Data01\V9\RLZ00001\Flow\GoldSim.tab
3	C:\SDF_RSI1Data01\V9\RLZ00001\Transport\De_Tc-99.tab
4	C:\SDF_FY19Data01\V9\DET001\BE\Flow\GoldSim.tab
5	C:\SDF_FY19Data01\V9\DET001\BE\Transport\De_I-129.tab
6	C:\SDF_FY19Data01\V9\DET001\CV\Flow\GoldSim.tab
7	C:\SDF_FY19Data01\V9\DET001\CV\Transport\De_I-129.tab
8	C:\SDF_FY19Data01\V9\DET001\CE\Flow\GoldSim.tab
9	C:\SDF_FY19Data01\V9\DET001\CE\Transport\De_I-129.tab
10	C:\SDF_RSI1Data01\V9\RLZ00001\SDU9\Sol1\SDU10Release.txt
11	C:\SDF_RSI1Data01\V9\RLZ00001\SDU9\Sol2\SDU10Release.txt
12	C:\SDF_RSI1Data01\V9\RLZ00001\SDU9\Sol3\SDU10Release.txt
13	C:\SDF_FY19Data01\DET-Tc99\BE\SDUXXRelease.txt
14	C:\SDF_FY19Data01\DET-Tc99\CV\SDUXXRelease.txt
15	C:\SDF_FY19Data01\DET-Tc99\CE\SDUXXRelease.txt
16	0 0 0 0 0 0 0 0 2 2 2 2 2 2 ! # of lines in the TOF header
17	1 1 1 1 1 1 1 1 0 0 0 0 0 0 ! # of rows in the header for each table
18	200 200 200 200 200 200 200 200 50001 50001 50001 50001 50001 50001
19	20 20 20 20 20 20 20 20 20 20 20 34 34 34
20	25 25 25 25 25 25 25 25 25 25 25 46 46 46

Note: Red text indicates changes relative to the input instruction from the SDF PA.

These changes, along with copying the files from the PORFLOW modeling (i.e., the Vadose Zone Flow and Vadose Zone Transport Models) into the appropriate directories ensures that the new flow fields and fluxes will be read into GoldSim as opposed to reading in the data from the SDF PA.

3.7 Setup for the Probabilistic RSI-5 Model File

For RSI-5, the NRC recommended as a Path Forward that a new sensitivity case be developed that is "consistent with the [U.S. Department of Energy] DOE responses to RSI-1, RSI-2, RSI-3, and RSI-4, which would include a run with the MCCs assumed in the PA and a run with the relative permeability equal to 1" (ML20254A003). Rather than a single deterministic sensitivity case, a probabilistic evaluation based on the RSI-1 modeling was prepared instead. This RSI-5 evaluation did not use all 1,000 realizations from RSI-1, but instead used a subset of 100 realizations for the RSI-5 analysis. Note that the DOE does not believe that assuming a relative permeability of 1 provides an appropriate representation of the SDF system (see Appendix A) but is nonetheless providing an RSI-5 analysis to be responsive to the NRC's request.

3.7.1 Selected Realizations for the RSI-5 Model

Based on Section 5.7.4.2 of the SDF PA (SRR-CWDA-2019-00001), infiltration rates are expected to be the most dominant factor in influencing releases and doses. Therefore, the selection of the representative sample of the Vadose Zone Flow Model realizations was based on an evaluation of the infiltration rates. The infiltration rates from the Probabilistic Saltstone Degradation Model described in SRR-CWDA-2021-00056 were used to select a wide range of realizations. The peak infiltration rates (within the first 10,000 years) were identified from each realization and then ranked (from highest flow rate to lowest flow rate). The five realizations with the highest infiltration rates were selected to ensure that high infiltration rates would be appropriately represented: these were realizations 941, 302, 346, 894, and 76. Then, continuing to use the peak infiltration rates for ranking the realizations, every 5th realization was selected up to the 50th ranked infiltration rate. Next, every 10th realization was selected up to Rank 290. Then, every 20th realization was selected up to Rank 690. Then every 10th realization up to Rank 960, then every 5th realization up to Rank 985. Then Ranks 985 through 991 were selected. The lowest 9 infiltration rates were not included in the selection as these are expected to provide relatively low risk results.

In addition to selecting realizations based on infiltration rates, a number of other key parameters were also considered. Specifically, the following realizations were also explicitly included in the selection:

- Realization #730 had the second highest *p*-averaging term,
- Realization #190 had the highest initial saturated hydraulic conductivity (K_{sat}) for the GCL, and
- Realization #350 had the highest *p*-averaging term and the highest initially damaged saltstone K_{sat}.

These realizations were explicitly included in the set of selected realizations because it was not known whether or not these other key parameters would have any unexpected behavior when the MCCs are replaced with an assumed relative permeability of 1. By including the realizations wherein these parameters sampled the most extreme values, it ensures that any potential influences will be included in the resulting analysis.

Table 3.7-1 provides the final listing of each of the selected realizations. The Vadose Zone Flow Model was run for each of these realizations. These flow models are identical to the equivalent realizations from the RSI-1 analysis (see Section 3.2) with one modification: the relative permeability for the cementitious materials was set equal to 1. The resulting flow fields were then used to process the Tc-99 fluxes from SDU 9 using the Vadose Zone Transport Model (see Section 3.3). Finally, the flows and the Tc-99 fluxes were read into a modified version of the SDF GoldSim Model (similar to the model described in Section 3.5).

Table 3.7-1: Selected Realizations Used for the RSI-5 Analysis

#2	#113	#307	#436	#585	#740	#894
#19	#114	#313	#439	#589	#742	#918
#21	#139	#314	#447	#610	#746	#927
#22	#141	#329	#448	#615	#765	#941
#31	#163	#337	#468	#638	#772	#949
#41	#176	#338	#470	#644	#779	#960
#51	#190	#346	#480	#666	#798	#971
#57	#196	#350	#490	#672	#805	#979
#59	#228	#356	#498	#678	#816	#991
#72	#245	#358	#533	#686	#831	#993
#75	#246	#360	#548	#692	#848	
#76	#259	#382	#551	#698	#859	
#100	#267	#388	#560	#730	#865	
#110	#291	#394	#562	#733	#867	
#111	#302	#434	#577	#735	#884	

3.7.2 Development of the RSI-5 Model

For the RSI-5 GoldSim model, the RSI-1 model (*SRS Saltstone RSI-1 v1.000.gsm*) was modified to add two new elements at the GoldSim directory path: \Inventory. These two new elements were a Lookup Table element and a data element. The Lookup Table element: *RSI5_Rlzs* provided a two-column table. The first column was numbered 1 to 1,000 (for each realization); the second column had a value of either 0 or 1. The 0 value indicates that the realization was not selected and the 1 value means that it was selected. The data element: *ActivateRLZ* reads the 0 or 1 value from *RSI5_Rlzs* based on whichever realization was being simulated.

Next, the existing Selector element: *ModeledInventory* was modified to multiply the inventory values based on *ActivateRLZ*. This way, if a realization is not used, it would apply a zero inventory and there would be no results. Similarly, the data from *ActivateRLZ* was passed into the looping submodel: *SDU_TransportSubmodel* where it was then applied as a multiplier to the Tc-99 flux data (via the Selector element: *Tc99FluxToUZ_SDU_a*). The resulting model file was saved as: *SRS Saltstone RSI-5 v1.000_selectedRLZs.gsm*. Like the RSI-1 analysis, this model file was also run for 1,000 realizations, but all results were prepared by filtering the output using *ActivateRLZ* = 1.

External to the GoldSim file, the external files for RSI-1 were copied into an RSI-5 directory and then the files for the selected realizations were replaced with the RSI-5 PORFLOW modeling results (i.e., flow fields from the Vadose Zone Flow Model and Tc-99 fluxes from the Vadose Zone Transport Model) so the appropriate files would be read in with the ReadFlowFields.DLL. Figure 3.7-1 shows the SDU 9 input instructions.

Figure 3.7-1: *ReadPFData9.in,* SDU 9 Read Flow Field Input Instructions for RSI-5

Line	Text
1	14 ! number of data files to be read
2	C:\SDF_RSI5Data01\V9\RLZ00001\Flow\GoldSim.tab
3	C:\SDF_RSI5Data01\V9\RLZ00001\Transport\De_Tc-99.tab
4	C:\SDF_FY19Data01\V9\DET001\BE\Flow\GoldSim.tab
5	C:\SDF_FY19Data01\V9\DET001\BE\Transport\De_I-129.tab
6	C:\SDF_FY19Data01\V9\DET001\CV\Flow\GoldSim.tab
7	C:\SDF_FY19Data01\V9\DET001\CV\Transport\De_I-129.tab
8	C:\SDF_FY19Data01\V9\DET001\CE\Flow\GoldSim.tab
9	C:\SDF_FY19Data01\V9\DET001\CE\Transport\De_I-129.tab
10	C:\SDF_RSI5Data01\V9\RLZ00001\SDU9\Sol1\SDU10Release.txt
11	C:\SDF_RSI5Data01\V9\RLZ00001\SDU9\Sol2\SDU10Release.txt
12	C:\SDF_RSI5Data01\V9\RLZ00001\SDU9\Sol3\SDU10Release.txt
13	C:\SDF_FY19Data01\DET-Tc99\BE\SDUXXRelease.txt
14	C:\SDF_FY19Data01\DET-Tc99\CV\SDUXXRelease.txt
15	C:\SDF_FY19Data01\DET-Tc99\CE\SDUXXRelease.txt
16	0 0 0 0 0 0 0 0 2 2 2 2 2 2 ! # of lines in the TOF header
17	1 1 1 1 1 1 1 1 0 0 0 0 0 0 ! # of rows in the header for each table
18	200 200 200 200 200 200 200 200 50001 50001 50001 50001 50001 50001
19	20 20 20 20 20 20 20 20 20 20 20 34 34 34
20	25 25 25 25 25 25 25 25 25 25 25 46 46 46

Note: Red text indicates changes relative to the input instruction from the SDF PA.

3.8 Context of the RSI Models

The models described above, and the prerequisite models described in SRR-CWDA-2021-00040 and SRR-CWDA-2021-00056, have been designed to provide insights relative to specific flow barriers and conditions that could affect the performance of those flow barriers. Due to the intent of these models, the design does not necessarily reflect expected long-term conditions. Instead, modeling decisions were made to incorporate implausible, unlikely, or unexpected conditions to facilitate extreme conditions for the purpose of exaggerating uncertainties. Similarly, some modeling decisions were made to explicitly address specific questions raised by the NRC (ML20254A003), even if the DOE does not see a basis for such decisions. Table 3.8-1 provides a detailed summary of the key modeling conditions or decisions that do not reflect expected future conditions.

Table 3.8-1: Key Modeling Conditions or Decisions That Do Not Reflect Expected Future Conditions

Modeling Parameter or Condition	Approach Used for RSI Models	Expected Conditions
HDPE failure condition for the HDPE in the closure cap	The closure cap and infiltration model described in SRR-CWDA-2021-00040 sampled equally between three different failure conditions: no failure, partial failure, or complete failure.	Partial failure is the most likely expected failure condition for HDPE. Degradation of the HDPE is expected to occur gradually at localized sites such the effects of HDPE failure would not occur as significant step-changes in the overall behavior of the system. The three failure conditions were each assumed to be plausible because there is currently insufficient long-term testing/service life data available to justify assuming only the partial failure condition.
HDPE Failure Condition for the HDPE at the SDU roof	As recommended in SRR-CWDA-2021-00057, the complete failure condition was assumed.	Partial failure is the most likely expected failure condition for HDPE. Degradation of the HDPE is expected to occur gradually at localized sites such that the effects of HDPE failure would not occur as significant step-changes in the overall behavior of the system. The complete failure condition was assumed to simplify the Vadose Zone Flow Modeling because the scoping runs described in SRR-CWDA-2021-00057 demonstrated that this failure condition posed the greatest potential risk with respect to Tc-99 fluxes.
HDPE Failure Condition for the HDPE between the SDU mud mats	As recommended in SRR-CWDA-2021-00057, the complete failure condition was assumed.	Partial failure is the most likely expected failure condition for HDPE. Degradation of the HDPE is expected to occur gradually at localized sites such the effects of HDPE failure would not occur as significant step-changes in the overall behavior of the system. The complete failure condition was assumed to simplify the Vadose Zone Flow Modeling because the scoping runs described in SRR-CWDA-2021-00057 demonstrated that this failure condition posed the greatest potential risk with respect to Tc-99 fluxes.
Silting-in of sand in the ULDL	The closure cap and infiltration model described in SRR-CWDA-2021-00040 assumed that silting-in will occur (i.e., the sand K_{sat} will gradually decrease due to migration of fines from the overlying backfill).	Silting-in is not expected to occur because significant silting-in of sand drainage layers has not been observed. However, because this hypothetical phenomenon remains plausible, and because the NRC staff has expressed concerns about the potential impacts if this phenomenon does occur (ML20254A003), it was explicitly included in the closure cap and infiltration model.
Silting-in of sand in the LLDL	The Vadose Zone Flow model described in Section 3.2 assumed that silting-in will occur (i.e., the sand K_{sat} will gradually decrease due to migration of fines from the overlying backfill).	Silting-in is not expected to occur because significant silting-in of sand drainage layers has not been observed. However, because this hypothetical phenomenon remains plausible, and because the NRC staff has expressed concerns about the potential impacts if this phenomenon does occur (ML20254A003), it was explicitly included in the closure cap and infiltration model.

Table 3.8-1: Key Modeling Conditions or Decisions That Do Not Reflect Expected Future Conditions (Continued)

Modeling Parameter or Condition	Approach Used for RSI Models	Expected Conditions
Initial K_{sat} of the GCL in the closure cap	As described in SRR-CWDA-2020-00040, the initial K_{sat} of the GCL is sampled over a wide distribution (from 1.4E-11 cm/s to 4.0E-07 cm/s) to address potential uncertainties.	As described in SRR-CWDA-2021-00040, manufacturers of GCL specify maximum K_{sat} values on the order of 3.0E-09 cm/s to 5.0E-09 cm/s. It is expected that once the final design of the closure cap is approved, it will incorporate design specifications that require the GCL to have maximum K_{sat} values on the order of 5.0E-09 cm/s, such that none of GCL used in the closure cap will have K_{sat} values higher than 5.0E-09 cm/s.
Final K_{sat} of the GCL in the closure cap	It is assumed that the GCL will undergo degradation due to cation exchange by increasing the GCL K_{sat} by as much as a factor of 354 (SRR-CWDA-2021-00040).	Based on local pore water chemistry expected for the SDF closure cap (i.e., very low ionic strength), and based on observations at the similar Barnwell site, no degradation of the GCL is expected.
Final K_{sat} of the combined HDPE/GCL in above the SDU roof	For the Vadose Zone Flow model described in Section 3.2, the HDPE and GCL layers are modeled as a single layer. Because the complete failure condition is being applied to the HDPE, the layer is modeled as impermeable until the HDPE fails, then the GCL K_{sat} based on degradation modeling defined in SRR-CWDA-2021-00040 is applied for both layers.	The HDPE is expected to undergo partial failure as opposed to complete failure, and the GCL is not expected to undergo any degradation (based on the low ionic strength of local pore water chemistry). Regardless, it is also expected that the overburden pressure from the overlying closure cap materials and lower backfill material would decrease the K_{sat} of the GCL, a phenomenon which has been observed but has not been credited because the data required to quantify this is not available.
Final K_{sat} of the combined HDPE/GCL between the SDU mud mats	For the Vadose Zone Flow model described in Section 3.2, the HDPE and GCL layers are modeled as a single layer. Because the complete failure condition is being applied to the HDPE, the layer is modeled as impermeable until the HDPE fails, then the GCL K_{sat} based on degradation modeling defined in SRR-CWDA-2021-00040 is applied for both layers.	The HDPE is expected to undergo partial failure as opposed to complete failure. However, unlike the other GCL layers (discussed above), it is possible that the GCL between the mud mats may undergo hydraulic degradation of the K_{sat} because it may be exposed to pore water that includes leachates from the saltstone waste form, and these leachates may invoke cation exchange. Regardless, it is also expected that the overburden pressure from the overlying closure cap materials, lower backfill material, and the SDU would decrease the K_{sat} of the GCL, a phenomenon which has been observed but has not been credited because the data required to quantify this is not available.

Table 3.8-1: Key Modeling Conditions or Decisions That Do Not Reflect Expected Future Conditions (Continued)

Modeling Parameter or Condition	Approach Used for RSI Models	Expected Conditions
p-averaging term for estimating the properties of partially degraded cementitious materials	As recommended in SRR-CWDA-2021-00052, the full range of potential uncertainties (from -1 to +1) has been sampled for the *p*-averaging term.	For the SDF, Brown and Garrabrants (2017) recommended using the geometric mean (effectively equivalent to a *p*-averaging term of 0). Similarly, Sanchez-Vila et al. (2006) indicated that the effective K_{sat} of a three-dimensional medium with isotropic heterogeneity may be determined with a *p*-averaging term of +0.33. As such, it is expected that a *p*-averaging term between 0 and +0.33 would probably provide the most realistic representation of the partially degraded cementitious materials for the SDF system.
Initial cracks in saltstone	As recommended in SRR-CWDA-2021-00052, initial cracking of saltstone is assumed to vary in frequency from no cracks up to 1 crack every foot, wherein each crack is assumed to be 1-cm thick. When the *p*-averaging term is sampled as value of +1, these cracks are effectively modeled as through-cracks (i.e., penetrating the full thickness of the saltstone monolith).	While some cracks have been observed in the surface of cured saltstone within SDU 4 (e.g., SRR-CWDA-2011-00105), these are expected to be limited to the thickness of individual pours, terminating at potential cold joints rather than being through-cracks (i.e., the depth of each crack is expected to be limited or near-surface only). Further, many SDU cells that have been inspected for cracks in saltstone have shown no cracks at all. Further, those SDU cells wherein the cracks have been observed have been much smaller than 1-cm (e.g., hairline fractures) and less frequent than one crack for every 10 feet. As such, the assumed modeling approach is expected to overpredict the influence of an initial damage to the saltstone.
Frequency of damage occurring due to seismic events	Saltstone-damaging seismic events are sampled as occurring with an average frequency of once every 2,500 years starting when the surrounding SDU concrete no longer affords any protection to the saltstone (SRR-CWDA-2021-00056).	Because the SDUs and the saltstone within the SDUs will be surrounded by backfill and covered beneath the closure cap, pressure will be applied to the SDUs from all directions. Further, seismic activity in South Carolina is generally rare and of relatively low magnitude. The one notable exception is the Charleston Earthquake of 1886 with an estimated peak ground acceleration of 0.18 g (K-ESR-Z-00008). As such, it is generally highly unlikely that any earthquake will occur with sufficient force to cause actual damage to the saltstone itself.

Table 3.8-1: Key Modeling Conditions or Decisions That Do Not Reflect Expected Future Conditions (Continued)

Modeling Parameter or Condition	Approach Used for RSI Models	Expected Conditions
Damage from seismic events	For every seismic event that is sampled as occurring, the total degradation fraction is increased. For simplicity, the amount of degradation is sampled once per realization rather than re-sampling for each event (SRR-CWDA-2021-00056). Thus, the degradation cumulative degradation fraction is assumed to increase by the same amount for every sampled seismic event. The sampled magnitude of the seismic degradation fraction was based on estimated depths of settlement.	As it is generally highly unlikely that any earthquake will occur with sufficient force to cause actual damage to the saltstone itself, applying any amount of damage is expected to result in an overprediction of saltstone degradation overtime. Further, even if seismic events of sufficient magnitudes to damage the saltstone do occur, it is expected that the amount of damage to saltstone would become smaller with each successive event. This is because structural damage to concrete structures release tension; once the tension is released it would take greater force to cause an equivalent amount of damage. Accordingly, each successive seismic event should be less likely to result in additional damage to the system.
Darcy velocity assumed for estimating the rate of advective decalcification	As described in Section 4.4 of SRR-CWDA-2021-00056, the Darcy velocity used for calculating the advection rate coefficient for saltstone decalcification was assumed to be equal to the time-dependent infiltration rate.	The assumed approach overpredicts saltstone degradation in two ways. First, due to previously mentioned modeling parameters and conditions (e.g., HDPE failure condition), the estimated infiltration rates from the RSI models are expected to overpredict actual infiltration rates. Second, this approach does not account for the influence of any of the flow barriers in the system (LLDL, composite HDPE/GCL barrier, or the SDU roof), so the assumed Darcy velocity is higher than would ever reasonably be expected. As shown in Section 6.3 of SRR-CWDA-2021-00056, the advective decalcification of saltstone is the leading degradation mechanism in the RSI model, so overpredicting the rate of advective decalcification results in a significant underprediction of the long-term performance of saltstone.

Given these modeling decisions, the RSI models and the associated results should be considered stylized sensitivity models. While the results from these models may be useful for informing risk-related decision-making, these results should not be construed as reflective of actual long-term conditions at the SDF.

4.0 RESULTS

The following presents the results from the probabilistic RSI-1 and RSI-5 models. The RSI-1 Model (*SRS Saltstone RSI-1 v1.000.gsm*) was run for 1,000 realizations and the RSI-5 Model (*SRS Saltstone RSI-5 v1.000.gsm*) was run for 100 realizations. Both were simulated over a period of 10,000 years. This period reflects the SDF PA Performance Period (i.e., 10,000 years per SRR-CWDA-2019-00001), which is 10 times longer than the 1,000-year Compliance Period.

Both of these models incorporate uncertainties based on recommendations developed via responses to RSI-2, RSI-3, RSI-4, and RSI-7, as well as the uncertainties already considered as part of Section 5.7 of the SDF PA (SRR-CWDA-2019-00001). For simplicity, these models only simulated the release and transport associated with SDU 9 (see Appendix B).

Section 4.1 presents probabilistic uncertainty analyses to characterize the variability in the model results and Section 4.2 presents probabilistic sensitivity analyses to identify the parameters that influence the uncertainty. Then Section 4.3 provides an analysis in response to RSI-5 (ML20254A003). Section 4.4 provides additional observations from the analysis of the model results. Finally, Section 4.5 provides a summary of recommendations and conclusions from these analyses.

4.1 Probabilistic Uncertainty Analysis of RSI-1 Model Results

This section provides uncertainty analyses for the Total Dose to the Member of the Public (MOP) for all 1,000 realizations (Section 4.1.1), the Total Dose to the MOP for the 334 realizations with partial failure of the HDPE (Section 4.1.2), and the Chronic Inadvertent Human Intruder (IHI) Dose for all 1,000 realizations (Section 4.1.3).

4.1.1 Probabilistic Uncertainty Analysis of Total Doses to the MOP from the RSI-1 Model for All 1,000 Realizations

Figure 4.1-1 shows the peak values from the total doses to the MOP at the 100-meter well. These results come from SDU 9 based on the RSI-1 Model (*SRS Saltstone RSI-1 v1.000.gsm*). These doses do not represent expected future conditions but are only provided to demonstrate where uncertainties in the system may pose the greatest risk relative to potential doses. The distinctive vertical groupings of the higher dose peaks coincide with the discrete time intervals that were applied in the Vadose Zone Flow Model (see Table 3.2-1). It is expected that increasing the temporal discretization of the flow fields would likely reduce the magnitudes of these peaks and the timing of the peaks would become more distributed. Regardless, Figure 4.1-1 demonstrates that the RSI-1 Model provides peak doses over a wide range for both timing and magnitude. Therefore, these results are sufficient for providing risk insights associated with the various uncertainties considered in the RSIs.

Of the 1,000 peak doses shown in Figure 4.1-1, 142 of them (14.2%) occur at 10,000 years (i.e., the end of the simulation); this indicates that peak doses for these realizations would likely occur at a point in time beyond 10,000 years.

Figure 4.1-2 shows the same peak dose results, but the data points have each been colored based on the sampled HDPE Failure Condition (HFC), where red (HFC = 3) indicates a complete failure

condition, gold (HFC = 2) indicates a partial failure condition, and blue (HFC = 1) indicates no failure (i.e., infiltration only occurs due to initial defects in the HDPE).

Figure 4.1-1: Peak Total Doses to the MOP at the 100-Meter Well from RSI-1

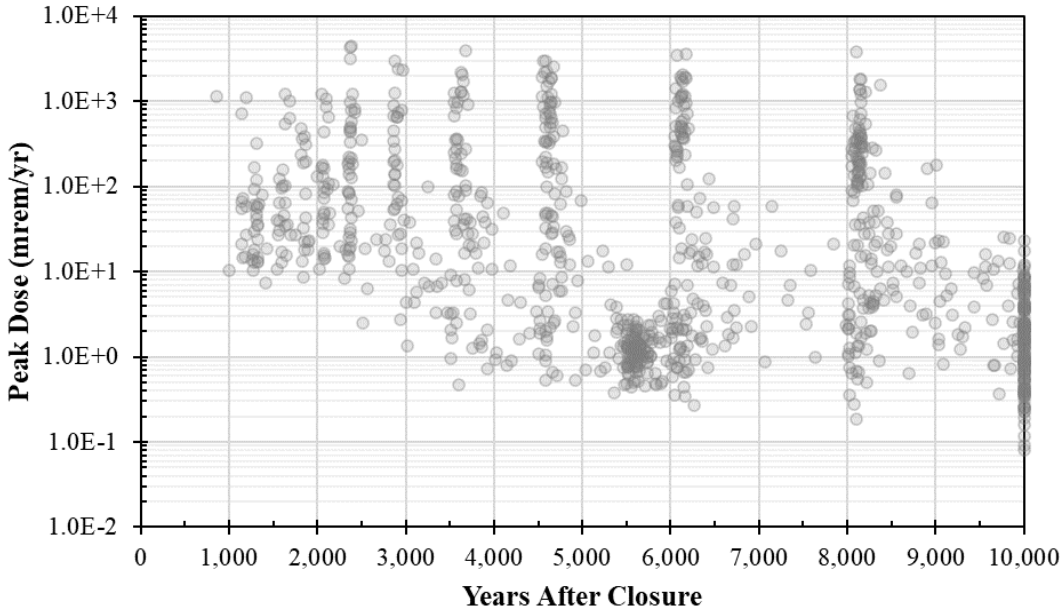

Figure 4.1-2: Peak Total Doses to the MOP at the 100-Meter Well from RSI-1 Based on HDPE Failure Condition

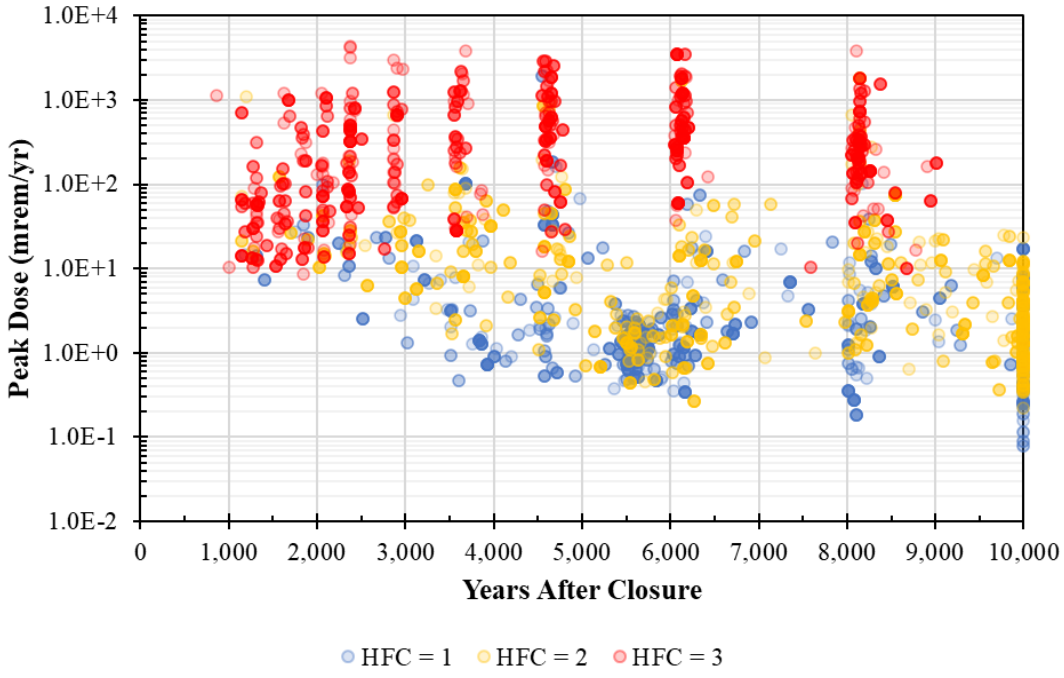

Note: HFC = HDPE failure condition: 1 = No HDPE Failure; 2 = Partial HDPE Failure; and 3 = Complete HDPE Failure.

As previously discussed in Section 3.2, the HFC is only sampled for the HDPE/GCL composite barrier within the closure cap (beneath the ULDL); for the other HDPE/GCL composite barriers (i.e., above the SDU and the between the mud mats), the complete failure condition has been assumed in every realization. As such, the sampling of the HFC only affects infiltration into the system.

The magnitudes of the red dose peaks in Figure 4.1-2 indicate that the dose results are likely to be strongly influenced by the HFC. Most of the realizations with the highest doses are realizations which sampled the complete failure condition for the HDPE. Because partial failure is expected to be the most likely failure condition, these results provide insights to the relative importance of this expectation.

Table 4.1-1 provides a summary of these peak MOP doses for both the Compliance Period and the Performance Period, as well as a summary based on each of the sampled HFC values. This table is similar to Table 5.7-5 from the SDF PA (SRR-CWDA-2019-00001). Aside from the realizations which sampled the complete HDPE failure condition (HFC = 3), the median values are generally similar in magnitude to the median values from the SDF PA, suggesting that while a greater range of variability is being considered, the central tendency has not changed significantly relative to the probabilistic uncertainty considered for the SDF PA.

Table 4.1-1: Statistics of Peak Total Doses to the MOP at the 100-Meter Well from RSI-1

Statistic	All Realizations	HDPE Failure Condition = 1	HDPE Failure Condition = 2	HDPE Failure Condition = 3
Count	**1,000**	**333**	**334**	**333**
Within the 1,000-Year Compliance Period				
Mean	3.5	0.23	0.27	10
Geometric Mean	**0.033**	**0.018**	**0.019**	**0.11**
Maximum	1,127	28	33	1,127
95th Percentile	10	0.28	0.29	30
75th Percentile	0.046	0.030	0.029	0.35
Median	**0.018**	**0.014**	**0.016**	**0.031**
25th Percentile	0.009	0.007	0.008	0.013
5th Percentile	0.003	0.003	0.003	0.006
Minimum	0.001	0.001	0.001	0.001
Within the 10,000-Year Performance Period				
Mean	191	12	43	518
Geometric Mean	**14**	**2.0**	**6.1**	**208**
Maximum	4,371	1,911	1,801	4,371
95th Percentile	1,140	25	133	2,042
75th Percentile	102	3.8	17	639
Median	**10**	**1.6**	**5.2**	**221**
25th Percentile	1.6	0.84	1.6	67
5th Percentile	0.53	0.36	0.65	16
Minimum	0.079	0.079	0.22	8.6

Figure 4.1-2 showed the individual peak doses from every realization. If we consider each realization as a unique timeline for estimating doses, a statistical time history may be generated by

analyzing the results as a function of time. Figure 4.1-3 shows the statistical time history of the total dose to the MOP from the RSI-1 Model (*SRS Saltstone RSI-1 v1.000.gsm*).

Figure 4.1-3: Statistical Time History of the Total Dose to the MOP from RSI-1

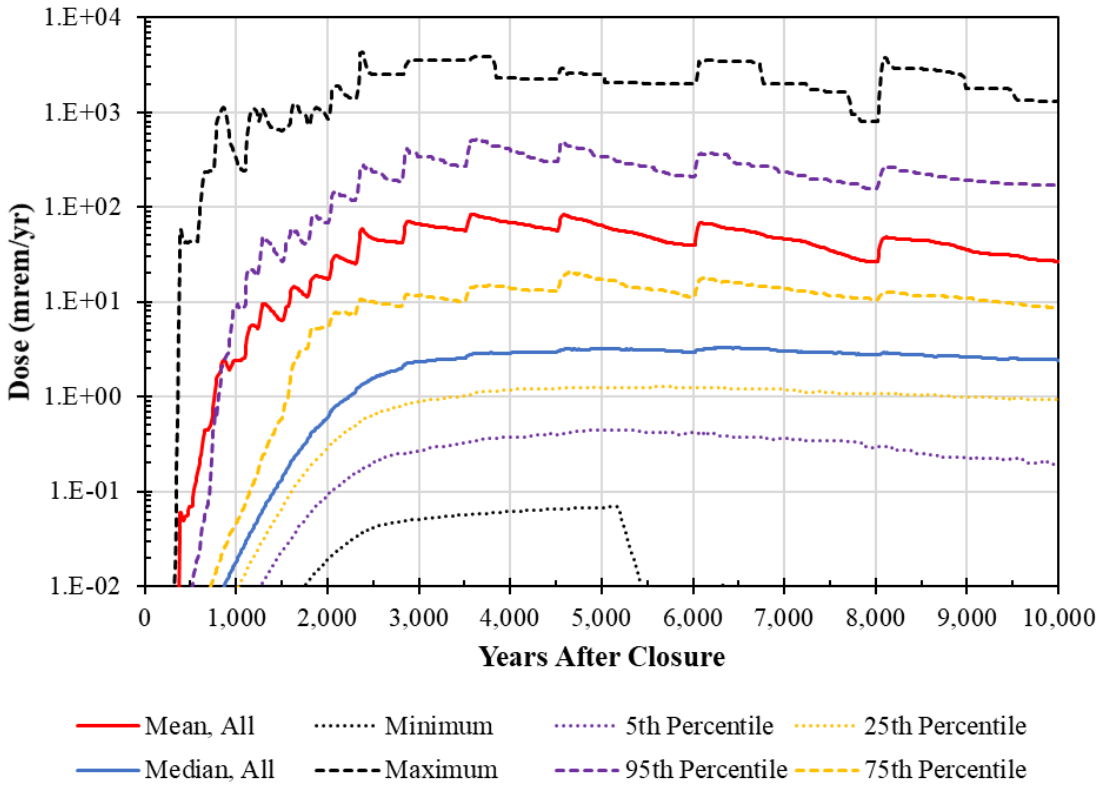

As shown, these doses exhibit significant variability. Despite this spread, and despite making a number of modeling decisions designed to emphasize the potential risks associated with various uncertainties, the 95th percentile dose result (purple dashed curve) peaks at 8.8 mrem/yr within the first 1,000 years (i.e., within the Compliance Period). Given the performance objective of 25 mrem/yr, these results indicate that even when all of the uncertainties from the RSIs and from the SDF PA are combined, it is still reasonable to expect that the SDF will meet performance objectives within the Compliance Period.

It is recognized that the mean dose (red curve) is skewed toward higher values due to the influence of a small number of realizations with extremely high doses. The mean dose generally falls midway between the 75th percentile (gold dashed curve) and the 95th percentile (purple dashed curve). For additional perspective, Figure 4.1-4 is identical to Figure 4.1-3, except that the arithmetic mean has been replaced with a geometric mean (dark red curve); this provides a more reasonable representation of the central tendency of these dose results. The geometric mean has a peak dose of 5.8 mrem/yr at 4,630 years after SDF closure, which is similar in magnitude to the 4.8 mrem/yr Total MOP Dose mean from Table 5.7-6 of the SDF PA (SRR-CWDA-2019-00001).

Figure 4.1-4: Statistical Time History of the Total Dose to the MOP from RSI-1, Using the Geometric Mean Instead of the Arithmetic Mean

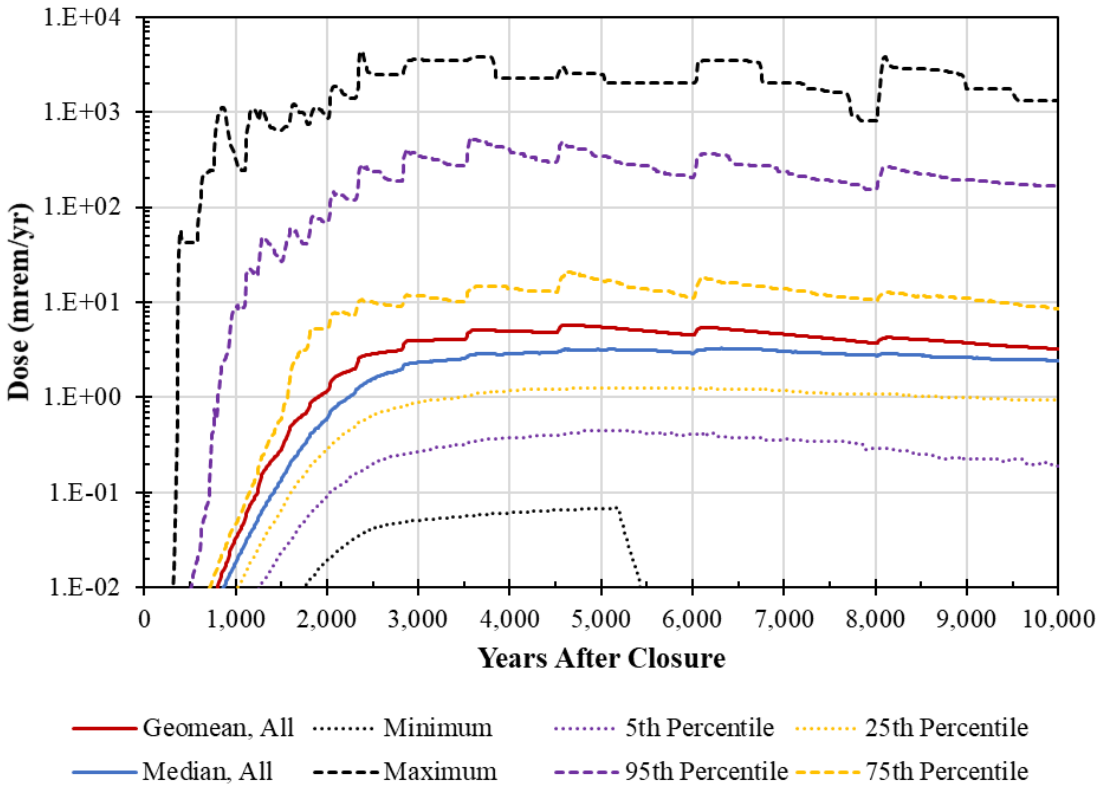

Table 4.1-2 provides a summary of the peaks for selected statistical values along these time histories. Note that HFC = 2 (partial failure condition for the HDPE) is expected to be the most likely and reasonable future condition.

Table 4.1-2: Peaks of the Statistics for the Total Doses to the MOP at the 100-Meter Well from RSI-1

Evaluated Endpoints	Peak of the Arithmetic Means		Peak of the Geometric Means		Peak of the Medians (50th Percentile)		Peak of the 95th Percentiles	
	Peak Dose (mrem/yr)	Time (yrs)	Peak Dose (mrem/yr)	Time (yrs)	Peak Dose (mrem/yr)	Time (yrs)	Peak Dose (mrem/yr)	Time (yrs)
Within the 1,000-Year Compliance Period								
Total MOP Dose (All)	2.4	870	0.033	1,000	0.018	1,000	8.8	990
Total MOP Dose for HFC = 1 (No Failure)	0.23	1,000	0.018	1,000	0.014	1,000	0.28	1,000
Total MOP Dose for HFC = 2 (Partial Failure)	0.27	1,000	0.019	1,000	0.016	1,000	0.29	1,000
Total MOP Dose for HFC = 3 (Complete Failure)	7.1	870	0.10	1,000	0.031	1,000	28	1,000
Within the 10,000-Year Performance Period								
Total MOP Dose (All)	85	3,590	5.8	4,630	3.3	6,320	516	3,640
Total MOP Dose for HFC = 1 (No Failure)	9.9	4,690	1.6	6,490	1.4	6,480	17	6,960
Total MOP Dose for HFC = 2 (Partial Failure)	22	4,700	3.7	8,340	3.2	8,590	59	8,210
Total MOP Dose for HFC = 3 (Complete Failure)	225	3,580	39	4,610	40	4,680	1,129	3,630

Next, Figure 4.1-5 shows that by simulating releases from only SDU 9, the (arithmetic) mean doses along Sector D dominate for the entire simulation. There is also a modest dose along Sector C. All of the other Sectors only exhibit doses because it is assumed that the MOP will consume contaminated fish, and swim and boat along the seepline of Fourmile Branch (beyond the 100-meter boundary); regardless of which sector the MOP draws their well water from, these activities will affect the MOP the same. This result may be compared to Figure 5.7-7 of the SDF PA (SRR-CWDA-2019-00001).

Figure 4.1-6 and Figure 4.1-7 show (arithmetic) mean dose contributors by radionuclide and by dose pathway, respectively. In the first 1,000 years, I-129 is the primary dose contributor, but shortly after 1,000 years, the contributions from Tc-99 exceed those from I-129. The two largest pathway contributors are plant ingestion and water ingestion. These results are similar to those shown in Figures 5.7-8 and 5.7-9 of the SDF PA (SRR-CWDA-2019-00001). This information indicates that applying the uncertainties from the various RSI responses does not alter the influence of the various dose contributors or pathways, relative to those discussed in the SDF PA.

Figure 4.1-5: Mean Doses to the MOP for Each Sector from RSI-1

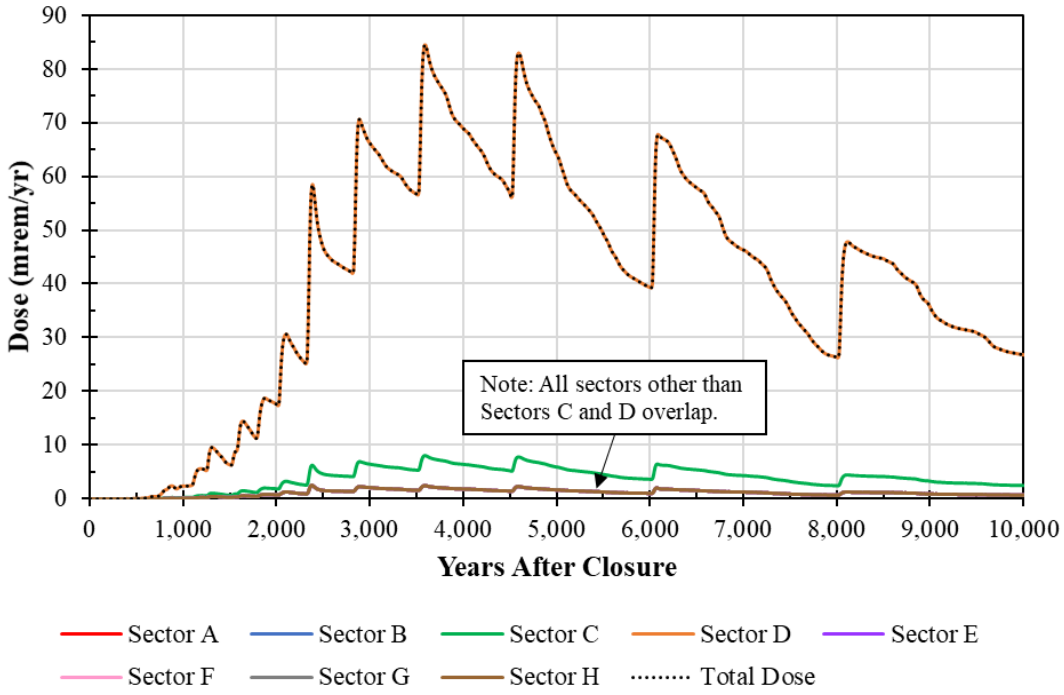

Figure 4.1-6: Mean Doses to the MOP for Each Radionuclide from RSI-1

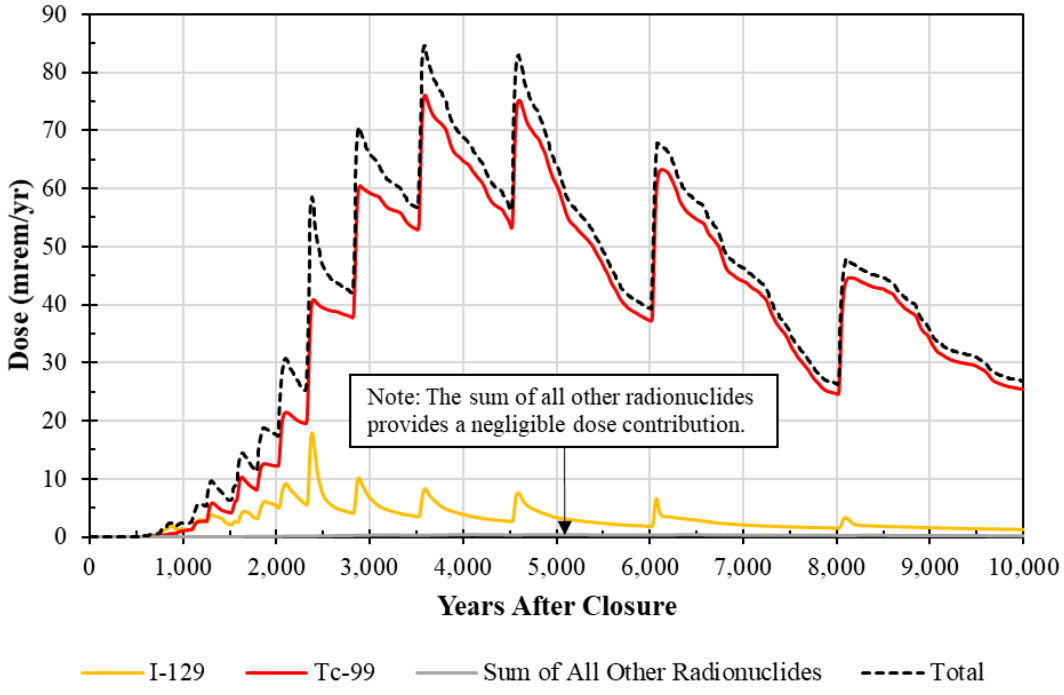

Figure 4.1-7: Mean Doses to the MOP for Each Pathway from RSI-1

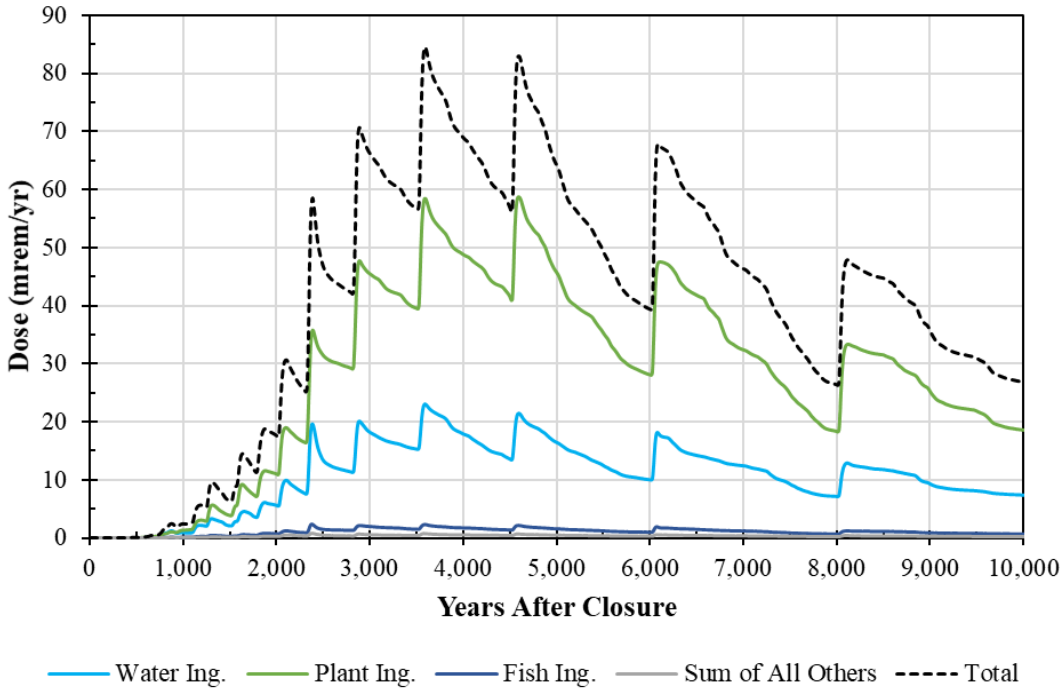

4.1.2 Probabilistic Uncertainty Analysis of Total Doses to the MOP from the RSI-1 Model for 334 Realizations wherein the HDPE Applied the Partial Failure Condition

Given the significance of the HFC, and the likelihood that any failure of the HDPE will be gradual and/or localized, this subsection is provided to offer additional insights relative to the 334 realizations from the RSI-1 Model (*SRS Saltstone RSI-1 v1.000.gsm*) wherein the expected partial failure condition (HFC = 2) was sampled.

Figure 4.1-8 shows the peak doses (for the total doses to the MOP at the 100-meter well) from SDU 9 based on the RSI-1 Model (*SRS Saltstone RSI-1 v1.000.gsm*) where HFC = 2. Compared to Figure 4.1-1, these peak doses are generally similar in range, but show less density for the doses in the upper values and less "clustering" of peaks at the times of the flow field time intervals. Table 4.1-1 provided a summary of the values for these peak doses.

Figure 4.1-8: Peak Total Doses to the MOP at the 100-Meter Well from RSI-1 for Realizations with Partial Failure of the HDPE

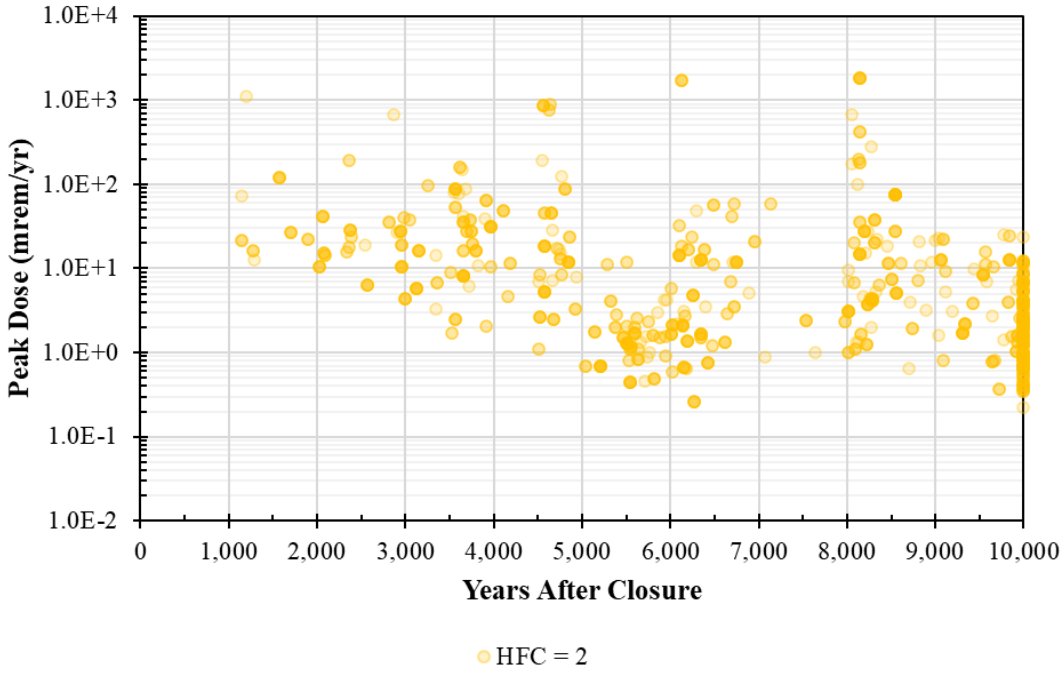

Note: HFC = HDPE failure condition: 2 = Partial HDPE Failure.

Figure 4.1-9 shows the statistical time history of the total dose to the MOP from the RSI-1 Model (*SRS Saltstone RSI-1 v1.000.gsm*) for the 334 realizations with partial failure of the HDPE. Similar to Figure 4.1-3, the doses in Figure 4.1-9 exhibit significant variability. While the maximum doses are similar in magnitude to Figure 4.1-3, the 95th percentile dose in Figure 4.1-9 is significantly lower, indicating that this subset of the results had relatively fewer outlier realizations.

Within the first 1,000 years (i.e., within the Compliance Period), the mean dose (red curve) and the 95th percentile dose (purple dashed curve) are both less than 0.3 mrem/yr. Within 10,000 years (i.e., within the Performance Period), the mean dose peaks at 22 mrem/yr at year 4,700 and the 95th percentile dose peaks at 59 mrem/yr at year 8,210.

For additional perspective, Figure 4.1-10 is identical to Figure 4.1-9, except that the arithmetic mean has been replaced with a geometric mean (dark red curve); this provides a more reasonable representation of the central tendency of these dose results. The geometric mean has a peak dose of 3.7 mrem/yr at 8,340 years after SDF closure. Table 4.1-2 provides a summary of the peaks for selected statistical values along these time histories.

Figure 4.1-9: Statistical Time History of the Total Dose to the MOP from RSI-1 for Realizations with Partial Failure of the HDPE

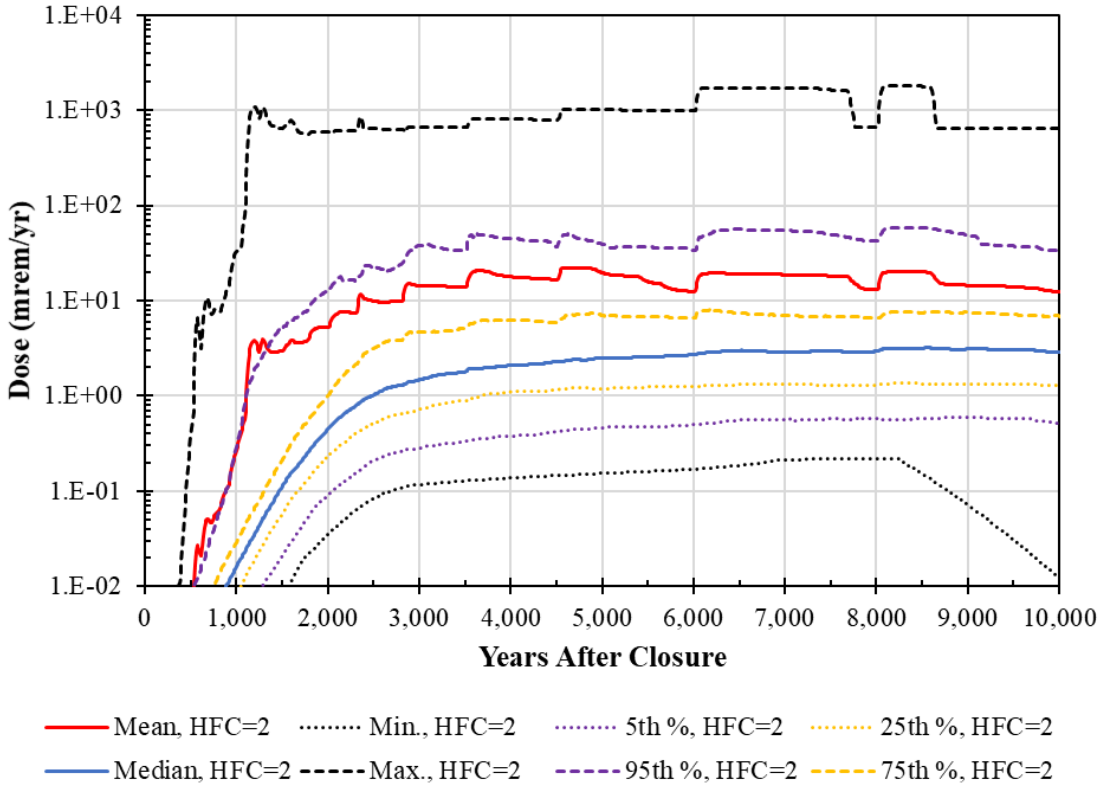

Figure 4.1-10: Statistical Time History of the Total Dose to the MOP from RSI-1 for Realizations with Partial Failure of the HDPE, Using the Geometric Mean Instead of the Arithmetic Mean

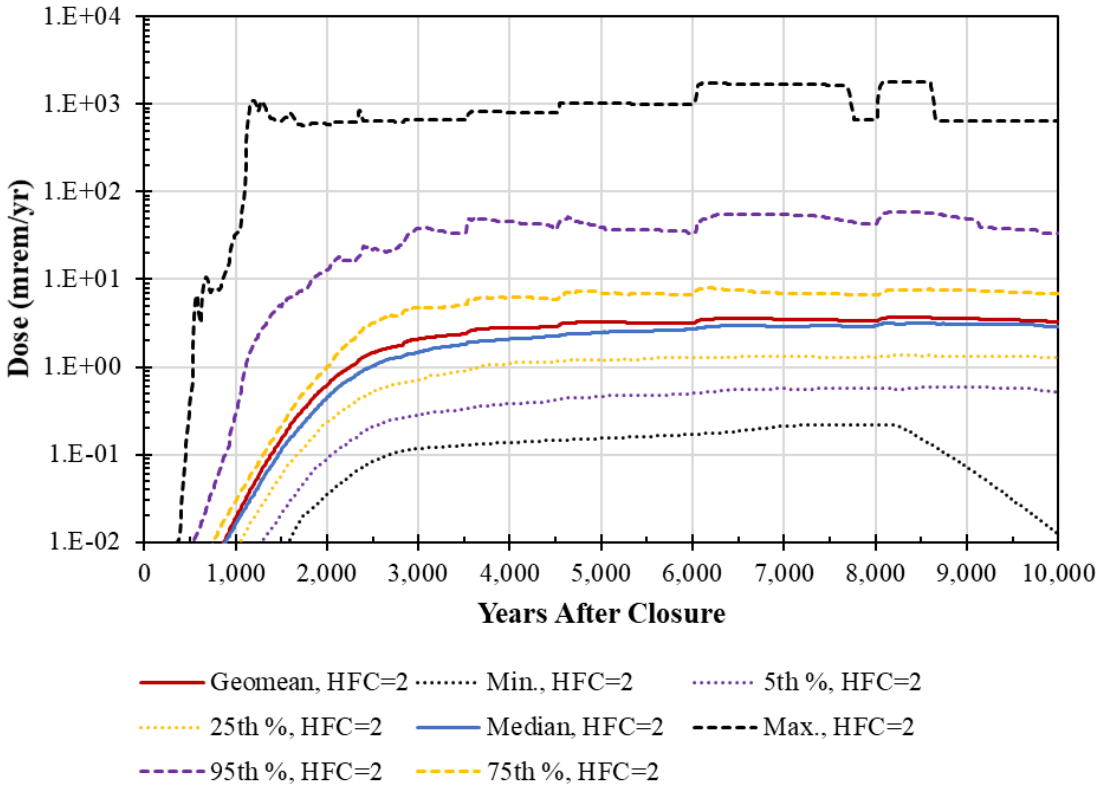

Next, Figure 4.1-11, Figure 4.1-12, and Figure 4.1-13 show the (arithmetic) mean doses by sector, by radionuclide, and by dose pathway, respectively. These results are similar to those presented for the full set of 1,000 realizations, albeit at a lower magnitude.

Figure 4.1-11: Mean Doses to the MOP for Each Sector from RSI-1 for Realizations with Partial Failure of the HDPE

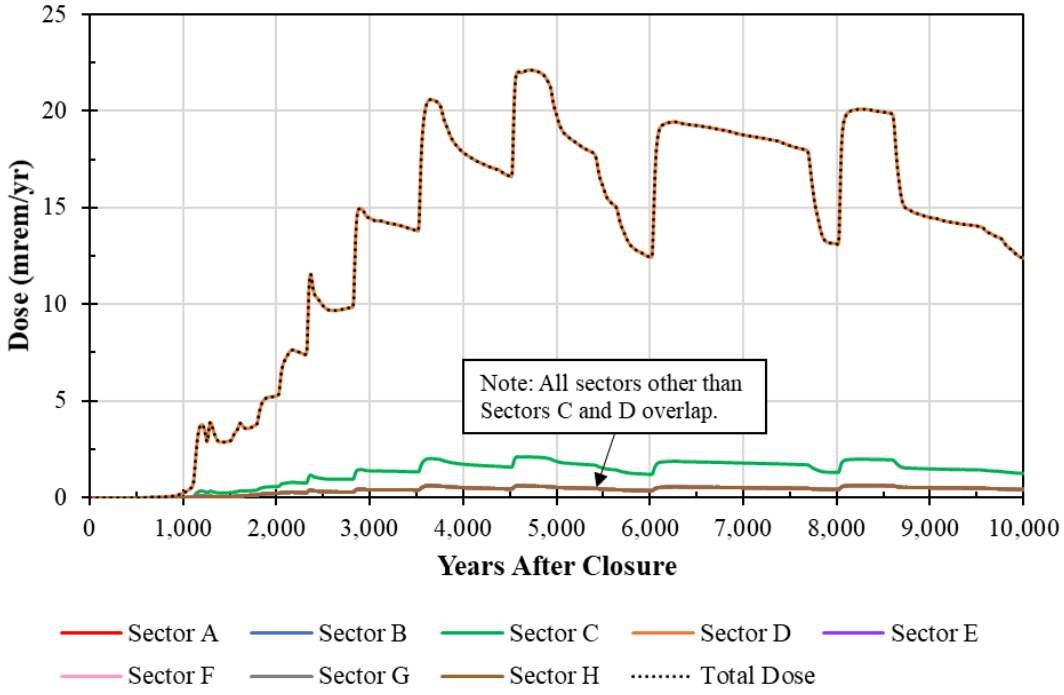

Figure 4.1-12: Mean Doses to the MOP for Each Radionuclide from RSI-1 for Realizations with Partial Failure of the HDPE

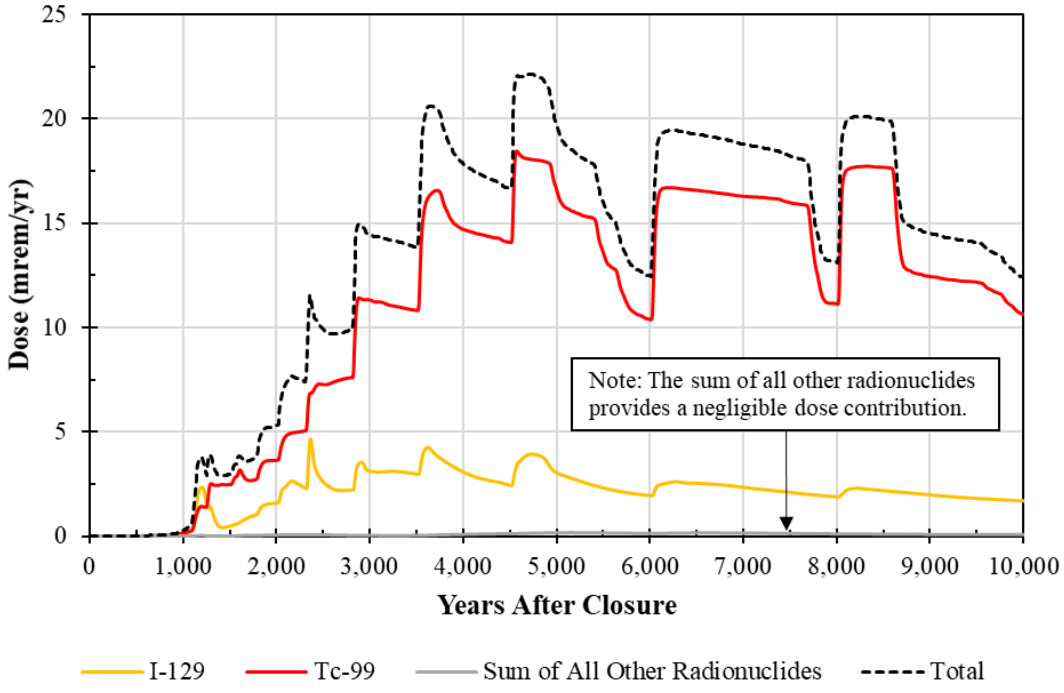

Figure 4.1-13: Mean Doses to the MOP for Each Pathway from RSI-1 for Realizations with Partial Failure of the HDPE

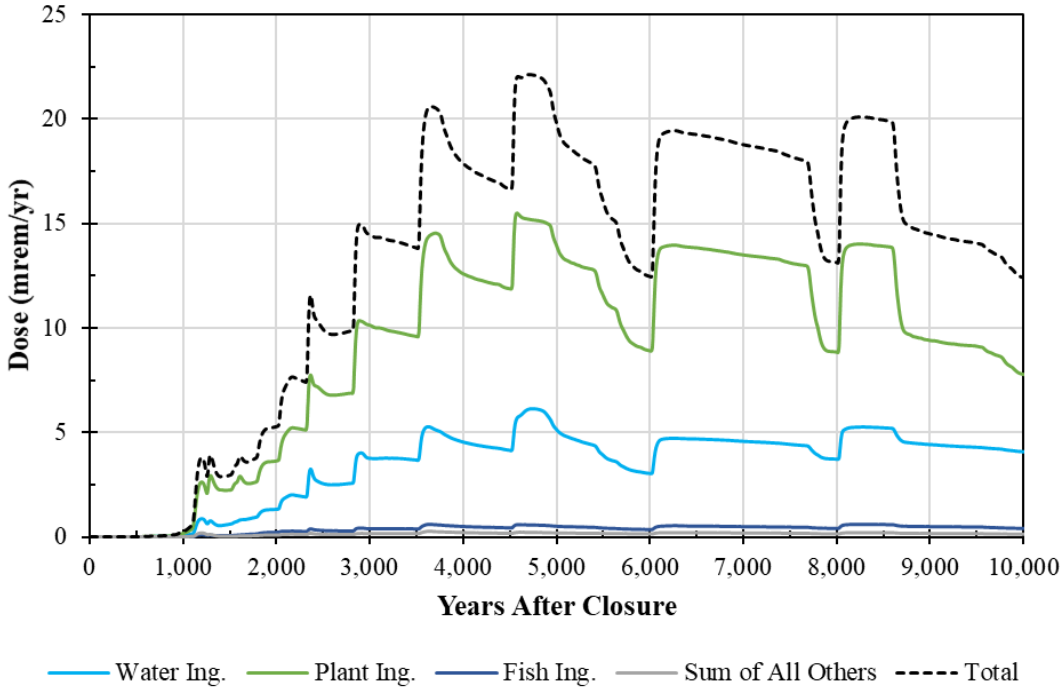

4.1.3 Probabilistic Uncertainty Analysis of Chronic IHI Doses from the RSI-1 Model for All 1,000 Realizations

Figure 4.1-14 shows the peak values from the Chronic IHI results at the 1-meter well. These results come from SDU 9 based on the RSI-1 Model (*SRS Saltstone RSI-1 v1.000.gsm*). These doses do not represent expected future conditions but are only provided to demonstrate where uncertainties in the system may pose the greatest risk relative to potential doses. These IHI results are very similar to the MOP results presented in Figure 4.1-1. This similarity is expected given that the Chronic IHI dose is strongly influenced by ground water concentrations (see Section 6.4.2 of the SDF PA (SRR-CWDA-2019-00001).

Figure 4.1-15 shows the same peak dose results, but the data points have each been colored based on the sampled HFC values. As with the MOP results, the magnitudes of the red dose peaks in Figure 4.1-15 indicate that the dose results are likely to be strongly influenced by the HFC.

Figure 4.1-14: Peak Chronic IHI Doses at the 1-Meter Well from RSI-1

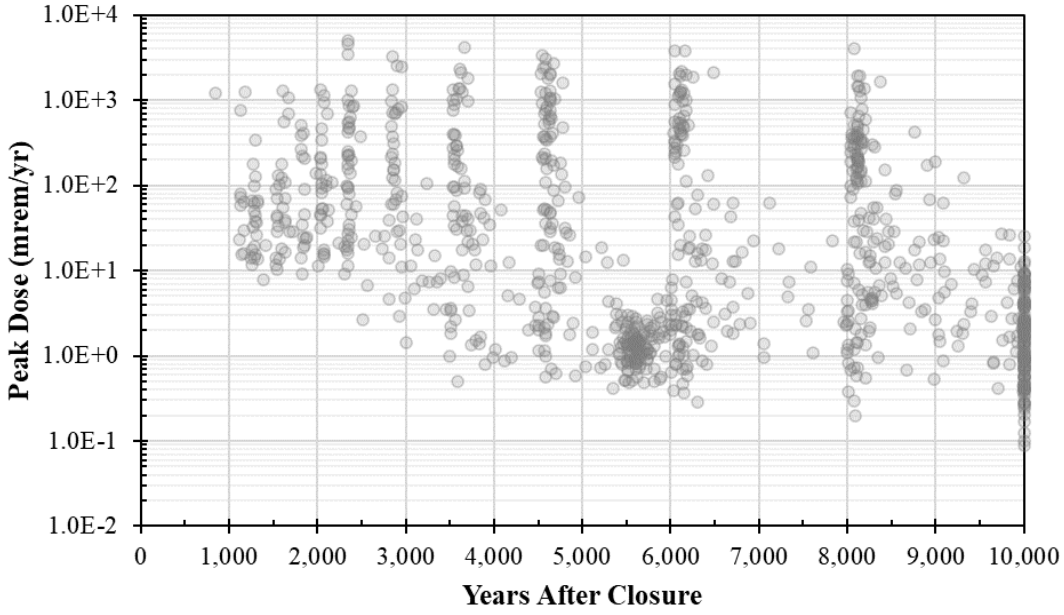

Figure 4.1-15: Peak Chronic IHI Doses at the 1-Meter Well from RSI-1 Based on HDPE Failure Condition

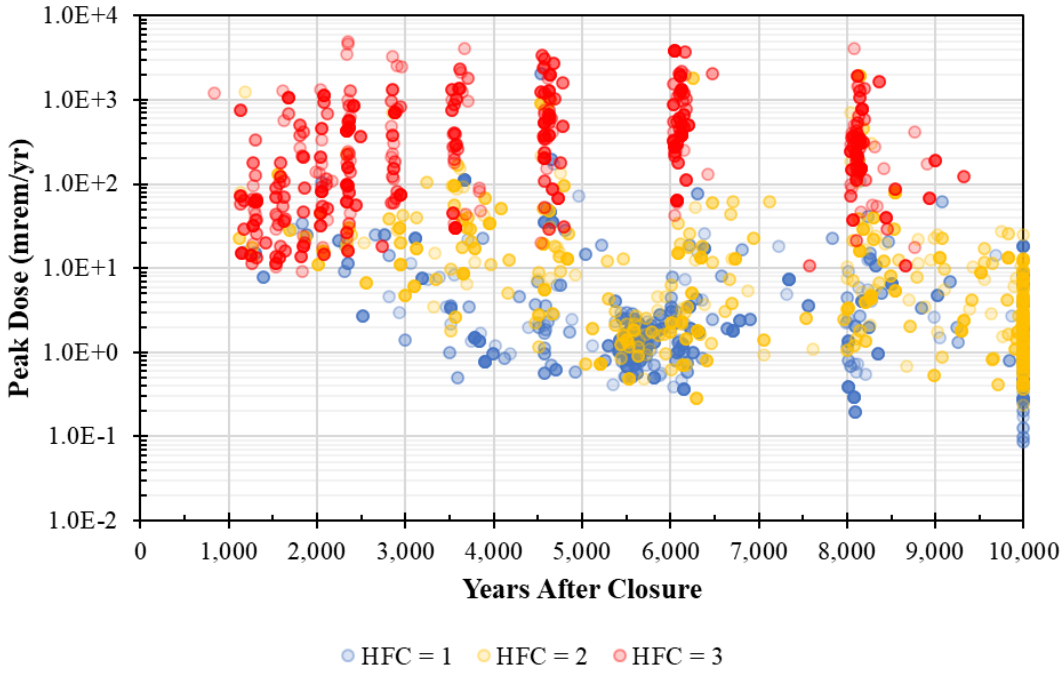

Note: HFC = HDPE failure condition: 1 = No HDPE Failure; 2 = Partial HDPE Failure; and 3 = Complete HDPE Failure.

Table 4.1-3 provides a summary of these peak Chronic IHI doses for both the Compliance Period and the Performance Period, as well as a summary based on each of the sampled HFC values.

Table 4.1-3: Statistics of Peak Chronic IHI Doses at the 1-Meter Well from RSI-1

Statistic	All Realizations	HDPE Failure Condition = 1	HDPE Failure Condition = 2	HDPE Failure Condition = 3
Count	**1,000**	**333**	**334**	**333**
Within the 1,000-Year Compliance Period				
Mean	3.8	0.26	0.33	11
Geometric Mean	**0.038**	**0.020**	**0.021**	**0.12**
Maximum	1,211	31	37	1,211
95th Percentile	12	0.32	0.36	34
75th Percentile	0.052	0.034	0.033	0.39
Median	**0.021**	**0.016**	**0.018**	**0.036**
25th Percentile	0.010	0.008	0.009	0.015
5th Percentile	0.004	0.003	0.003	0.007
Minimum	0.001	0.001	0.001	0.001
Within the 10,000-Year Performance Period				
Mean	206	13	46	559
Geometric Mean	**15**	**2.2**	**6.6**	**225**
Maximum	4,978	2,046	1,926	4,978
95th Percentile	1,231	27	141	2,149
75th Percentile	110	4.0	18	682
Median	**11**	**1.7**	**5.5**	**242**
25th Percentile	1.7	0.91	1.8	72
5th Percentile	0.57	0.39	0.70	18
Minimum	0.088	0.088	0.24	9.3

Figure 4.1-16 shows the statistical time history of the total dose to the MOP from the RSI-1 Model (*SRS Saltstone RSI-1 v1.000.gsm*). As with the MOP doses, these IHI doses exhibit significant variability. Despite this spread, and despite making a number of modeling decisions designed to emphasize the potential risks associated with various uncertainties, the 95th percentile dose result (purple dashed curve) peaks at 9.7 mrem/yr within the 1,000-year Compliance Period and 551 mrem/yr within the 10,000-year Performance Period.

Figure 4.1-16: Statistical Time History of the Chronic IHI Dose from RSI-1

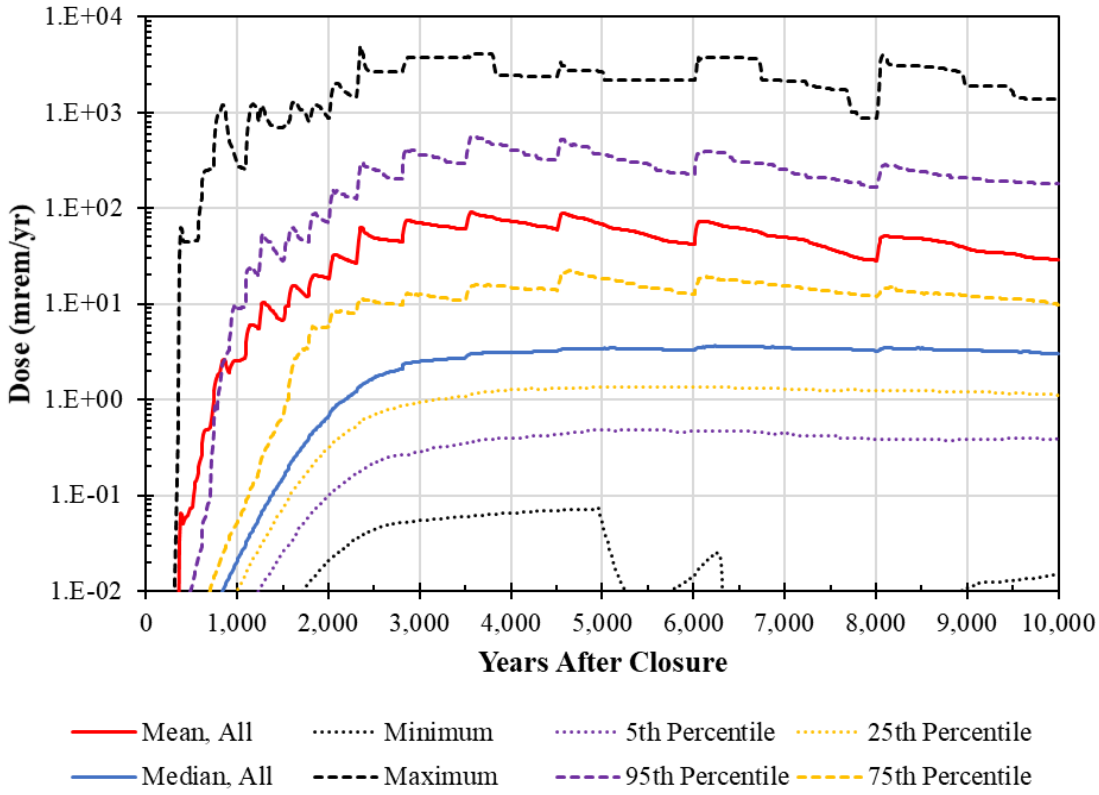

It is recognized that the mean dose (red curve) is skewed toward higher values due to the influence of a small number of realizations with extremely high doses. The mean dose generally falls midway between the 75th percentile (gold dashed curve) and the 95th percentile (purple dashed curve). For additional perspective, Figure 4.1-17 is identical to Figure 4.1-16, except that the arithmetic mean has been replaced with a geometric mean (dark red curve); this provides a more reasonable representation of the central tendency of these dose results. The geometric mean has a peak dose of 6.2 mrem/yr at 4,610 years after SDF closure.

Figure 4.1-17: Statistical Time History of the Chronic IHI Dose from RSI-1, Using the Geometric Mean Instead of the Arithmetic Mean

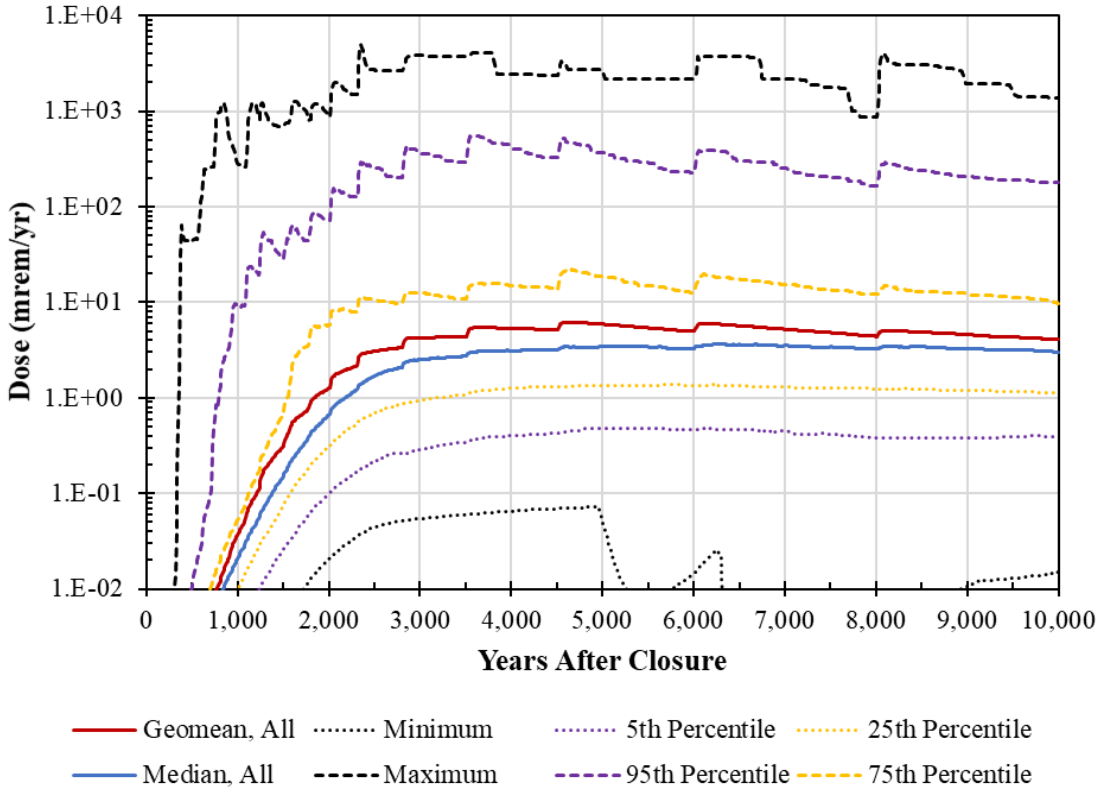

Table 4.1-4 provides a summary of the peaks for selected statistical values along these time histories. Note that HFC = 2 (partial failure condition for the HDPE) is expected to be the most likely and reasonable future condition.

Table 4.1-4: Peaks of the Statistics for the Chronic IHI Doses at the 1-Meter Well from RSI-1

Evaluated Endpoints	Peak of the Arithmetic Means		Peak of the Geometric Means		Peak of the Medians (50th Percentile)		Peak of the 95th Percentiles	
	Peak Dose (mrem/yr)	Time (yrs)	Peak Dose (mrem/yr)	Time (yrs)	Peak Dose (mrem/yr)	Time (yrs)	Peak Dose (mrem/yr)	Time (yrs)
Within the 1,000-Year Compliance Period								
Total MOP Dose (All)	2.6	850	0.037	1,000	0.021	1,000	9.7	990
Total MOP Dose for HFC = 1 (No Failure)	0.26	1,000	0.020	1,000	0.016	1,000	0.32	1,000
Total MOP Dose for HFC = 2 (Partial Failure)	0.33	1,000	0.021	1,000	0.018	1,000	0.36	1,000
Total MOP Dose for HFC = 3 (Complete Failure)	7.6	850	0.12	1,000	0.036	1,000	30	980
Within the 10,000-Year Performance Period								
Total MOP Dose (All)	90	3,570	6.2	4,610	3.6	6,240	551	3,620
Total MOP Dose for HFC = 1 (No Failure)	10.6	4,670	1.7	6,490	1.5	6,520	18	6,990
Total MOP Dose for HFC = 2 (Partial Failure)	24	4,680	4.0	8,330	3.5	8,110	63	8,210
Total MOP Dose for HFC = 3 (Complete Failure)	241	3,570	43	4,590	42	4,670	1,208	3,610

Next, Figure 4.1-18 shows that by simulating releases from only SDU 9, the (arithmetic) mean doses at IHI Well 4 dominate for the entire simulation. As a result, this well and the 1-Meter Well are identical. All of the other IHI Wells only exhibit doses due to contributions from seepline activities (fish ingestion, swimming, boating, etc.). This result may be compared to Figure 6.6-5 of the SDF PA (SRR-CWDA-2019-00001).

Figure 4.1-18: Mean Doses to the Chronic IHI for Each IHI Well from RSI-1

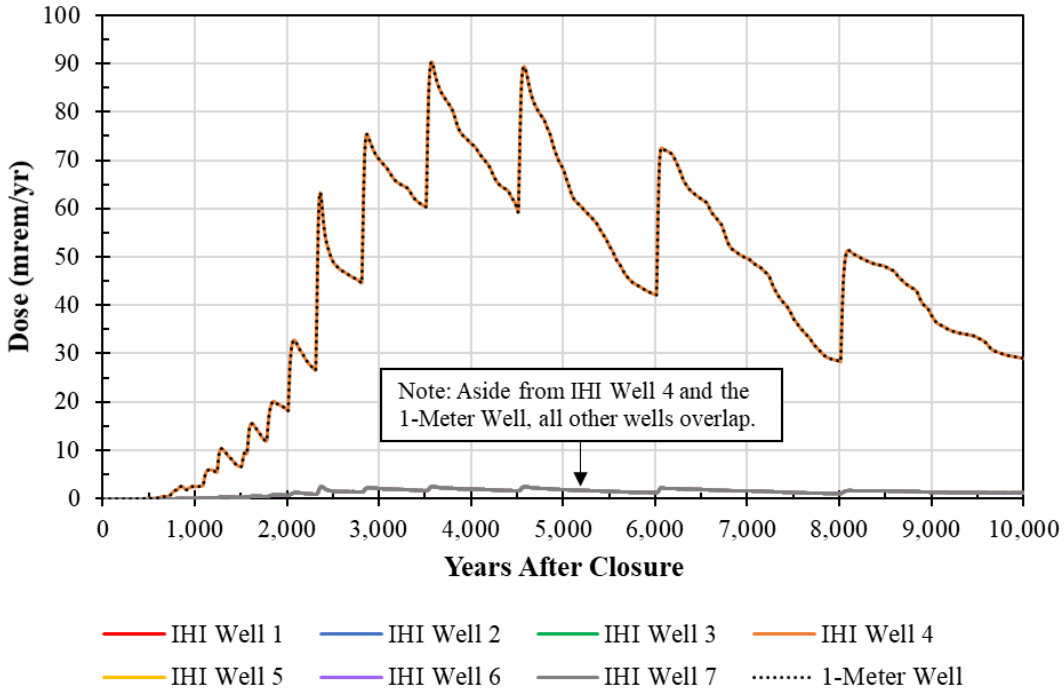

4.2 Probabilistic Sensitivity Analysis of the RSI-1 Model Results

This section presents probabilistic sensitivity analysis results for the doses from the RSI-1 Model (*SRS Saltstone RSI-1 v1.000.gsm*). These sensitivity analyses include partially ranked correlation coefficients (PRCCs) and stepwise ranked regression coefficients (SRRCs), which are statistical measures used to identify the parameters with the greatest influence over selected dose results. Refer to Appendix C for an introduction to PRCC and SRRC analyses. Section 4.2.1 provides the sensitivity analysis for the total dose to the MOP for all 1,000 realizations, Section 4.2.2 provides the sensitivity analysis for the total dose to the MOP for the 334 realizations with partial failure of the HDPE, and Section 4.2.3 provides the sensitivity analysis for the Chronic IHI dose for all 1,000 realizations.

4.2.1 Probabilistic Sensitivity Analysis of Total Doses to the MOP from the RSI-1 Model for All 1,000 Realizations

The top ten PRCCs for the total dose to the MOP are depicted in Figure 4.2-1. These PRCC results show that within the first 1,000 years, the SDU 9 vadose zone thickness (orange curve) is the most dominant parameter influencing the uncertainty in the system, with a PRCC of -0.75. This is consistent with equivalent findings in the SDF PA (see Figure 5.7-10 of SRR-CWDA-2019-00001). After the first 1,000 years, the HFC (red curve) becomes the dominant parameter, with a PRCC of +0.72. This is consistent with equivalent findings in Figure 6.2-1 of SRR-CWDA-2021-00040 and in Figure 6.2-1 of SRR-CWDA-2021-00056, which indicated that the sampled HFC influences the infiltration rates and the saltstone degradation rates.

Figure 4.2-1: Top Ten PRCCs for the Total MOP Dose Results of RSI-1

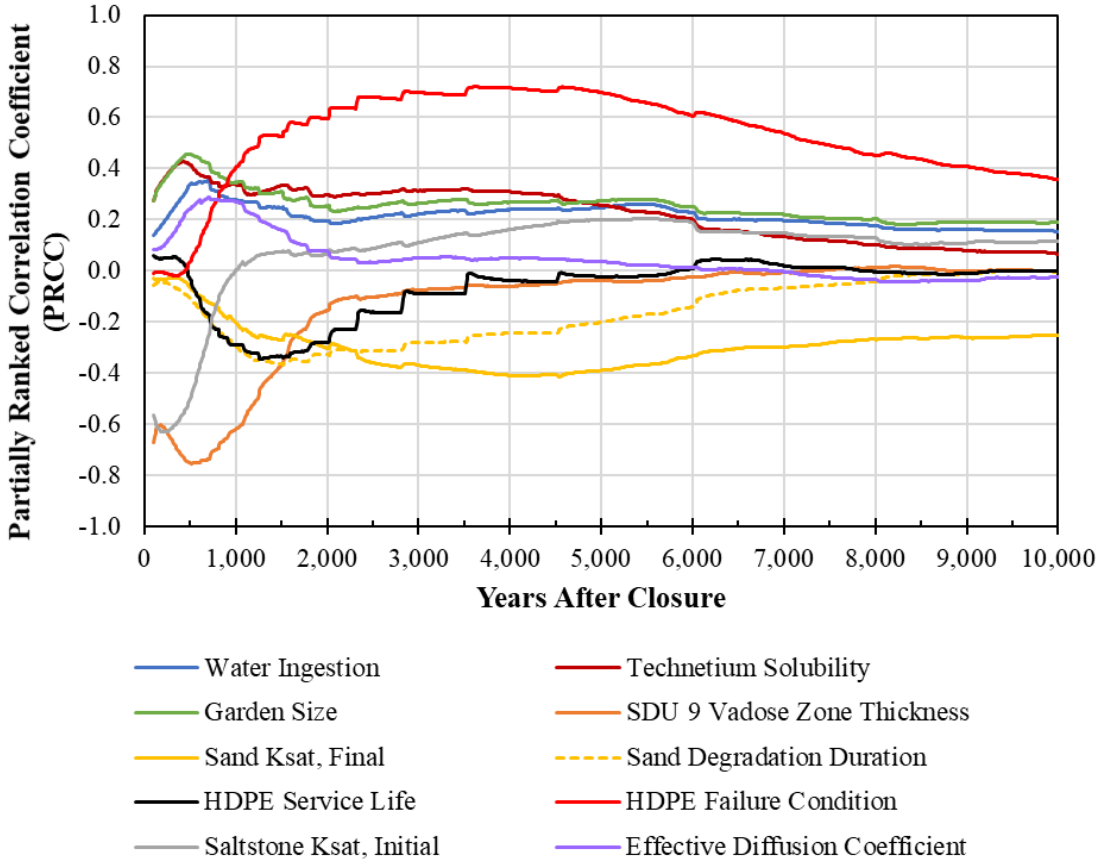

These PRCC results also indicate that releases from the system are initially dominated by diffusion, then later by advection. This is evidenced by the effective diffusion coefficient (purple curve), which peaks within 1,000 years, then decreases to a nearly negligible influence. Similarly, the initial saltstone K_{sat} (gray curve) is initially negative (with a value of less than -0.6), which then transitions to a positive value at approximately 1,000 years. This indicates that when the system is diffusion-dominated, a lower saltstone K_{sat} value would promote greater doses because it is less likely that any contaminants which are released would diffuse back into the saltstone whereas a higher saltstone K_{sat} value may allow for some degree of backwards diffusion. Once the HDPE reaches the end of its service life (black curve), infiltration rates and flow rates increase such that the releases become dominated by advection, at which point a higher saltstone K_{sat} value would promote higher doses.

Table 4.2-1 shows the results from the stepwise regression analysis for the total dose to the MOP. This table only shows the first eight variables from the SRRC analysis of the RSI-1 Model parameters. The importance of each variable quickly diminishes with each successive analysis step. In this analysis, the first three or four variables effectively dominate any influence over the dependent variable (e.g., total dose to the MOP) at the time analyzed. For this SRRC analysis, the doses were analyzed at 1,000 and 4,700 years. These results are similar to the PRCC results.

Table 4.2-1: Top Eight SRRC Results for the Total MOP Dose Results of RSI-1

Time = 1,000 Years, Cumulative R^2 = 0.651			Time = 4,700 Years [a], Cumulative R^2 = 0.673		
Variable	**Cumulative R^2**	**SRRC**	**Variable**	**Cumulative R^2**	**SRRC**
SDU 9 Vadose Zone Thickness	0.2186	-0.4807	HDPE Failure Condition	0.3858	0.5971
HDPE Failure Condition	0.2951	0.2687	Sand K_{sat}, Final	0.4528	-0.2613
Garden Size	0.3455	0.2250	Technetium Solubility	0.4794	0.1680
Technetium Solubility	0.3931	0.2162	Garden Size	0.5051	0.1637
Water Ingestion Rate	0.4243	0.1750	*p*-Averaging Term	0.5293	0.1415
Sand Degradation Duration	0.452	-0.1831	GCL K_{sat}, Initial	0.5515	0.1620
Effective Diffusion Coefficient (D_{eff})	0.4784	0.1692	Water Ingestion Rate	0.5699	0.1421
HDPE Service Life	0.5048	-0.1830	Sand Degradation Duration	0.5843	-0.1275

Notes: (a) 4,700 years was used because the peak of the geometric mean occurs at 4,630 years (see Table 4.1-2), and this value was rounded up to the nearest 100-year value.

4.2.2 Probabilistic Sensitivity Analysis Results from the RSI-1 Model for 334 Realizations wherein the HDPE Applied the Partial Failure Condition

Given the significance of the HFC, and the greater likelihood that failure of the HDPE will be gradual and/or localized, this subsection is provided to offer additional insights relative to the 334 realizations from the RSI-1 Model (*SRS Saltstone RSI-1 v1.000.gsm*) wherein the partial failure condition (HFC = 2) was sampled.

The top ten PRCCs for the total dose to the MOP (for realizations with partial failure of the HDPE) are depicted in Figure 4.2-2. In general, these results are similar to those presented in Figure 4.2-1. However, by removing the influence of the HFC, the HDPE service life no longer shows up as one of the top ten parameters. Instead, the final sand K_{sat} (in the LLDL) (solid gold curve) and the duration of the sand degradation (dashed gold curve) become more important. For both of these parameters, lower values are expected to result in higher dose results because higher values would lead to greater lateral drainage (i.e., more water would shed away from the SDU). Additionally, the GCL parameters (magenta curves) now show up as important parameters.

With respect to the importance of the sand conditions, it is noted that all of the RSI-1 realizations assume that the sand will undergo silting-in (i.e., clays and other fines will migrate from the overlying backfill and into the sand), resulting in long-term changes to the material properties of the sand. While this process might be plausible, it is not expected as there is little evidence of such a process occurring in natural systems. Regardless, it has been explicitly included in the RSI analyses to address questions raised by the NRC (ML20254A003).

If silting-in of the sand does not occur (as is expected), the infiltration rates and flow rates into the vadose zone will remain relatively low and greater lateral drainage above the SDUs would occur. Under such conditions, the doses are expected to be lower than those modeled in this analysis. Also, removing the influence of the sand conditions would likely promote the importance of the GCL parameters relative to those shown in Figure 4.2-2.

Figure 4.2-2: Top Ten PRCCs for the Total MOP Dose Results of RSI-1 for Realizations with Partial Failure of the HDPE

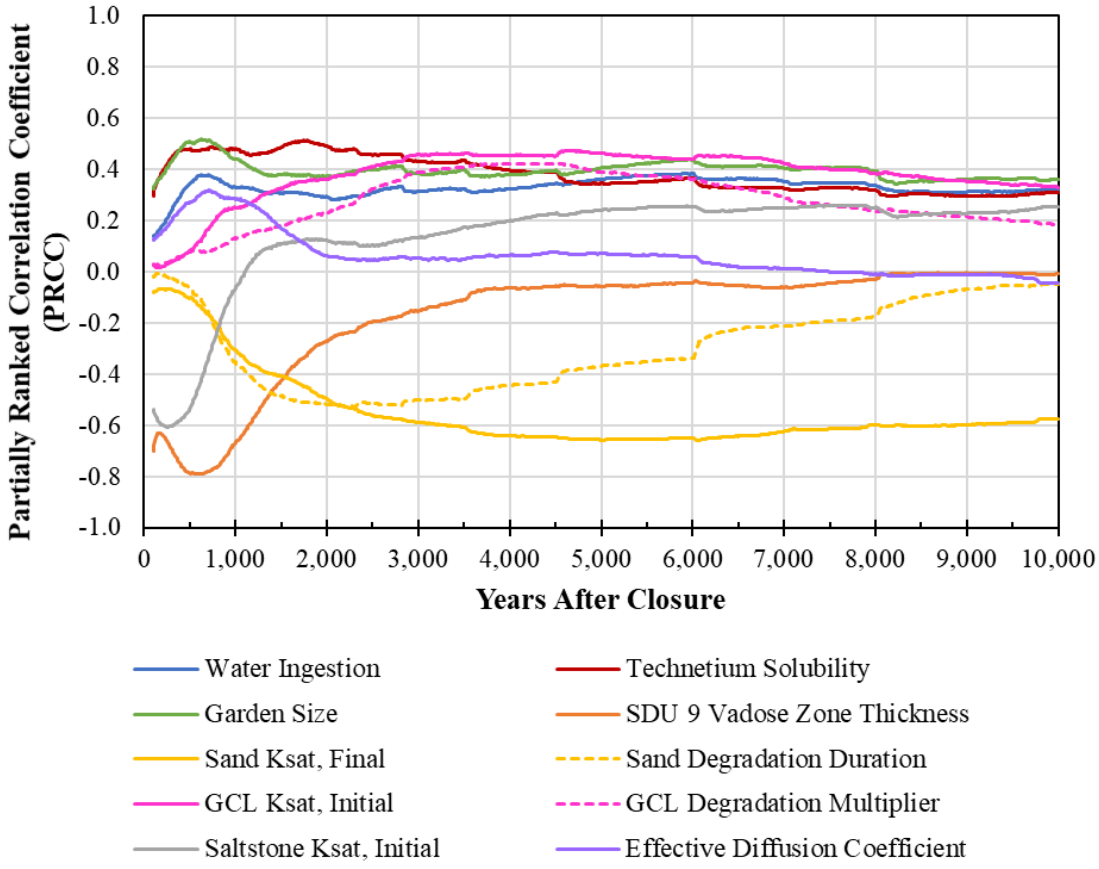

Table 4.2-2 shows the results from the stepwise regression analysis for the total dose to the MOP for those realizations wherein the partial failure condition of the HDPE was sampled. This table only shows the first eight variables. In this analysis, the first three or four variables effectively dominate any influence over the dependent variable (e.g., total dose to the MOP) at the time analyzed. For this SRRC analysis, the doses were analyzed at 1,000 and 4,700 years. These results are similar to the PRCC results and to the results from the analysis of the full suite of realizations (see Table 4.2-1).

Table 4.2-2: Top Eight SRRC Results for the Total MOP Dose Results of RSI-1 for Realizations with Partial Failure of the HDPE

Time = 1,000 Years, Cumulative R^2 = 0.709			Time = 4,700 Years [a], Cumulative R^2 = 0.711		
Variable	**Cumulative R^2**	**SRRC**	**Variable**	**Cumulative R^2**	**SRRC**
SDU 9 Vadose Zone Thickness	0.2682	-0.5126	Sand K_{sat}, Final	0.2349	-0.4984
Garden Size	0.3477	0.2859	GCL Degradation Multiplier	0.3141	0.2723
Technetium Solubility	0.4340	0.3116	GCL K_{sat}, Initial	0.3782	0.2974
Water Ingestion Rate	0.468	0.2017	Sand Degradation Duration	0.4334	-0.2595
Sand Degradation Duration	0.4974	-0.2055	Garden Size	0.4734	0.2524
Effective Diffusion Coefficient (D_{eff})	0.5195	0.1794	Water Ingestion Rate	0.5145	0.1827
GCL K_{sat}, Initial	0.5425	0.1596	Technetium Solubility	0.5459	0.2293
Irrigation Rate	0.5638	0.1355	Initial HDPE Defects per Hectare	0.5780	0.1783

Notes: (a) 4,700 years was used to be consistent with Table 4.2-1.

4.2.3 Probabilistic Sensitivity Analysis of Chronic IHI Doses from the RSI-1 Model for All 1,000 Realizations

The top ten PRCCs for the Chronic IHI doses are depicted in Figure 4.2-3. These results are nearly identical to analysis of the total doses to the MOP shown in Figure 4.2-1. The agreement between these two figures is expected given that the Chronic IHI dose is strongly influenced by ground water concentrations (see Section 6.4.2 of the SDF PA (SRR-CWDA-2019-00001)). Similarly, the SRRC results shown in Table 4.2-3 are very similar to those from Table 4.2-1. These results are complimentary of the PRCC analyses, showing that within 1,000 years the SDU 9 vadose zone thickness is most important and beyond 1,000 years, the HFC becomes most important.

Figure 4.2-3: Top Ten PRCCs for the Chronic IHI Dose Results of RSI-1

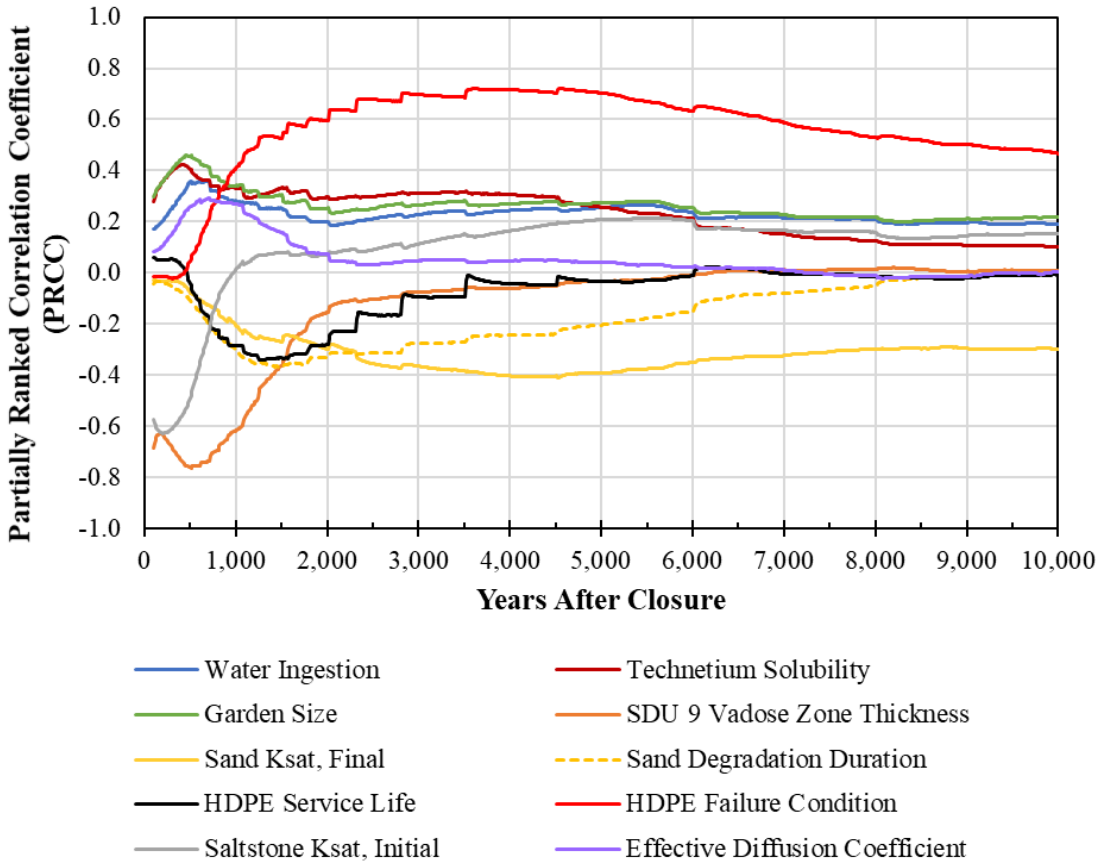

Table 4.2-3: Top Eight SRRC Results for the Chronic IHI Dose Results of RSI-1

Time = 1,000 Years, Cumulative R^2 = 0.653			Time = 4,700 Years [a], Cumulative R^2 = 0.676		
Variable	**Cumulative R^2**	**SRRC**	**Variable**	**Cumulative R^2**	**SRRC**
SDU 9 Vadose Zone Thickness	0.2159	-0.4775	HDPE Failure Condition	0.3858	0.5948
HDPE Failure Condition	0.2953	0.2739	Sand K_{sat}, Final	0.4533	-0.2577
Garden Size	0.3443	0.2198	Technetium Solubility	0.4797	0.1663
Technetium Solubility	0.3903	0.2131	Garden Size	0.5060	0.1681
Water Ingestion Rate	0.4218	0.1755	*p*-Averaging Term	0.5304	0.1435
Sand Degradation Duration	0.4504	-0.1895	GCL K_{sat}, Initial	0.5526	0.1607
Effective Diffusion Coefficient (D_{eff})	0.4768	0.1694	Water Ingestion Rate	0.5716	0.1455
HDPE Service Life	0.5029	-0.1795	Sand Degradation Duration	0.5860	-0.1276

Notes: (a) 4,700 years was used to be consistent with Table 4.2-1.

4.3 Analysis of RSI-5 Model (Relative Permeability = 1) Results

Section 3.7 described the setup for a 100-realization analysis developed to evaluate the impact from the SDF PA using MCCs rather than assuming a relative permeability of 1. As discussed in Appendix A, the DOE does not consider the use of a relative permeability of 1 to be a realistic representation of permeability under partially saturated conditions; however, this analysis was developed to be responsive to the request from the NRC.

Before discussing the results, a basis for comparison will be established based on the results from the RSI-1 model. Specifically, the results from *SRS Saltstone RSI-1 v1.000.gsm* were filtered to show only results from those realizations that were selected to support the RSI-5 analysis (see Table 3.7-1). Using only the 100 selected realizations from the RSI-1 Model, the statistical time history of the results appears as shown in Figure 4.3-1. The mean and median values from this set of selected realizations are similar in magnitude to the mean and median values from the complete set of 1,000 realizations shown in Figure 4.1-3. Comparing Figure 4.3-1 to Figure 4.1-3 establishes that the 100 selected realizations identified in Table 3.7-1 provides a reasonable sample set for analysis.

Figure 4.3-1: Statistical Time History of the Total Dose to the MOP Using Only 100 Selected Realizations from RSI-1

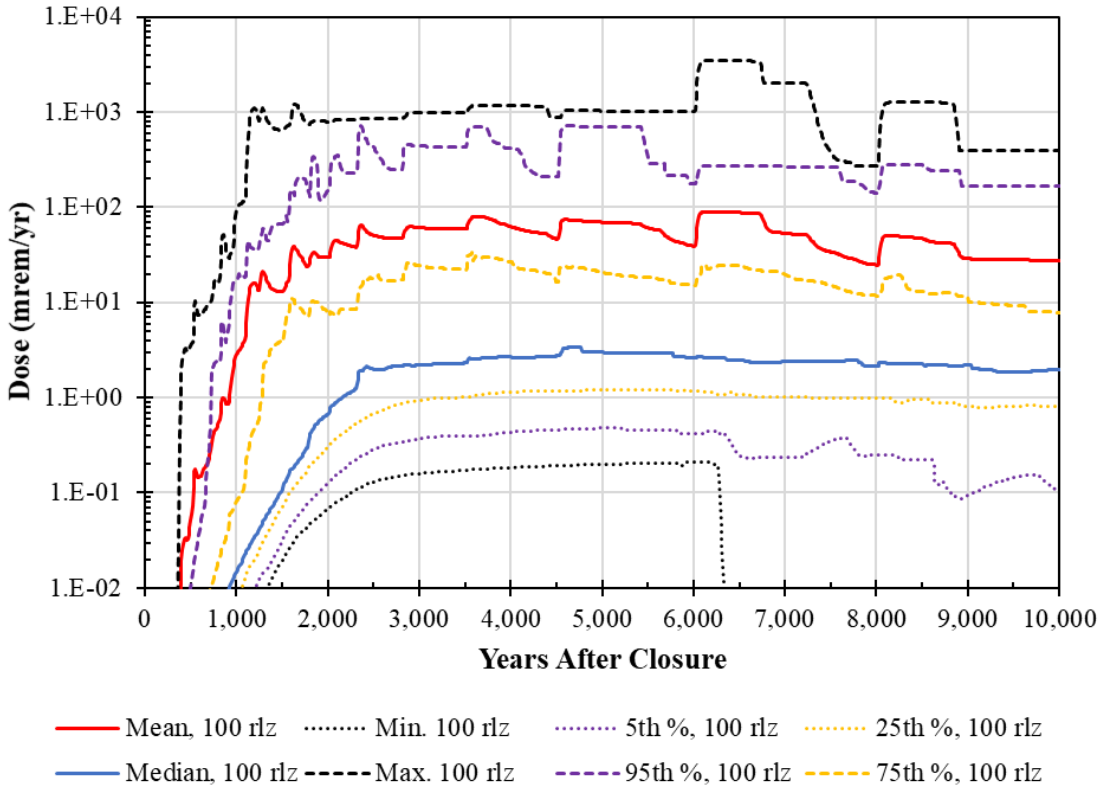

Next, the 100 selected realizations were modeled in the Vadose Zone Flow Model and the Vadose Zone Transport Model, using the exact same settings at the RSI-1 analysis, except that instead of applying the MCCs, a relative permeability of 1 was assumed for all the cementitious materials

(i.e., SDU concretes and saltstone). This model is hereafter referred to as the RSI-5 Model. The resulting statistical time history is shown in Figure 4.3-2. These results are very similar to those shown in Figure 4.3-1. To better illustrate this similarity, Figure 4.3-3 is provided to show both sets of time histories on a single figure. In Figure 4.3-3, the darker curves (labeled "100 rlz") show the time histories from Figure 4.3-1 and the lighter curves (labeled "RSI-5") show the time histories from Figure 4.3-2.

Figure 4.3-2: Statistical Time History of the Total Dose to the MOP from RSI-5

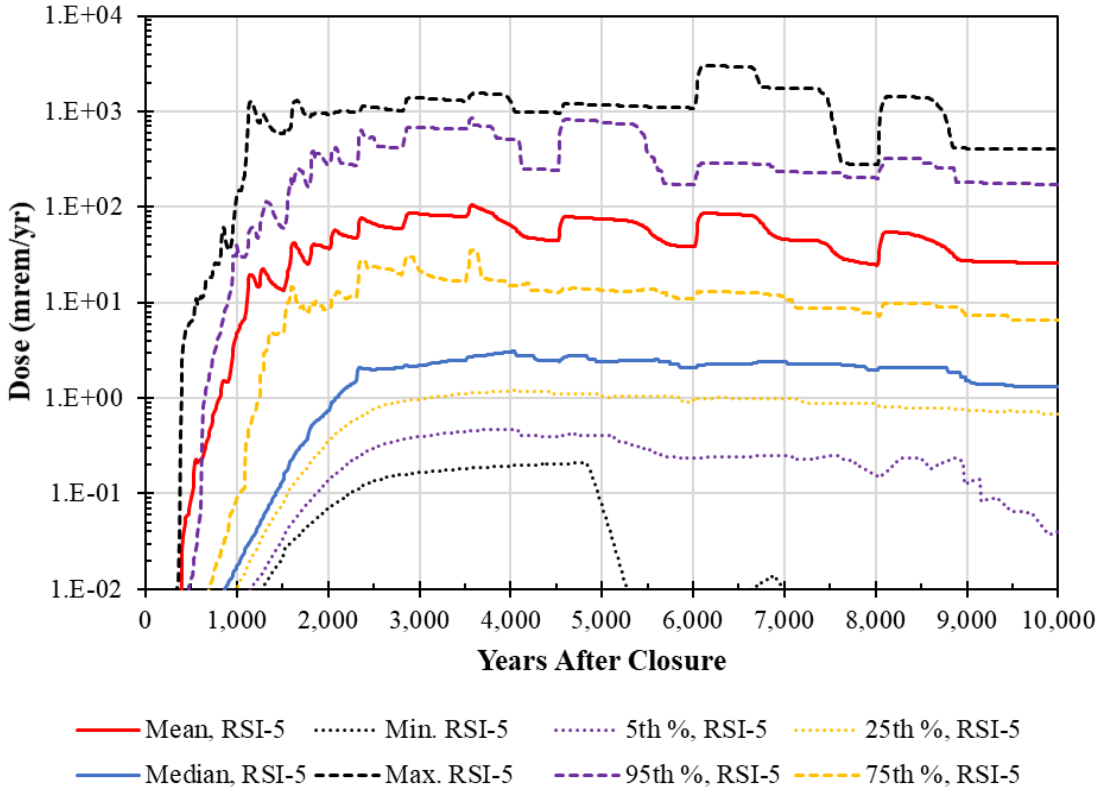

Figure 4.3-3: Comparison of the Statistical Time Histories of the Total Doses to the MOP from RSI-1 (Using 100 Selected Realizations) and RSI-5

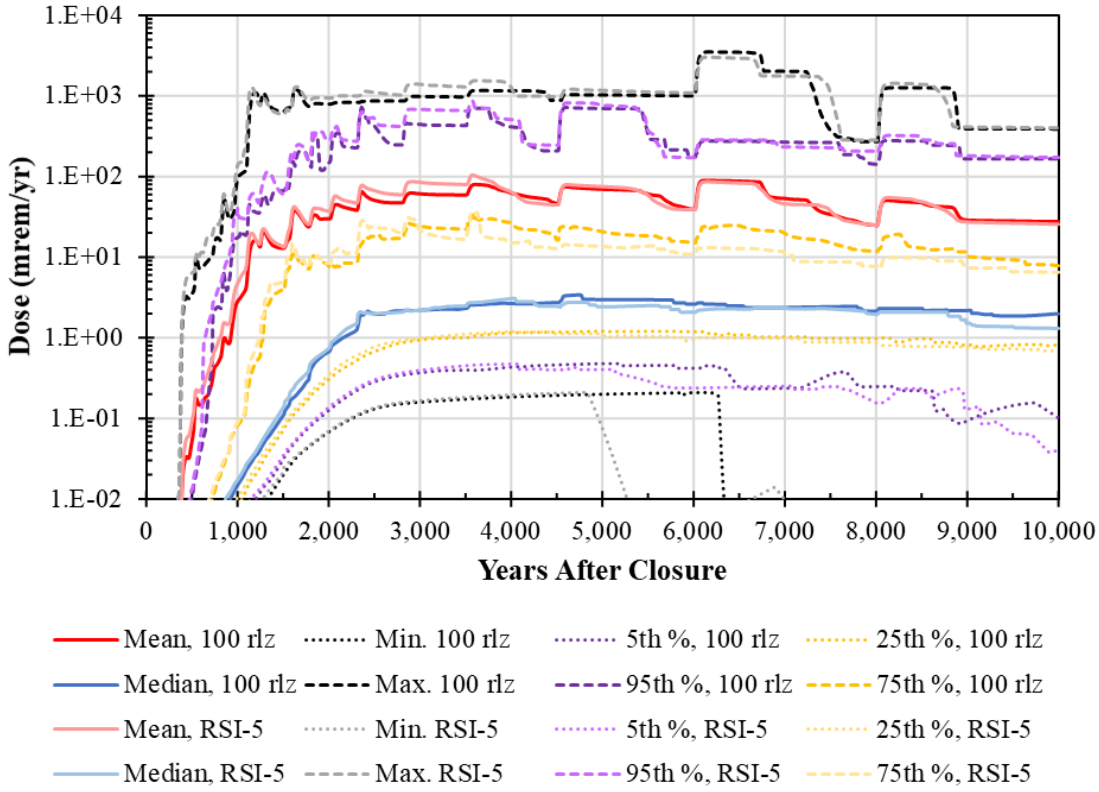

As an additional comparison, Figure 4.3-4 shows the peak MOP doses within 10,000 years from both models. The RSI-5 peak doses are plotted along the X-axis and the equivalent RSI-1 peak doses are plotted along the Y-axis. The solid black line crossing diagonally through the figure represents a 1-to-1 relationship: data points on this line represent peak doses of equal value between the two models. The dashed lines are provided as a guide to show where values would lie if they were different by an order of magnitude or more. As shown, all of the peak doses are relatively close to the 1-to-1 line, which confirms that the general impact from applying the MCCs (as opposed to assuming a relative permeability of 1) is relatively minor.

The biggest difference was observed for Realization #72 where the RSI-1 Model exhibited a peak dose of 181 mrem/yr and the RSI-5 Model exhibited a peak dose of 617 mrem/yr (i.e., a factor of 3.4 times larger). This factor of increase is not typical of most of the model results; on average, the RSI-5 dose peaks were only approximately 18% higher than the respective RSI-1 dose peaks.

Figure 4.3-4: Comparison of the Total MOP Dose Peaks within 10,000 Years from RSI-1 (Using 100 Selected Realizations) and RSI-5

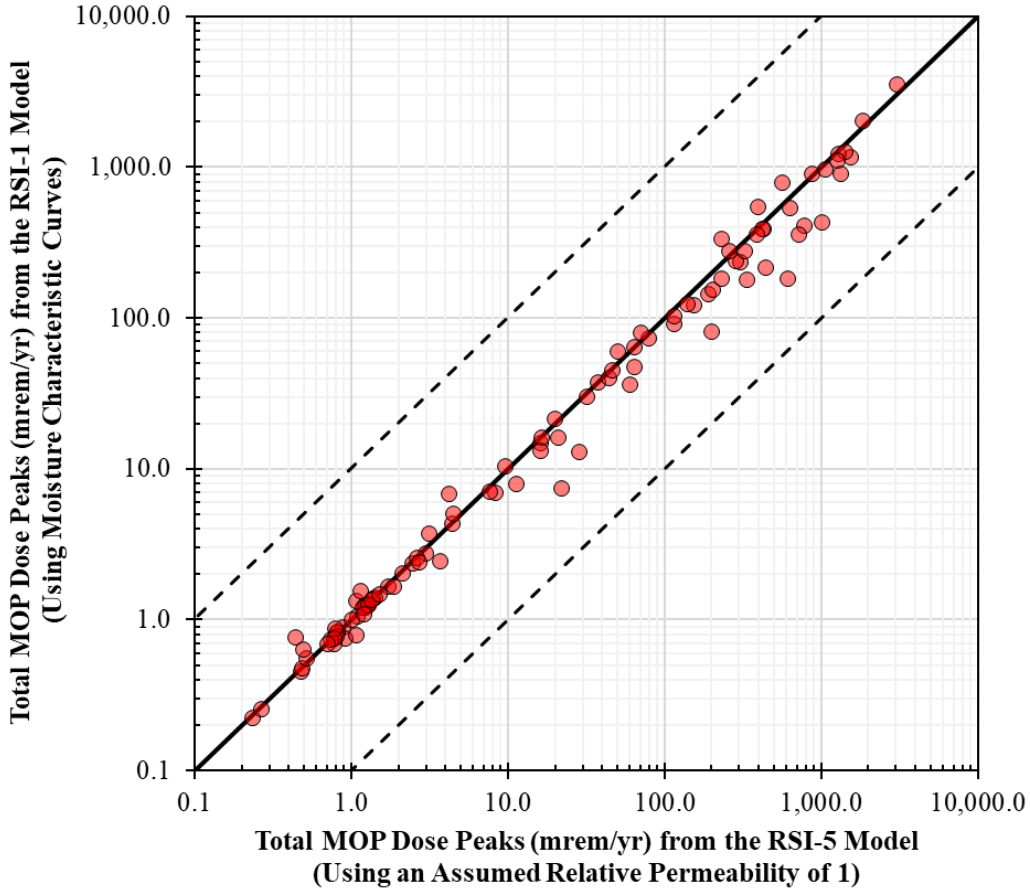

Next, an additional analysis was performed to also assume a relative permeability of 1 for all materials that are assigned the properties of gravel (water stops, joints, etc.). As with the RSI-5 Model, this analysis was limited to the 100 realizations selected in Table 3.7-1. Other than applying the assumed relative permeability of 1 to gravel, this model was identical in setup to the RSI-5 Model, so the model from this additional analysis is hereafter referred to as the RSI-5a Model.

Figure 4.3-5 is identical to Figure 4.3-3, except that the RSI-5 Model results have been replaced with the RSI-5a Model results. Similarly, Figure 4.3-6 is identical to Figure 4.3-4 except, again, the RSI-5 Model results have been replaced with the RSI-5a Model results. Comparisons of these figures indicate that applying a relative permeability of 1 to gravel has a negligible impact relative to the overall influence of cementitious materials.

Figure 4.3-5: Comparison of the Statistical Time Histories of the Total Doses to the MOP from RSI-1 (Using 100 Selected Realizations) and RSI-5a

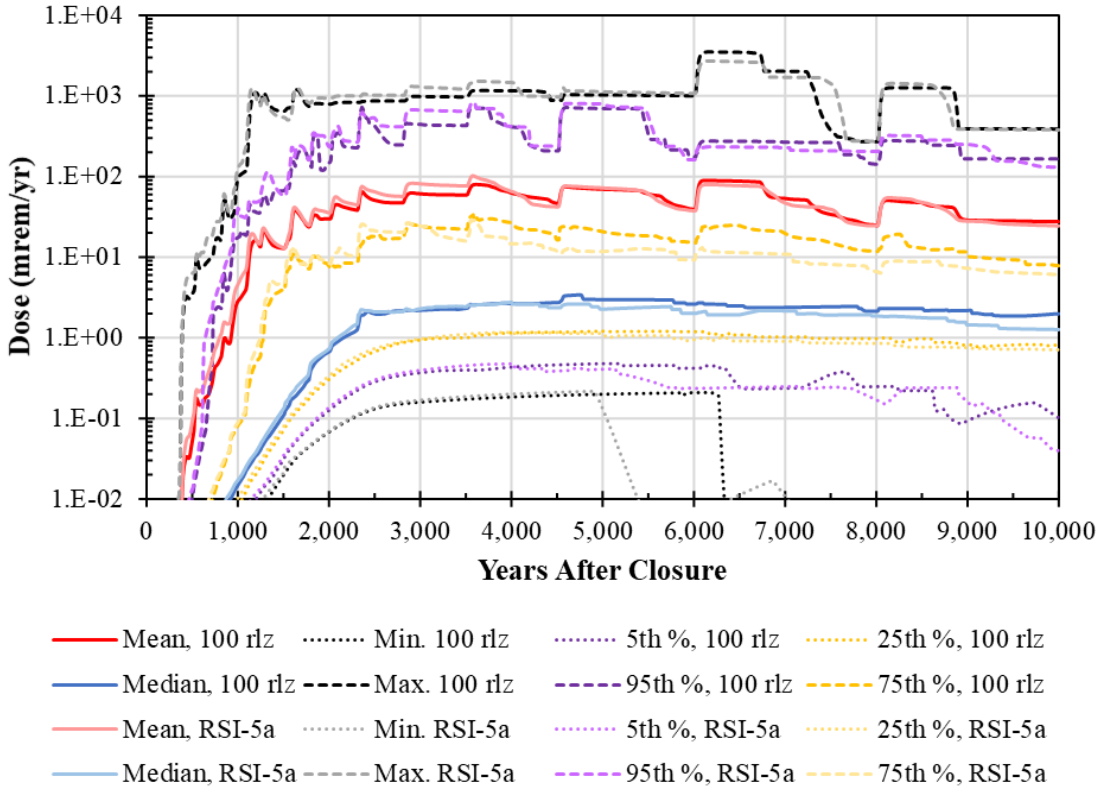

Figure 4.3-6: Comparison of the Total MOP Dose Peaks within 10,000 Years from RSI-1 (Using 100 Selected Realizations) and RSI-5a

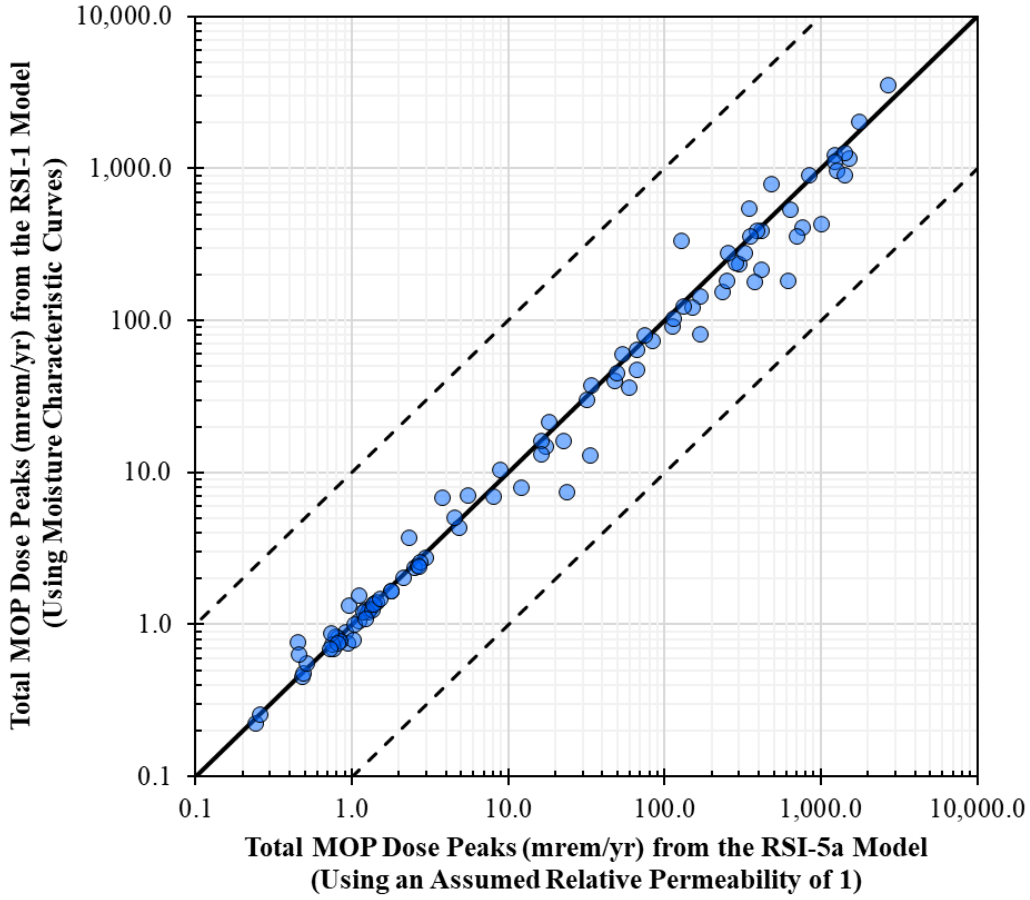

Table 4.3-1 provides a final comparison using the peaks from selected statistics from an analysis of the time histories. This table is similar to Table 4.1-2, except it focuses on providing values from the selected realizations. Note the comparisons of the arithmetic mean and 95th percentiles exaggerate the differences between the different model results as these statistics are driven by outlier realizations, especially given the limited selection of infiltration rates used. Alternatively, the geometric mean and the median provide reasonable comparisons of the central tendencies of the time histories. Over 10,000 years the RSI-1, the RSI-5, and the RSI-5a Models show peaks of the geometric means that are all near 6 mrem/yr and peaks of the medians that are all near 3 mrem/yr. When the relative permeability of 1 is applied to the cementitious materials only, the dose results are generally slightly higher than when the relative permeability of 1 is applied to both the cementitious materials and the materials that are assigned gravel properties (water stops, joints, etc.).

Table 4.3-1: Peaks of the Statistics for the Total Doses to the MOP at the 100-Meter Well from RSI-1, RSI-5, and RSI-5a

Evaluated Endpoints	Peak of the Arithmetic Means		Peak of the Geometric Means		Peak of the Medians (50th Percentile)		Peak of the 95th Percentiles	
	Peak Dose (mrem/yr)	Time (yrs)	Peak Dose (mrem/yr)	Time (yrs)	Peak Dose (mrem/yr)	Time (yrs)	Peak Dose (mrem/yr)	Time (yrs)
Within the 1,000-Year Compliance Period								
Total MOP Dose from RSI-1: MCCs applied (1,000 Realizations)	2.4	870	0.033	1,000	0.018	1,000	8.8	990
Total MOP Dose from RSI-1: MCCs applied (100 Selected Realizations)	2.8	1,000	0.044	1,000	0.015	1,000	17.5	1,000
Total MOP Dose from RSI-5: $k_r = 1$ assumed for cementitious materials	4.7	1,000	0.060	1,000	0.017	1,000	40.4	1,000
Total MOP Dose from RSI-5a: $k_r = 1$ assumed for cementitious materials and gravel	4.5	1,000	0.059	1,000	0.017	1,000	40.4	1,000
Within the 10,000-Year Performance Period								
Total MOP Dose from RSI-1: MCCs applied (1,000 Realizations)	85	3,590	5.8	4,630	3.3	6,320	516	3,640
Total MOP Dose from RSI-1: MCCs applied (100 Selected Realizations)	89	6,110	5.8	4,700	3.4	4,760	724	2,360
Total MOP Dose from RSI-5: $k_r = 1$ assumed for cementitious materials	104	3,580	6.3	3,590	3.1	4,040	861	3,580
Total MOP Dose from RSI-5a: $k_r = 1$ assumed for cementitious materials and gravel	102	3,580	6.0	3,590	2.8	4,000	833	3,590

Note: k_r = relative permeability.

These comparisons demonstrate that regardless of whether MCCs are applied or a relative permeability of 1 is assumed, the impact on the overall performance is relatively limited. This is consistent with similar conclusions provided in Section 5.8.8.3 of the SDF PA (SRR-CWDA-2019-00001).

4.4 Additional Analysis of Results

This section provides additional analyses and insights not previously discussed. Section 4.4.1 provides an analysis of peak doses, Section 4.4.2 presents the sampled parameter values from the three realizations with the highest peak doses, and Section 4.4.3 identifies which realizations will be used to satisfy RSI-6 (water balance data).

4.4.1 Additional Analysis of RSI-1 Model Peak Doses

This section provides additional analyses and insights related to the peak dose results from the RSI-1 Model. Because the Chronic IHI dose results are similar to the Total MOP dose results, the analyses in this section only uses the peak doses to the MOP.

Figure 4.1-2 in Section 4.1.1 showed the peak doses to the MOP with each data point colored based on the sampled HFC value, where red (HFC = 3) indicated a complete failure condition, gold (HFC = 2) indicated a partial failure condition, and blue (HFC = 1) indicated no failure (i.e., infiltration only occurs due to initial defects in the HDPE). Figure 4.4-1 is similar, except instead of showing the peaks over the entire 10,000-year simulation, these are the peak doses within the 1,000-year Compliance Period. Nearly all of the peaks occur at 1,000 years. For most of the realizations, the doses are only starting to climb during the early years of the simulation. Note that red HFC = 3 data points are obscuring the other results. In general, most of the blue HFC = 1 data points and gold HFC =2 data points fall between 1.0E-03 mrem/yr and 1.0E-01 mrem/yr.

Figure 4.4-1: Peak Total Doses to the MOP at the 100-Meter Well within 1,000 Years from RSI-1 Based on HDPE Failure Condition

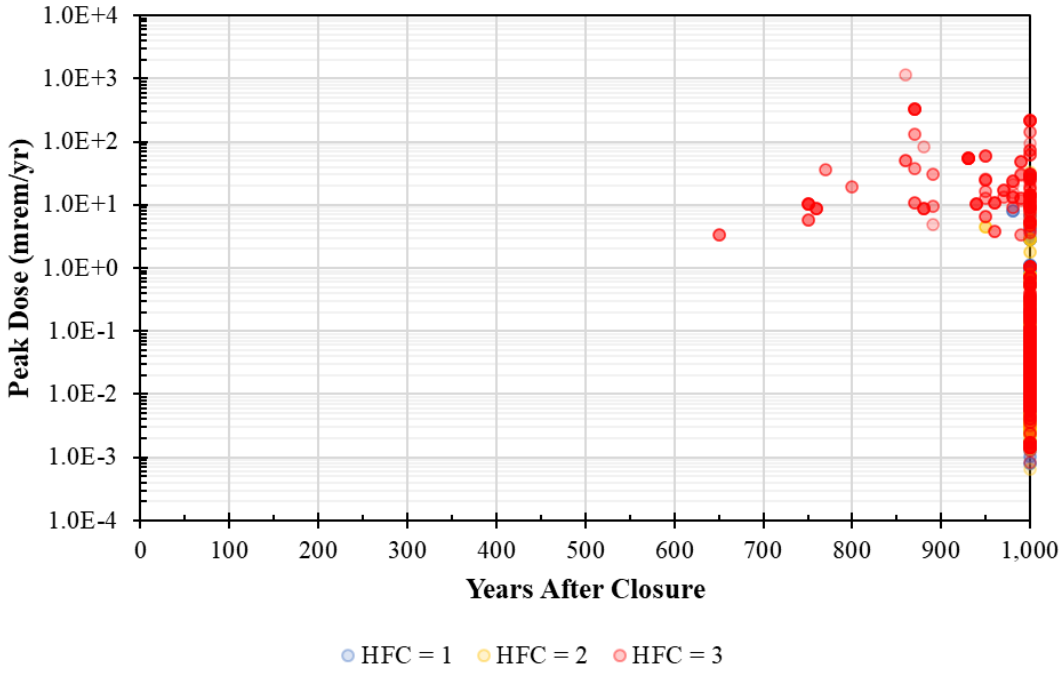

Note: HFC = HDPE failure condition: 1 = No HDPE Failure; 2 = Partial HDPE Failure; and 3 = Complete HDPE Failure.

Because most of the data points in Figure 4.4-1 fall along the 1,000-year axis, this presentation of the peak doses is not especially informative. As discussed in Section 4.2.1, within the first 1,000 years the SDU 9 vadose zone thickness is the dominant parameter influencing the uncertainty in the system. So as an alternative presentation of the peak doses, rather than using time (years after closure) for the X-Axis, Figure 4.4-2 uses the sampled vadose zone thickness of SDU 9. This figure is presented as four panels: (a) shows all three HFC values, (b) shows only HFC = 1, (c) shows only HFC = 2, and (d) shows only HFC = 3. All three HFC values exhibit similar behavior where

most of the peaks are clustered around the lower doses. In general, higher dose peaks occur when the lower SDU 9 vadose zone thicknesses were sampled and lower doses when the higher SDU 9 vadose zone thicknesses were sampled. This is expected because a thicker vadose zone means that contaminants must be transported over a greater distance before reaching the water table. Note that because Tc-99 fluxes were simulated with the Vadose Zone Transport Model and not as part of the contaminant transport simulated in the RSI-1 Model, Tc-99 doses are not sensitive to this parameter. If Tc-99 fluxes had been simulated using the sampled SDU 9 vadose zone thicknesses, the shape of this cluster would likely have been steeper.

Figure 4.4-2: Peak Total Doses to the MOP at the 100-Meter Well within 1,000 Years from RSI-1 Based on HDPE Failure Condition as a Function of SDU 9 Vadose Zone Thickness

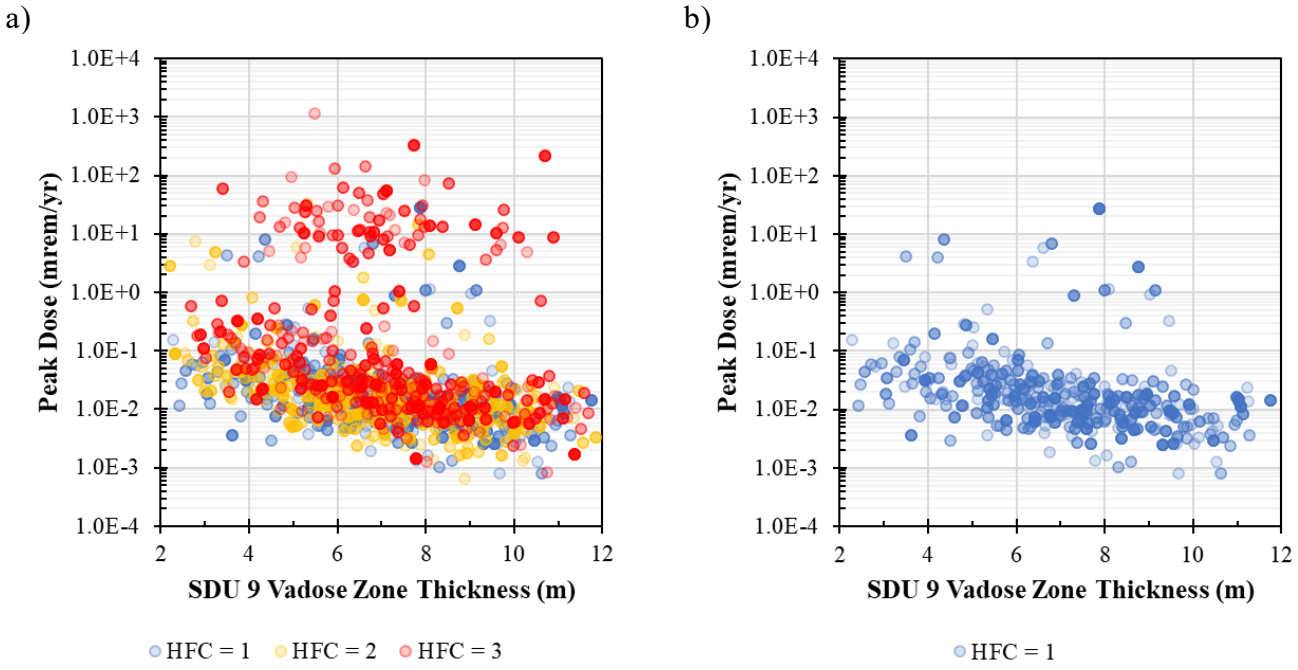

c)

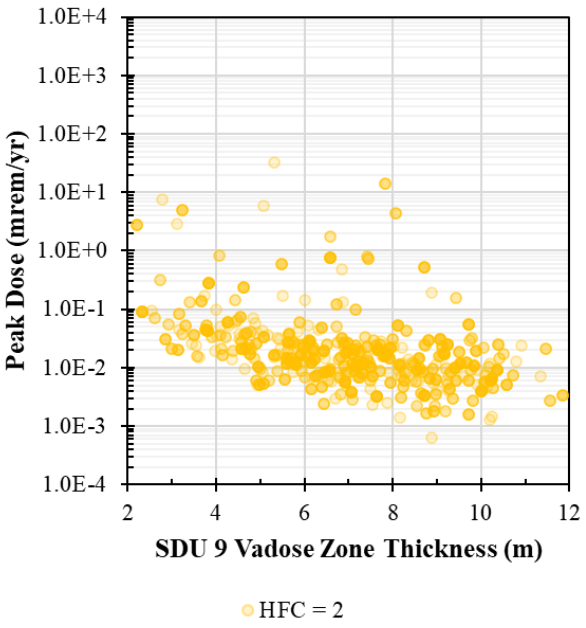

d)

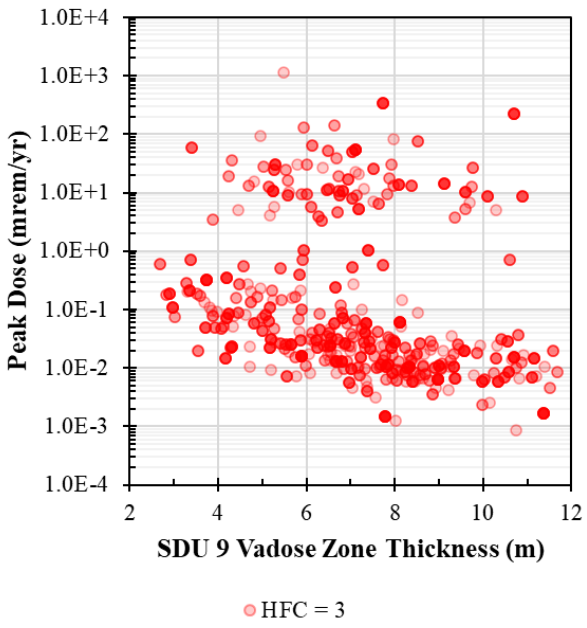

Note: HFC = HDPE failure condition: 1 = No HDPE Failure; 2 = Partial HDPE Failure; and 3 = Complete HDPE Failure.

In Figure 4.4-2(d), the peak doses associate with HFC = 3 has a second (but less dense) cluster of peaks with significantly higher doses. The other HFC samples also have a few of these higher peaks. These are dose peaks that are predominantly associated with realizations in which the HDPE service life was sampled to be less than 1,000 years. Figure 4.4-3 illustrates this. This figure shows the same data as the red (HFC = 3) data in Figure 4.4-2(d), but the data points have been re-colored based on whether or not the HDPE service life was sampled as greater than 1,000 years (magenta) or less than 1,000 years (dark red). This indicates that the timing of the HDPE failure can significantly influence the magnitudes of the doses.

Figure 4.4-3: Peak Total Doses to the MOP at the 100-Meter Well within 1,000 Years from RSI-1 for HFC = 3 as a Function of SDU 9 Vadose Zone Thickness and HDPE Service Life

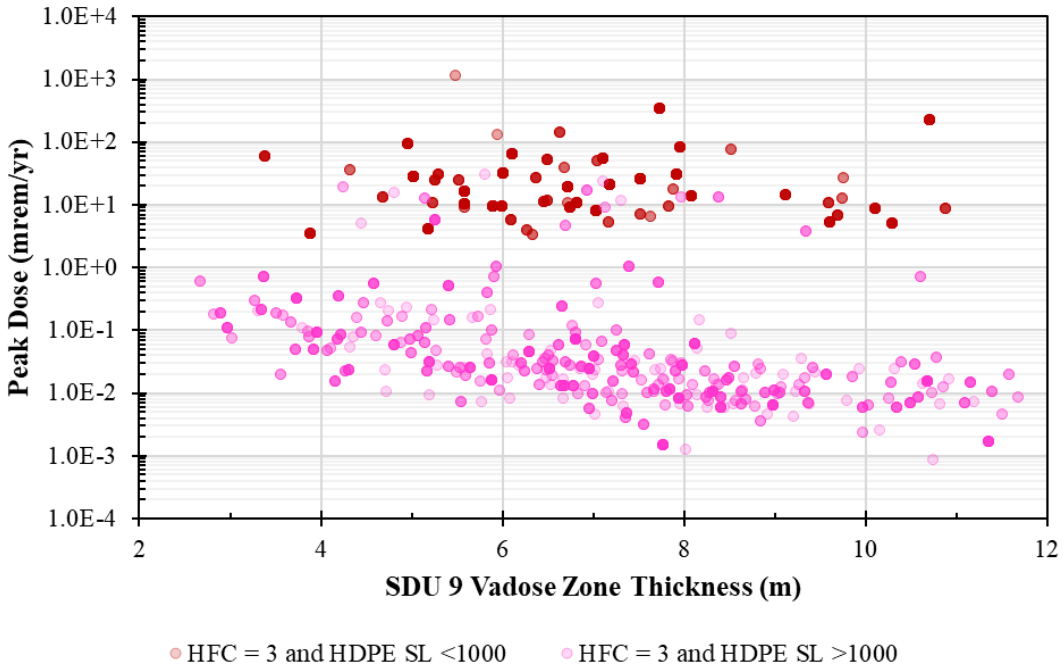

Note: HFC = HDPE failure condition: 3 = Complete HDPE Failure and SL = Service Life (years)

Based on this observation, it was postulated that the timing of the peak doses over 10,000 years would be correlated to the timing of the HDPE failures. To test this, Figure 4.1-2 from Section 4.1.1 was modified: instead of using the Y-Axis of the figure to show the peak doses, Figure 4.4-4 uses the Y-Axis to show the sampled HDPE service life. This figure shows that, for most realizations, the time of the peak dose occurs on or after the year of the HDPE service life. This is especially clear for HFC = 3 because for this HDPE failure condition, the infiltration rates and the SDU flows are both contingent on the sampled HDPE service life.

Figure 4.4-4: Peak Total Doses to the MOP at the 100-Meter Well within 1,000 Years from RSI-1 Based on HDPE Failure Condition

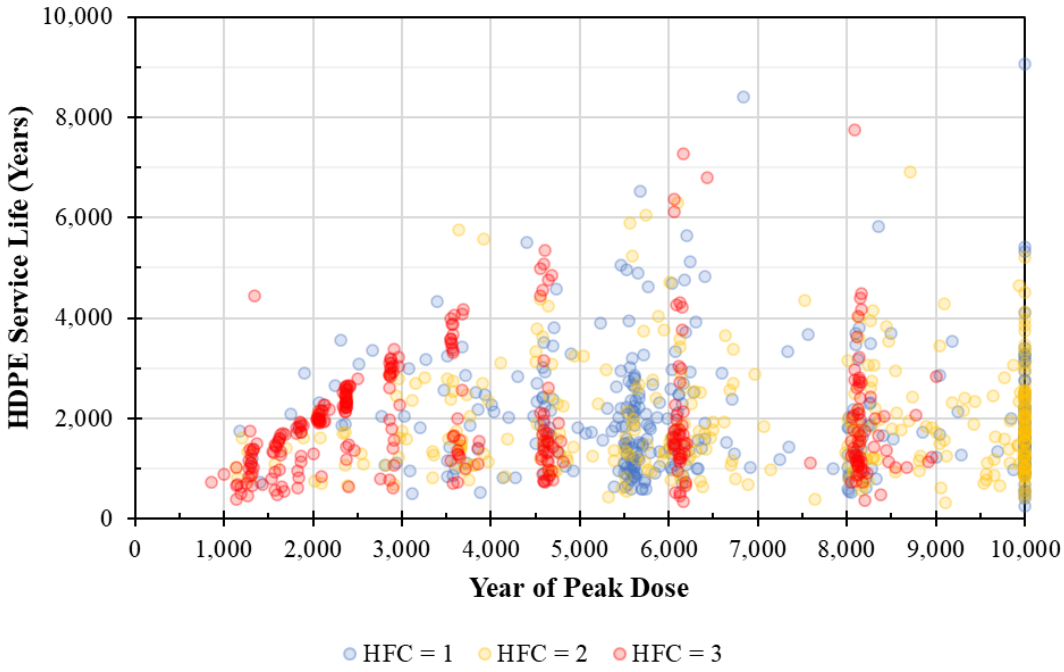

Just as Figure 4.4-2 modified the X-Axis of Figure 4.4-1 to use the SDU vadose zone thickness, Figure 4.4-5 modified Figure 4.1-2 to use the X-Axis to show the final K_{sat} of the sand in the LLDL because this was identified as a major influencing parameter in Section 4.2.1. As with Figure 4.4-2, Figure 4.4-5 is presented as four panels: (a) shows all three HFC values, (b) shows only HFC = 1, (c) shows only HFC = 2, and (d) shows only HFC = 3. Here we see that when the no failure conditions (blue, HFC = 1) and the partial failure condition (gold, HFC = 2) are sampled, the final sand K_{sat} has a strong influence on the resulting magnitude of the dose peaks: most realizations with peak doses greater than 10 mrem/yr have final sand K_{sat} values of less than 1.0E-02 cm/s.

Figure 4.4-5(d) also shows that when the complete failure condition (red, HFC = 3) is sampled, the peak doses are higher, but there appears to be no influence from the sampled final sand K_{sat}. However, while the magnitude of these dose peaks is generally higher than the other HFC values, the relative range of variability for these dose peaks is smaller. For HFC = 1 and HFC = 2, the dose peaks generally spanned a range of three to four orders of magnitude, while the HFC = 3 dose peaks varied over less than three orders of magnitude. This range of variability is closer to the range of variability presented from the probabilistic analyses from the SDF PA (e.g., see Figure 5.7-2 of SRR-CWDA-2019-00001).

Figure 4.4-5: Peak Total Doses to the MOP at the 100-Meter Well from RSI-1 Based on HDPE Failure Condition as a Function of the Final Sand K_{sat}

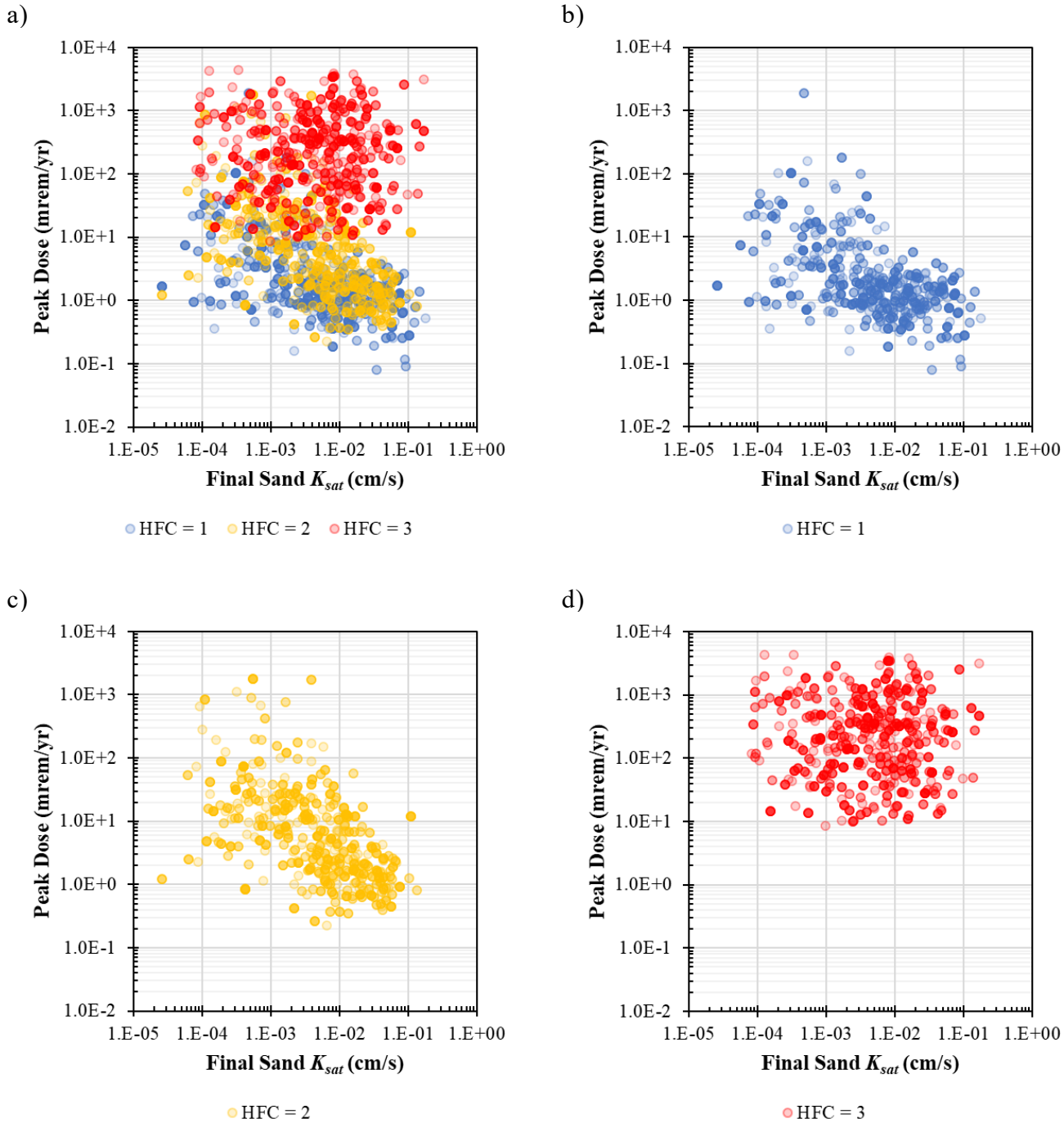

Note: HFC = HDPE failure condition: 1 = No HDPE Failure; 2 = Partial HDPE Failure; and 3 = Complete HDPE Failure.

4.4.2 Uncertainty Analysis of RSI-1 Model Realizations with the Highest Doses

This section identifies individual parameters that impact uncertainty analyses by investigating realizations that affect the overall results. Recognizing that the realizations with the highest doses to the MOP have the most impact on the uncertainty analyses, the three realizations with the highest dose peaks were studied for this evaluation.

The realizations with the highest dose consequences are those that have a combination of parameters with values significantly different from what is expected, such that when they occur concurrently, they produce dose results that are higher than others. The three RSI-1 realizations with the greatest doses were: Realization #185, Realization #87, and Realization #973, with peak doses of 4,371 mrem/yr, 4,250 mrem/yr, and 3,876 mrem/yr, respectively. Table 4.4-1 provides a summary of these realizations. This table is similar to Table 5.7-7 of the SDF PA (SRR-CWDA-2019-00001).

Table 4.4-1: Overview of Realizations with the Highest Peak Doses

Realization	Peak Dose (mrem/yr)	Time of Peak (yr)	Sector of Peak	Radionuclide Contributors to Peak Doses	Pathway Contributors to Peak Doses
Realization #185	4,371	1,000	D	I-129 (45%) Tc-99 (55%)	Water Ingestion (16%) Plant Ingestion (77%)
Realization #87	4,250	1,000	D	I-129 (52%) Tc-99 (48%)	Water Ingestion (43%) Plant Ingestion (49%)
Realization #973	3,876	1,000	D	I-129 (0%) Tc-99 (100%)	Water Ingestion (44%) Plant Ingestion (54%)

Table 4.4-1 indicates that even though the peak doses from these individual realizations are higher than those from the other realizations, the locations of the peaks (Sector D), the major radionuclide dose contributors (I-129 and Tc-99), and the major pathway contributors (water ingestion and plant ingestion) are the same (see Section 4.1.1).

The individual realizations are analyzed below by identifying those uncertainty parameters that have a direct impact on the magnitude or timing of the peak dose. Because all these realizations show I-129 and Tc-99 are always the most dominant radionuclide dose contributors, the analyses only mention these two radionuclides. As described, all three of these of the realizations simulated very similar conditions.

Realization #185

Realization #185 had a peak dose of 4,371 mrem/yr at year 2,380. This realization sampled the complete failure condition (HFC = 3). The time of the peak dose coincides closely with the sampled HDPE service life (2,343 years). The radionuclides contributing the most to this peak dose were I-129 with 45% (1,947 mrem/yr) and Tc-99 with 55% (2,423 mrem/yr). Similarly, the primary dose pathways were water ingestion with 16% (719 mrem/yr) and plant ingestion with 77% (3,350 mrem/yr).

The sampled precipitation rate of 58 in/yr was higher than current average conditions (estimated to be 49.4 in/yr in SRR-CWDA-2021-00036). The sand in the ULDL (and the LLDL) underwent significant silting-in such that the initial K_{sat} for the sand decreased from 1.6E-01 cm/s to 3.3E-04

cm/s. As a result of the closure cap modeling, the infiltration rate into the vadose zone peaked at approximately 19 in/yr when the HDPE failure occurred. This infiltration rate is higher than natural infiltration (i.e., recharge) rates for the General Separations Area (estimated to be 15.4 in/yr in SRR-CWDA-2021-00036).

For saltstone degradation, the initial damage fraction was relatively high (>0.02) such that when this value was coupled with the higher-than-expected *p*-averaging term (0.78), the resulting initial K_{sat} for saltstone was extremely high (2.88E-07 cm/s). The seismic events were not a factor in this realization as the initial damage and the subsequent high advective decalcification of saltstone completely dominated the saltstone degradation.

The saturated zone Darcy velocity multiplier was 0.88, meaning that ground water flow was slower than average conditions. The sampled saturated zone thickness (16.6 m) was smaller than the expected 20 m thickness and the saturated zone width (364 ft) was smaller than the expected 375 ft. These factors all contribute to conditions in which lower-than-expected dilution would occur as contaminants are transported into the saturated zone. This sampling is inconsistent with the modeled precipitation and infiltration rates; under higher precipitation rates, the water table would rise, resulting in higher subsurface flow rates and greater dilution (not less dilution) of the contaminants in the ground water.

The higher technetium solubility condition was sampled, the inventory multiplier for I-129 in SDU 9 was 1.38, and the sampled garden size was 730 m^2 (or 7.3 times larger than the compliance case).

Collectively, these multiple conditions resulted in a realization in which flow into the saltstone was fairly limited up until the HDPE failure occurred. Because of the limited flow conditions early on, some amount of Tc-99 and I-129 was able to diffuse into the surrounding soils and migrate to the water table so that just prior to the HDPE failure, the total dose to the MOP at approximately 2,300 years was approximately 1.4 mrem/yr. Then, once the HDPE failure occurred, a very large amount of water effectively flushed most of the mass of I-129 out of SDU 9 within a few hundred years. The Tc-99 release was limited by solubility controls, so it took a few thousand years, but it was also flushed from the SDU. Once released to the water table, there was insufficient dilution to moderate the ground water concentrations, so doses were high.

Realization #87

Realization #87 had a peak dose of 4,250 mrem/yr at year 2,370. This realization sampled the complete failure condition (HFC = 3). Due the discretization of the time intervals applied for generating the flow fields (see Table 3.2-1), the time of the peak dose is slightly earlier than the sampled HDPE service life; this is because the HDPE service life (2,496 years) occurs during Time Interval 22, which spans from 2,300 years to 2,800 years, so the change to the flow field conditions was applied starting at 2,300 years. The radionuclides contributing the most to this peak dose were I-129 with 52% (2,199 mrem/yr) and Tc-99 with 48% (2,049 mrem/yr). Similarly, the primary dose pathways were water ingestion with 43% (1,822 mrem/yr) and plant ingestion with 49% (2,070 mrem/yr).

The sampled precipitation rate of 62 in/yr was higher than current average conditions (estimated to be 49.4 in/yr in SRR-CWDA-2021-00036). The sand in the ULDL (and the LLDL) underwent significant silting-in such that the initial K_{sat} for the sand decreased from 6.4E-02 cm/s to 1.3E-04

cm/s. As a result of the closure cap modeling, the infiltration rate into the vadose zone reached approximately 21 in/yr when the HDPE failure occurred, and then peaked at 30 in/yr when a climate change was sampled to occur at approximately 5,300 years. These infiltration rates are much higher than natural infiltration (i.e., recharge) rates for the General Separations Area (estimated to be 15.4 in/yr in SRR-CWDA-2021-00036).

For saltstone degradation, the initial damage fraction was relatively high (>0.02) such that when this value was coupled with the higher-than-expected *p*-averaging term (0.66), the resulting initial K_{sat} for saltstone was extremely high (1.17E-07 cm/s). The seismic events were not a factor in this realization as the initial damage and the subsequent high advective decalcification of saltstone completely dominated the saltstone degradation.

The saturated zone Darcy velocity multiplier was 0.80, meaning that ground water flow was slower than average conditions. The sampled saturated zone thickness (18.9 m) was smaller than the expected 20 m thickness and the saturated zone width (315 ft) was smaller than the expected 375 ft. These factors all contribute to conditions in which lower-than-expected dilution would occur as contaminants are transported into the saturated zone. This sampling is inconsistent with the modeled precipitation and infiltration rates; under higher precipitation rates, the water table would rise, resulting in higher subsurface flow rates and greater dilution (not less dilution) of the contaminants in the ground water.

The higher technetium solubility condition was sampled, the inventory multiplier for I-129 in SDU 9 was 1.04, and the sampled garden size was 275 m^2 (or 2.75 times larger than the compliance case).

As with Realization #185, these multiple conditions resulted in a realization in which flow into the saltstone was fairly limited up until the HDPE failure occurred. Because of the limited flow conditions early on, some amount of Tc-99 and I-129 was able to diffuse into the surrounding soils and migrate to the water table so that just prior to the HDPE failure, the total dose to the MOP at approximately 2,300 years was approximately 1.9 mrem/yr. Then, once the HDPE failure occurred, a very large amount of water effectively flushed most of the mass of I-129 out of SDU 9 within a few hundred years. The Tc-99 release was limited by solubility controls, so it took a few thousand years, but it was also flushed from the SDU. Once released to the water table, there was insufficient dilution to moderate the ground water concentrations, so doses were high.

Realization #973

Realization #973 had a peak dose of 3,876 mrem/yr at year 3,680. This realization sampled the complete failure condition (HFC = 3). While the doses increased significantly due to the flow changes applied in association with the HDPE service life (2,575 years), this peak dose doesn't actually occur until approximately 1,000 years later because this is when a transition to a wetter climate (with a 25% increase to precipitation) is sampled to occur. Although the initial dose peak associated with the HDPE failure had a significant I-129 dose contribution, the inventory from I-129 was exhausted before the climate change transition occurred, so Tc-99 was the only major dose contributor, accounting for nearly 100% (3,871 mrem/yr) of the dose contribution. The primary dose pathways were water ingestion with 44% (1,697 mrem/yr) and plant ingestion with 54% (2,079 mrem/yr).

The sampled precipitation rate of 57 in/yr was higher than current average conditions (estimated to be 49.4 in/yr in SRR-CWDA-2021-00036). The sand in the ULDL (and the LLDL) underwent modest silting-in such that the initial K_{sat} for the sand decreased from 7.1E-02 cm/s to 8.2E-03 cm/s. As a result of the closure cap modeling, the infiltration rate into the vadose zone reached approximately 18 in/yr when the HDPE failure occurred, and then peaked at 25 in/yr when the climate change transition occurred at approximately 3,700 years. These infiltration rates are much higher than natural infiltration (i.e., recharge) rates for the General Separations Area (estimated to be 15.4 in/yr in SRR-CWDA-2021-00036).

For saltstone degradation, the initial damage fraction was not particularly significant (<0.01). However, the higher-than-expected *p*-averaging term (0.64) still resulted in an initial K_{sat} for saltstone was relatively high (1.15E-08 cm/s). The seismic events were not a factor in this realization as the initial damage and the subsequent high advective decalcification of saltstone completely dominated the saltstone degradation.

The saturated zone Darcy velocity multiplier was 0.93, meaning that ground water flow was slower than average conditions. The sampled saturated zone thickness (16.8 m) was smaller than the expected 20 m thickness and the saturated zone width (319 ft) was smaller than the expected 375 ft. These factors all contribute to conditions in which lower-than-expected dilution would occur as contaminants are transported into the saturated zone. This sampling is inconsistent with the modeled precipitation and infiltration rates; under higher precipitation rates, the water table would rise, resulting in higher subsurface flow rates and greater dilution (not less dilution) of the contaminants in the ground water.

The higher technetium solubility condition was sampled and the sampled garden size was 510 m^2 (or 5.10 times larger than the compliance case). Additionally, the water ingestion multiplier (1.80) and the plant ingestion multiplier (1.66) both ensured that the MOP consumed high amounts of contaminated material.

As with Realizations #185 and #87, these multiple conditions resulted in a realization in which flow into the saltstone was fairly limited up until the HDPE failure occurred. Because of the limited flow conditions early on, some amount of Tc-99 and I-129 was able to diffuse into the surrounding soils and migrate to the water table so that just prior to the HDPE failure, the total dose to the MOP at approximately 2,300 years was approximately 1.5 mrem/yr. Then, once the HDPE failure occurred, a very large amount of water effectively flushed most of the mass of I-129 out of SDU 9 within a few hundred years. The Tc-99 release was limited by solubility controls, so it took a few thousand years, but it was also flushed from the SDU. Once released to the water table, there was insufficient dilution to moderate the ground water concentrations, so doses were high.

4.4.3 Water Balance Data for Response to RSI-6

To support the response to RSI-6 (ML20254A003), water balance data shall be provided for the three cases performed for RSI-1 that resulted in the greatest dose and the three cases that resulted in the greatest amount of water flowing through the saltstone. The three RSI-1 realizations with the greatest doses were: Realization #185, Realization #87, and Realization #973, with peak doses of 4,371 mrem/yr, 4,250 mrem/yr, and 3,876 mrem/yr, respectively. The three RSI-1 realizations with the greatest cumulative volumetric flows through saltstone were: Realization #302, Realization #87, and Realization #604, with cumulative flow volumes (over 10,000 years) of

6.97E+13 cm^3 (1.84E+10 gal), 5.04E+13 cm^3 (1.33E+10 gal), and 4.71E+13 cm^3 (1.25E+10 gal), respectively. Therefore, to be responsive to the request from the NRC, water balance data for the following realizations shall be provided:

- Realization #87 (for both high doses and high saltstone flow rates),
- Realization #185 (for high doses),
- Realization #302 (for high saltstone flow rates),
- Realization #604 (for high saltstone flow rates), and
- Realization #973 (for high doses).

This water balance data will be provided via external files equivalent to a previous data transmittal (SRR-CWDA-2020-00077).

4.5 Conclusions and Recommendations

At face value, many of the doses presented in Section 4.1 may appear to be problematic from a compliance perspective. However, as described in Section 3.8, while the RSI models and the associated results may be useful for informing risk-related decision-making, they do not represent actual long-term conditions at the SDF and are not intended to represent the expected conditions as would be necessary for demonstrating compliance. Additionally, even with the many modeling decisions designed to accentuate the negative effects of potential risks (see Table 3.8-1), when considering these results from a health-risk perspective, most of the doses presented in Section 4.1 are below the average radiation dose (620 mrem/yr) for persons in the United States (NCRP-160) as depicted in Figure 4.5-1.

Figure 4.5-1: Major Sources of Radiation Exposure to the Average US Citizen

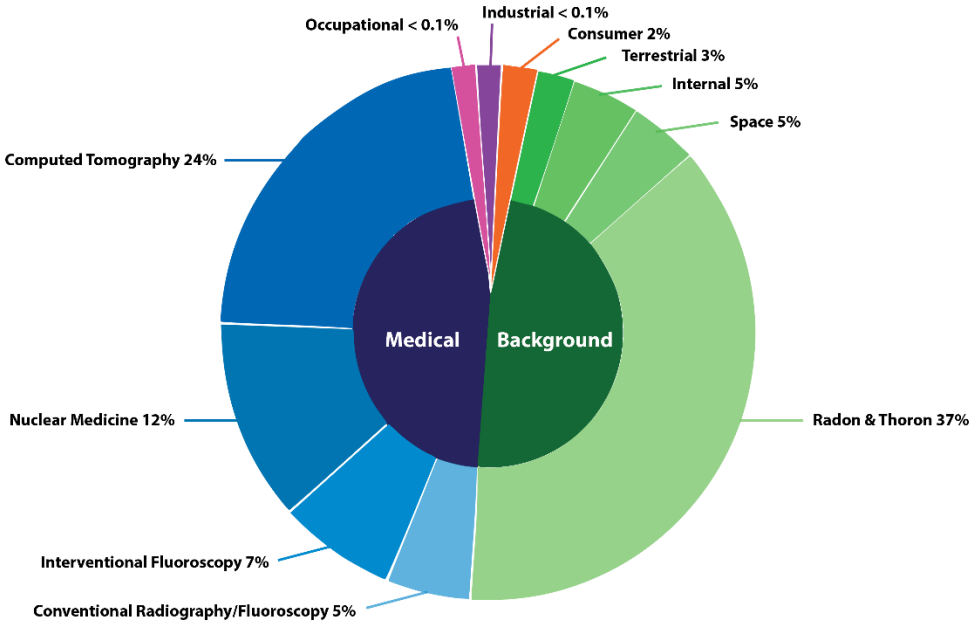

Average Annual Radiation Dose

Sources	Radon & Thoron	Computed Tomography	Nuclear Medicine	Interventional Fluoroscopy	Space	Conventional Radiography/ Fluoroscopy	Internal	Terrestrial	Consumer	Occupational	Industrial
Units											
mrem (United States)	228 mrem	147 mrem	77 mrem	43 mrem	33 mrem	33 mrem	29 mrem	21 mrem	13 mrem	0.5 mrem	0.3 mrem
mSv (International)	2.28 mSv	1.47 mSv	0.77 mSv	0.43 mSv	0.33 mSv	0.33mSv	0.29 mSv	0.21 mSv	0.13 mSv	0.005 mSv	0.003 mSv

[Source: NCRP-160, via https://www.epa.gov/radiation/radiation-sources-and-doses]

Based on the probabilistic analyses of the model results described in Sections 4.1 through 4.4 and the related analyses provided in SRR-CWDA-2021-00040 and SRR-CWDA-2021-00056, the parameters that pose the most significant risks associated with the performance of the flow barriers are the HDPE failure condition, the assumed silting-in of the sand drainage layers, and the *p*-averaging term used for estimating saltstone conditions for partially degraded saltstone.

For the HDPE failure condition, three conditions were considered (complete failure, partial failure, and no failure); however, only the partial failure condition of the HDPE is considered plausible. The sampling of this parameter and the modeling approaches that were applied in association with the sampling of the complete failure condition result in higher-than-expected infiltration rates as well as accelerated degradation rates for saltstone (via advective decalcification).

Accordingly, research associated with HDPE performance under conditions that are more representative of the SDF closure cap and SDUs could help develop a better understanding of how HDPE failures are most likely to occur, as well as how such failures would influence infiltration and flow conditions. Such research could significantly reduce the ranges of uncertainties associated with HDPE performance.

For the silting-in of the sand drainage layers, the NRC expressed concern that silting-in will occur because "NUREG/CR-7028 [ML12005A110] described the discovery of fine particles within the exhumed geotextiles, geonets, and geosynthetic drainage layers that apparently were transported

there due to the migration of those fines" (ML20254A003). Despite this concern, the reference itself stated that "Changes in … drainage layers were modest or small. Greater reductions in transmissivity and permittivity were observed for drainage layers covered with soils having higher fines content. However, this effect was modest, and all of the drainage layers functioned as anticipated." Further, Dr. Craig Benson, one of the authors of NUREG/CR-7028 (ML12005A110), was consulted on this topic and he provided feedback, stating that silting-in of sand drainage layers "is a hypothetical issue, which is not supported by observed [conditions] in engineered cover systems or natural analogs" (Benson (2021)). He also stated that "the presence or accumulation of fines on the surface of geotextiles or directly above a coarse earthen layer is common and expected, but is not indicative of 'silting-in' that might occur in a fluvial environment with higher energy. The finer particles that accumulate at the interface with a sand drainage layer or a geotextile form bridges across the larger pores in the coarser material below, creating a thin 'filter' layer directly above the drainage layer. This filter mechanism keeps the underlying drainage material free of fines" (Benson (2021)).

Based on this consultation with the subject matter expert and based on studies of analog sites (see Section 4.3.1 of SRR-CWDA-2021-00031), the DOE maintains that this silting-in phenomenon is not expected and that the sand drainage layers are expected to perform as designed. While it might not be possible to prove that this hypothetical phenomenon will not occur, identifying additional analog sites with similar site conditions may help to alleviate the NRC's concerns.

Additionally, for the *p*-averaging term used for estimating saltstone conditions, literature reviews or additional analyses may be prepared to better define the appropriate value to use for blending the material properties of intact and degraded saltstone.

Finally, if future modeling efforts will apply probabilistic modeling to develop variable infiltration rates and flow rates, as was developed per the RSI models, the ground water (aquifer) transport models should also be modified such that increased precipitation and infiltration would coincide with a rise in the water table and increased saturated zone Darcy velocities to provide more realistic model results.

5.0 REFERENCES

B-SQP-C-00002, Hommel, S.P., *Software Quality Assurance Plan for GoldSim© for Savannah River Site's Liquid Waste Program*, Savannah River Site, Aiken, SC, Rev. 3, May 2018.

B-SQP-C-00003, Lester, B., *Software Quality Assurance Plan for ReadPORFLOWData.dll for the Savannah River Site's Liquid Waste Program*, Savannah River Site, Aiken, SC, Rev. 1, June 2013.

B-SQP-C-00005, Hommel, S., *Software Quality Assurance Plan for mView*, Savannah River Site, Aiken, SC, Rev. 0, January 2013.

Benson, C.H. (2021). Personal communication with Steve Hommel, March 11, 2021.

Environmental Protection Agency (EPA) Website, Radiation Sources and Doses, Accessed July 23, 2021: https://www.epa.gov/radiation/radiation-sources-and-doses

GTG-2018a, *GoldSim User's Guide: Probabilistic Simulation Environment*, GoldSim Technology Group LLC, Issaquah, WA, 2018. (Copyright)

LBL-18473, Wang, J. S. Y., and Narasimhan, T. N., *Hydrologic Mechanisms Governing Fluid Flow in a Partially Saturated, Fractured, Porous Tuff at Yucca Mountain*, Lawrence Berkeley Laboratory, University of California, Berkeley, CA, October 1984.

ML20254A003, Koenick, S. S., *Preliminary Review of the U.S. Department of Energy's Submittal of the 2020 Savannah River Site Saltstone Disposal Facility Performance Assessment*, U.S. Nuclear Regulatory Commission, Washington DC, October 2020.

NCRP-160, *Ionizing Radiation Exposure of the Population of the United States (2009)*, National Council on Radiation Protection and Measurements, Bethesda, MD, 2009. (Copyright)

Or, D. and Tuller, M. (2000), *Flow in unsaturated fractured porous media: Hydraulic conductivity of rough surfaces*, Water Resources Research, Vol. 36 (5), May 2000. DOI: 10.1029/2000WR900020

SRNL-STI-2018-00275, Whiteside, T.S., *PORFLOW 6.42.9 Testing and Verification Document*, Savannah River National Laboratory, Aiken, SC, Rev. 0, June 2018.

SRR-CWDA-2018-00068, Watkins, D., *Performance Assessment for the Saltstone Disposal Facility at the Savannah River Site: Quality Assurance Report*, Savannah River Site, Aiken, SC, Rev. 2, January 2020.

SRR-CWDA-2019-00001, *Performance Assessment for the Saltstone Disposal Facility at the Savannah River Site*, Savannah River Site, Aiken, SC, Rev. 0, March 2020.

SRR-CWDA-2019-00046, Watkins, D., *QA Addendum to FY2019 SDF PA QA Report, SRR-CWDA-2018-00068*, Savannah River Site, Aiken, SC, Rev. 3, March 2020.

SRR-CWDA-2020-00005, *Closure Plan for the Z-Area Saltstone Disposal Facility*, Savannah River Site, Aiken, SC, Rev. 1, August 2020.

SRR-CWDA-2020-00064, *FY2020 Special Analysis for the Saltstone Disposal Facility at the Savannah River Site*, Savannah River Site, Aiken, SC, Rev. 1, April 2021.

SRR-CWDA-2020-00077, Flach, G.P., *Electronic Data Associated with the 2020 Saltstone Disposal Facility Performance Assessment, Transmittal 2*, Savannah River Site, Aiken, SC, Rev. 0, November 2020.

SRR-CWDA-2020-00081, Arnett, B.E., *Determination of the SDF Inventory through 9/30/2020*, Savannah River Site, Aiken, SC, Rev. 0, December 2020.

SRR-CWDA-2021-00031, Hommel, S.P., *Closure Cap Model Parameter Evaluation: Saturated Hydraulic Conductivity of Sand*, Savannah River Site, Aiken, SC, Rev. 1, May 2021.

SRR-CWDA-2021-00033, Hommel, S.P., *Closure Cap Model Parameter Evaluation: High Density Polyethylene (HDPE) and Geosynthetic Clay Liner (GCL) Composite Barrier Performance*, Savannah River Site, Aiken, SC, Rev. 1, May 2021.

SRR-CWDA-2021-00036, Hommel, S.P., *Evaluation of the Potential for Erosion in the Vicinity of Z Area*, Savannah River Site, Aiken, SC, Rev. 0, June 2021.

SRR-CWDA-2021-00040, Hommel, S.P., *Evaluation of the Uncertainties Associated with the SDF Closure Cap and Long-Term Infiltration Rates*, Savannah River Site, Aiken, SC, Rev. 0, June 2021.

SRR-CWDA-2021-00052, Flach, G.P., *Supplemental Information and Proposed Probabilistic Inputs Related to NRC RSI-4: Saltstone Degradation*, Savannah River Site, Aiken, SC, Rev. 0, July 2021.

SRR-CWDA-2021-00056, Hommel, S.P., *Evaluation of the Uncertainties Associated with Long-Term Saltstone Degradation*, Savannah River Site, Aiken, SC, Rev. 0, July 2021.

SRR-CWDA-2021-00057, Hommel, S.P., *Selected PORFLOW Modeling Configurations to Support RSI-4 Analysis*, Savannah River Site, Aiken, SC, Rev. 0, July 2021.

SRR-LWP-2009-00001, Chew, D.P., Hamm, B.A., and Wells, M.N., *Liquid Waste System Plan*, Savannah River Site, Aiken, SC, Rev. 21, January 2019.

Tuller, M. and Or, D. (2002), *Unsaturated Hydraulic Conductivity of Structured Porous Media: A Review of Liquid Configuration–Based Models*, Vadose Zone Journal Vol 1 (1), August 2002. DOI: 10.2113/1.1.14

APPENDIX A. MOISTURE CHARACTERISTIC CURVES

This appendix provides an overview of the moisture characteristic curves and provides a basis for why the application of the moisture characteristic curves in the SDF PA provides a reasonable and defensible approximation of degraded saltstone conditions.

A.1 Conceptualization of Water Storage

A moisture characteristic curve (MCC), also known as a water retention curve or soil water characteristic curve, is a curve (i.e., a line plotted on a chart) which represents the relationship between the volumetric water content (θ) and the pressure head (ψ) or matric suction (-ψ) of a partially saturated permeable media. Defining the MCC of saltstone and other materials in the SDF PA models is important because it can have a major influence on flow conditions.

A common way to introduce the concept of MCCs is by using a sponge as an example of a permeable media. For example, one may imagine a dry sponge. Adding a few drops of water to the dry sponge will increase the volumetric water content, but the matric suction of the sponge will prevent those few drops from dripping out of the bottom of the sponge. As one adds more water to the sponge, the sponge will become more saturated and water will eventually begin to exit the sponge. Once the sponge is fully saturated, outflow will be equal to the inflow of water. But if one stops adding water, the flow rate of water passing out of the sponge will decrease as the volumetric water content within the sponge decreases. Once the pressure head or matric suction within the sponge reaches equilibrium with external conditions, the sponge will no longer drip even though there is still water present within the sponge.

This conceptualization may be applied to media other than sponges, such as sands, clays, and concretes. And for any media that water may pass through, a different MCC must be defined.

A.2 Richards Equations and MCCs

The SDF PA simulated vadose zone flow in PORFLOW using a modified form of Richards Equation (see SDF PA Section 4.4.4.2). In one-dimension, the equation takes the form:

$$\frac{\partial(nS_w)}{\partial t} = \frac{\partial}{\partial z}\left[K_{sat} k_r \frac{\partial(\psi + z)}{\partial z}\right] + Q \qquad \text{Eq. A-1}$$

Where:

n = porosity (unitless),

S_w = the water saturation (unitless: volume of water (cm^3) divided by volume of pore space (cm^3)),

t = time (s),

K_{sat} = the saturated hydraulic conductivity (cm/s),

k_r = the relative permeability (unitless),

ψ = pressure head (cm),

z = elevation (cm), and

Q = the volumetric rate of fluid injection (> 0) or withdrawal (< 0).

The relative permeability is a function of saturation:

$$k_r = k_r(S_w) \quad \text{Eq. A-2}$$

Where:

k_r = the relative permeability (unitless) and

S_w = the water saturation (unitless).

Similarly, saturation is a function of pressure head:

$$S_w = S_w(\psi) \quad \text{Eq. A-3}$$

Where:

S_w = the water saturation (unitless) and

ψ = pressure head (cm).

Equations A-2 and A-3 are empirical functions referred to as the MCCs. Equations A-1 through A-3 form a system of equations that describe variably saturated porous medium flow in terms of the unknowns ψ, S_w, and k_r. The Vadose Zone Flow Model in the SDF PA (SRR-CWDA-2019-00001) comprises a sequence of steady-state simulations with no internal flow sources/sinks. As such, the Richards Equation becomes:

$$0 = \frac{\partial}{\partial z}\left[K_{sat} k_r \frac{\partial(\psi + z)}{\partial z}\right] \quad \text{Eq. A-4}$$

Where:

K_{sat} = the saturated hydraulic conductivity tensor (cm/s),

k_r = the relative permeability (unitless),

ψ = pressure head (cm), and

z = elevation (cm).

Next, the unknown saturation variable can be eliminated by substituting Equation A-3 into Equation A-2 such that:

$$k_r = k_r(\psi) \quad \text{Eq. A-5}$$

or equivalently:

$$K_{sat} k_r = K(\psi) \quad \text{Eq. A-6}$$

Where:

K_{sat} = the saturated hydraulic conductivity tensor (cm/s),

k_r = the relative permeability (unitless),

K = the unsaturated hydraulic conductivity (cm/s), and

ψ = pressure head (cm).

With this change, the governing equation set for vadose zone flow becomes:

$$0 = \frac{\partial}{\partial z}\left[K(\psi)\frac{\partial(\psi + z)}{\partial z}\right] \quad \text{Eq. A-7}$$

Where:

K = the unsaturated hydraulic conductivity (cm/s),

ψ = pressure head (cm), and

z = elevation (cm).

Note that the unsaturated hydraulic conductivity function $K(\psi)$ embedded in Equation A-7 is fully equivalent to the separate water retention and relative permeability functions defined by Equations A-2 and A-3. Subsequent discussion of moisture characteristics is posed in terms of unsaturated hydraulic conductivity $K(\psi)$ to avoid interpretation of multiple functions and the intermediate variable S_w.

A.3 Use of MCCs in the SDF PA

The morphology of degraded saltstone is uncertain and expected to vary depending on the degradation mechanism. The SDF PA conceives saltstone degrading via gradual decalcification as infiltrate slowly dissolves cement binders. Decalcification is expected to increase the hydraulic conductivity of saltstone by increasing porosity and average pore size. The DOE continues to believe that a granular soil such as backfill is a reasonable surrogate for saltstone degraded by decalcification. For convenient reference, Figure A-1 illustrates the unsaturated hydraulic conductivity functions assumed in the SDF PA for intact saltstone ("Grout" = 0% degraded (black curve)) and fully degraded saltstone ("Backfill" = 100% (orange curve)). Also, shown are three intermediate stages of physical degradation as estimated by blending the intact and fully degraded conditions in varying proportions using geometric averaging: 25%, 50%, and 75% (dashed gray curves).

Figure A-1: Unsaturated Hydraulic Conductivity for Selected Materials Including Fractured Grout with a Crack Spacing of 1 Meter

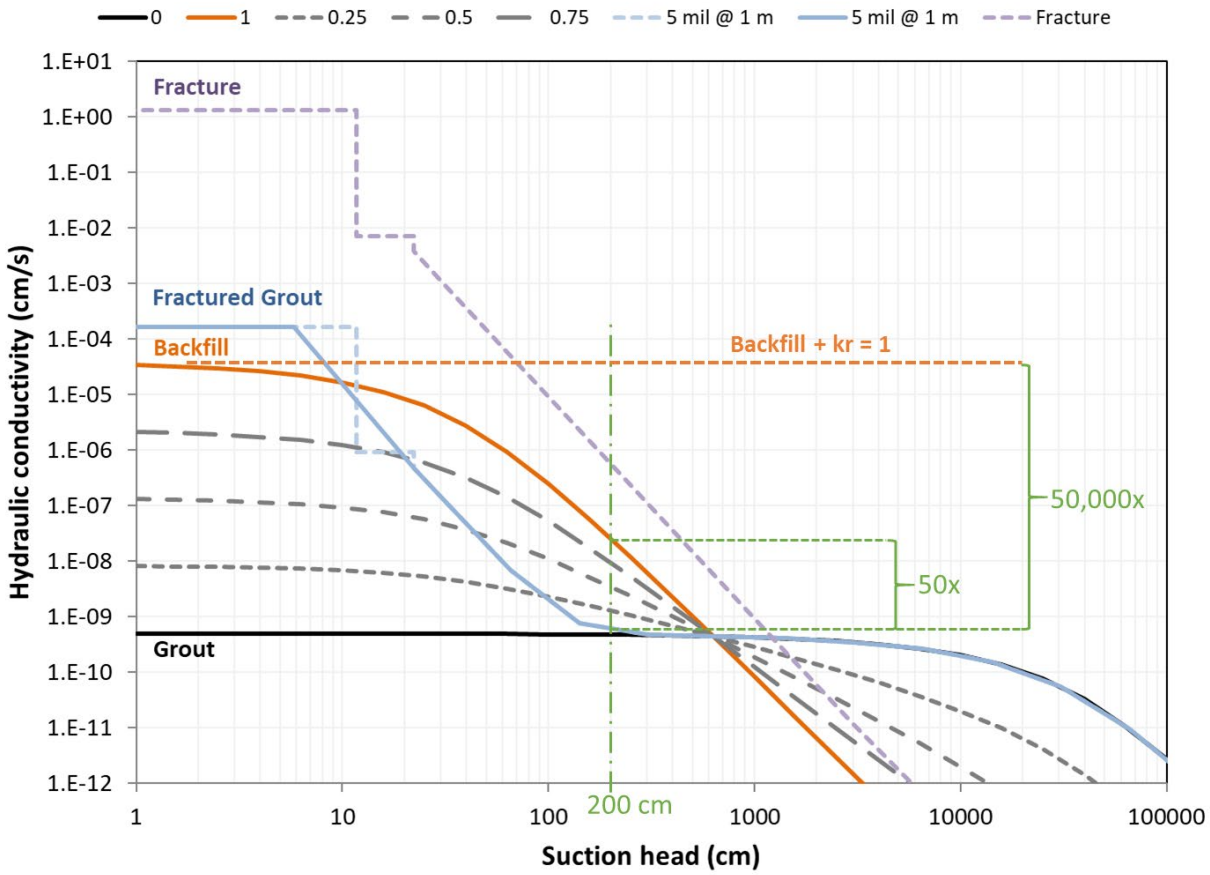

A.4 Use of MCCs in the RSI Analyses

For other physical degradation mechanisms postulated in the responses to RSI-1 and RSI-4, such as seismic events, damage is more likely to take the form of fractures. The saturated hydraulic conductivity of a saturated fracture is approximated by that of a smooth-wall planar gap (e.g., LBL-18473):

$$K_f = \frac{\rho g b^2}{12\eta} \qquad \text{Eq. A-1}$$

Where:

K_f = the saturated hydraulic conductivity (cm/s) of a saturated fracture,

ρ = liquid density (g/cm^3),

g = gravitational acceleration (cm^2/s),

b = fracture aperture (cm), and

η = liquid viscosity (g/cm/s).

Given a density of water of approximately 1 g/cm^3 and a liquid viscosity of approximately 1 mPa/s (or 0.01 g/cm/s) and given an assumed gravitational acceleration of 9.81 cm/s^2, a crack with a fracture aperture of 5 mil (0.0127 cm) is estimated to have a K_{sat} of approximately 1.3 cm/s, while intact (or undegraded) saltstone has a K_{sat} of 5.0E-10 cm/s (per SRR-CWDA-2019-00001, Table 4.3-3). Based on this, for saltstone with parallel cracks spaced 1 meter apart, the effective K_{sat} would increase from 5.0E-10 cm/s to 1.7E-04 cm/s.

However, an aperture of width b will only be water-filled if (e.g., LBL-18473):

$$\psi > -\frac{2\sigma}{\rho g b} \qquad \text{Eq. A-2}$$

Where:

ψ = pressure head (cm),

σ = surface tension (N/m),

ρ = liquid density (g/cm^3),

g = gravitational acceleration (cm^2/s), and

b = fracture aperture (cm).

For a 5-mil (0.0127 cm) fracture, suction head (-ψ) must be less than 11.7 cm for the aperture to be water-filled; otherwise, water will be present as a thin film on each fracture face. The abrupt transition to film flow initially reduces flow and corresponding effective conductivity by roughly two orders of magnitude. The higher the suction the less significant the film flow in fractures compared to matrix flow. At sufficiently high suctions, the effective hydraulic conductivity of a fractured medium differs little from that of an intact condition.

The above concepts are illustrated in Figure A-1 which shows the hydraulic conductivity of a 5 mil (0.0127 cm) aperture with periodic V-shaped grooves to mimic roughness ("Fracture"), following Or and Tuller (2000). Tuller and Or (2002) show that theoretical constructs of this nature can reproduce the hydraulic properties of fractured rock systems. The abrupt decrease in $K(\psi)$ at $-\psi$ = 11.7 cm reflects the transition from a water-filled aperture to film-flow. The smaller abrupt decrease at roughly 20 cm reflects the transition from water-filled grooves to meniscus-flow. At higher suctions film thickness and flow rate decrease, causing a gradual decline in $K(\psi)$.

Also shown in Figure A-1 is the effective conductivity of fractured saltstone ("Fractured Grout" (blue curves)) assuming a 1-meter fracture spacing. The dashed line is the theoretical result from Or and Tuller (2000) and the solid line is a more realistic variation reflecting a distribution of crack widths centered around 5 mil (0.0127 cm). A crack spacing of 1-meter was selected to achieve a conductivity like that of backfill for suctions in the 0 cm (saturated flow) to 20 cm range. Suction heads vary in SDF PA simulations depending on infiltration rate and material properties. Selecting 200 cm as a representative example, the assumed "Backfill" $K(\psi)$ curve is 50 times higher than the "Fractured Grout" curve. Thus, the selection of backfill as a surrogate for degraded saltstone is a very conservative assumption when damage takes the form of fractures. Backfill K_{sat} coupled

with a relative permeability ($k_r(\psi)$) of 1 plots as a horizontal line in Figure A-1. At a suction of 200 cm this curve is roughly 50,000 times higher than the "Fractured Grout" curve. The DOE does not consider backfill with a relative permeability of 1 to be a realistic condition. Nonetheless, simulations with $k_r = 1$ are provided to support parameter sensitivity studies within this report.

A.5 Consideration of Extremely Degraded Saltstone

Figure A-2 shows the "Fractured Grout" curve when the fracture spacing is only 1-centimeter (100 times as many cracks as assumed in Figure A-1). Even under this extremely degraded condition, "Fractured Grout" $K(\psi)$ approaches but still does not reach that of "Backfill" when suction head ranges from several tens to a few hundred centimeters. The Backfill + $k_r(\psi) = 1$ curve continues to be unrealistically high.

Figure A-2: Unsaturated Hydraulic Conductivity for Selected Materials Including Fractured Grout with a Crack Spacing of 1 Centimeter

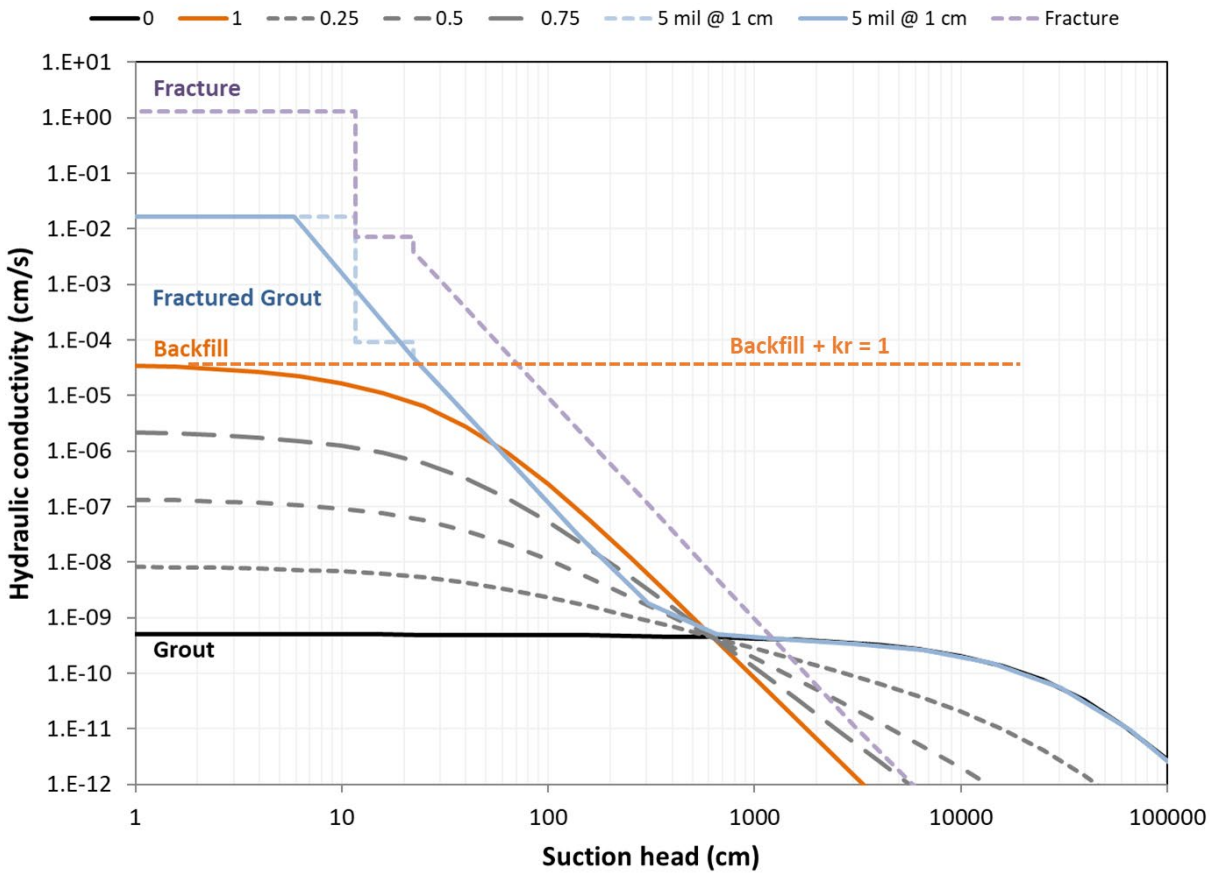

To summarize, the DOE believes "Backfill" to be a reasonable assumption for saltstone degraded by decalcification and pessimistic under typical unsaturated conditions if damage takes the form of cracks. "Backfill" coupled with a relative permeability of 1.0 is considered an unrealistic condition.

APPENDIX B. BASIS FOR USING ONLY SDU 9 FOR THE RSI ANALYSES

As described in this report, the SDF has 15 SDUs but only a single SDU (SDU 9) was used for the models and analyses described in Sections 3.0 and 4.0. SDU 9 was selected to provide computational efficiency and to reduce statistical noise associated with evaluating uncertainties associated with doses from multiple SDUs. This appendix is provided to demonstrate why doses based on contaminants released from SDU 9 provide a reasonable representation of the system as a whole.

B.1 Selection of SDU 9

The selection of SDU 9 as the basis for modeling was recommended in the interoffice memorandum *Selected PORFLOW Modeling Configurations to Support RSI-4 Analysis* (SRR-CWDA-2021-00057), which states:

> "SDU 9 was selected because it is a 375-foot Diameter SDU. These larger SDUs are assigned more inventory than any of the other SDU designs (see Section 3.3 of the SDF PA), which means that there is more potential risk associated with them. Of the 375-foot Diameter SDUs, SDUs 6, 7, and 11 are considered lower risk than SDUs 8, 9, 10, and 12 based on their locations within the SDF, proximity to the 100-meter SDF boundary, and predominant directions of ground water flow (see Section 4.4.8 of the SDF PA). Having down selected the SDUs to SDUs 8, 9, 10 and 12, SDU 9 was selected because in the SDF PA it is assumed to be constructed closer to the water table than the other SDUs (see Section 4.4.4.3 of the SDF PA). Being closer to the water table, releases from SDU 9 have been shown to dominate the model results within the 1,000-year Compliance Period and for a significant portion of the 10,000-year Performance Period (see Sections 5.5 and 5.7 of the SDF PA)."

B.2 Comparison of SDF PA Results Versus Equivalent Results for SDU 9 Only

Section 5.7 of the SDF PA (SRR-CWA-2019-00001) described the probabilistic analysis that was developed for evaluating various uncertainties. The analysis simulated MOP dose results for eight "sectors" along the 100-meter boundary based on releases from all 15 SDUs. Despite using all 15 SDUs, dose along Sector D generally dominated the results for the first 4,000 years after closure (see Figure 5.7-7 of SRR-CWDA-2019-00001). Even after the first 4,000 years, the doses along Sector D remained high and relatively close to the total dose to the MOP. As explained in the SDF PA, the Sector D doses are highest during the first few thousand years due to releases from SDU 9. SDU 9 is simulated as being constructed at a lower elevation and closer to the water table. As such, releases from SDU 9 reach the 100-meter boundary first, such that the SDU 9 releases generally dominate the system.

To provide some context for how SDU 9 only releases compare to the combined releases from all SDUs, one of the three GoldSim model files used in the SDF PA probabilistic analyses (*SRS Saltstone v5.053_RS1a.gsm*) has been modified to only include releases from SDU 9. This model file (*SRS Saltstone v5.053_RS1a_SDU9-Only.gsm*) was set to run for SDU 9 only and to run for

only 10,000 years (as opposed to 20,000 years). Otherwise, this model is identical to *SRS Saltstone v5.053_RS1a.gsm*. The results from this simulation were then compared to the results from the SDF PA probabilistic analyses.

The most direct way to communicate the uncertain nature of the model results is to show graphs of certain key model endpoints. Figure 5.7-2 in the SDF PA (SRR-CWDA-2019-00001) shows the peak doses (for the total doses to the MOP at the 100-meter well) from all 3,000 realizations that were performed in the SDF PA. This figure has been reproduced here as Figure B-1. The colors of the data points indicate the random seed (RS) of the corresponding GoldSim file (see Table 5.7-4 in the SDF PA).

Figure B-1: Peak Doses to the MOP at the 100-Meter Well from 3,000 Realizations from the SDF PA

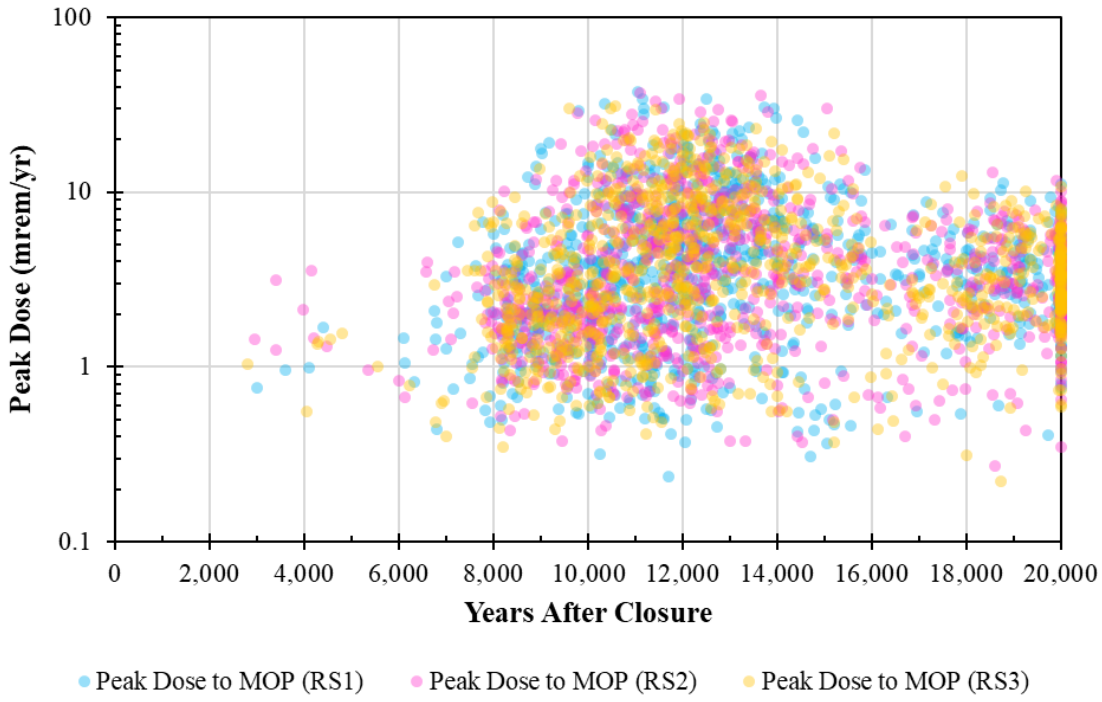

[SOURCE: SRR-CWDA-2019-00001, Figure 5.7-2]

For the RSI-1 analyses described within this report, the modeling was limited to only the realizations generated with Random Seed = 1. Figure B-2 shows the equivalent peak doses from the SDF GoldSim Model for only the realizations which used Random Seed = 1. Figure B-3 shows the equivalent peak doses within 10,000 years. This is effectively equivalent to the RSI-1 Model, except that these dose peaks are based on releases from all SDUs whereas the RSI-1 Model only models the SDU 9 releases.

Figure B-2: Peak Doses to the MOP at the 100-Meter Well from the 1,000 Realizations from the SDF PA with Random Seed =1

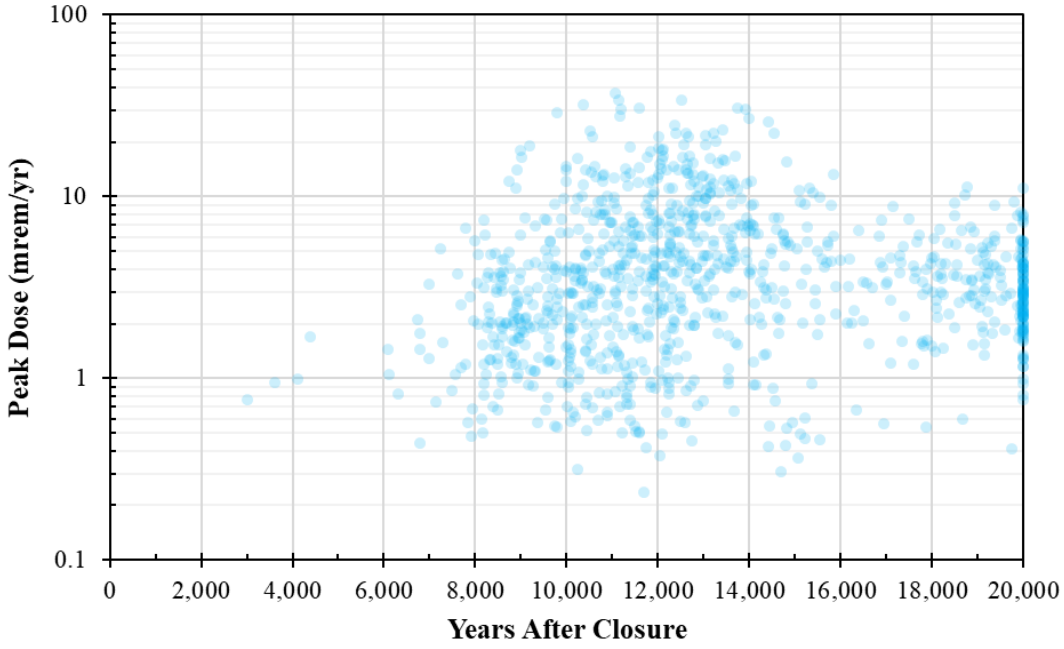

Figure B-3: Peak Doses to the MOP at the 100-Meter Well within 10,000 Years from the 1,000 Realizations from the SDF PA with Random Seed =1

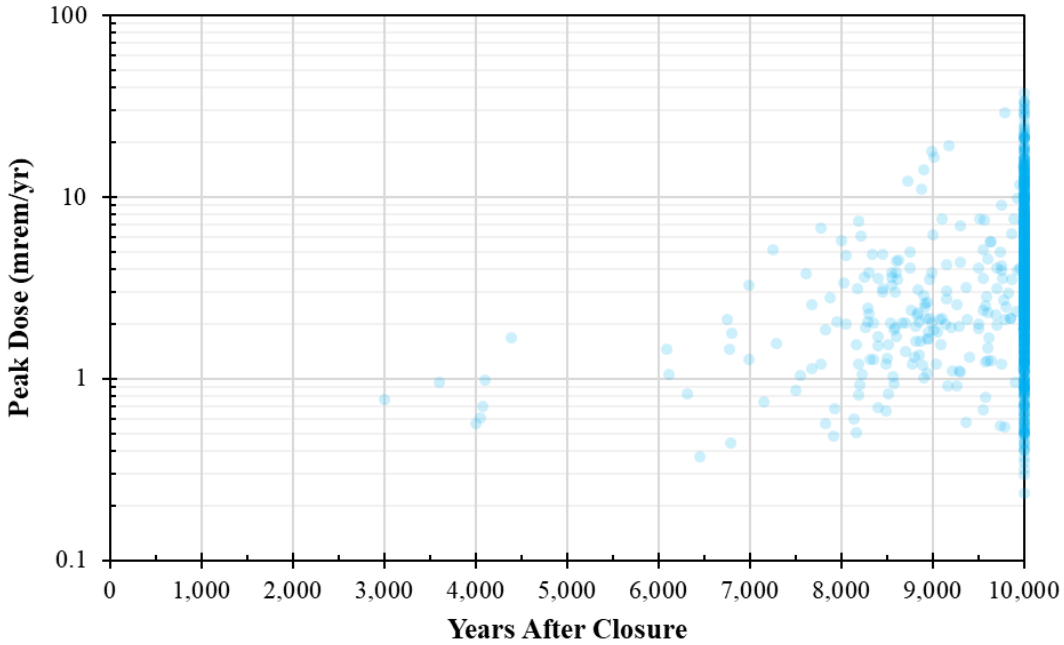

To provide the most direct comparison possible, Figure B-4 shows the equivalent dose peaks within 10,000 years from the SDF GoldSim Model for only the realizations which used Random Seed = 1, except that the model was re-ran using only SDU 9 releases. This figure is comparable to Figure 4.1-1.

Figure B-4: Peak Doses to the MOP at the 100-Meter Well within 10,000 Years from the 1,000 Realizations from the SDF PA with Random Seed =1 and Only Simulating Releases from SDU 9

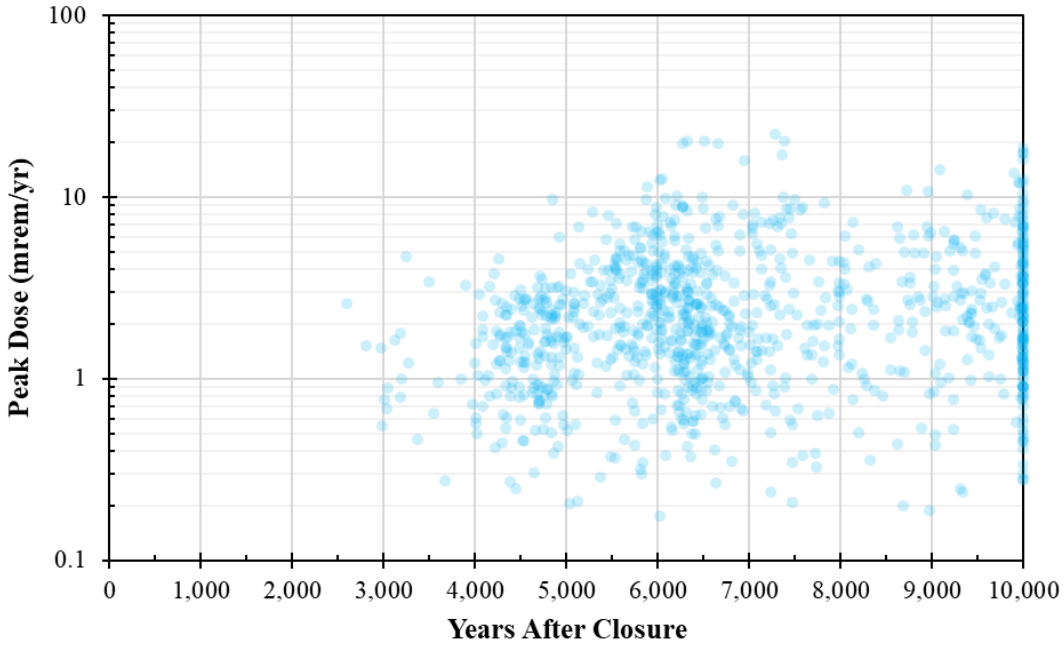

Next, to demonstrate that releases from SDU 9 may be reasonably used to represent the entire SDF system, the peak doses from Figure B-3 and from Figure B-4 were plotted together as shown in Figure B-5. In this figure, the peak doses from the version of the model using all 15 SDUs are plotted along the X-axis and the equivalent peak doses from the version of the model using only SDU 9 are plotted along the Y-axis. The solid black line crossing diagonally through the figure represents a 1-to-1 relationship: data points on this line represent peak doses of equal value between the two versions of the model. The dashed lines are provided as a guide to show where values would lie if they were different by an order of magnitude or more. As shown, although the SDU 9 doses are slightly lower than the SDF system doses, all of the peak doses are relatively close to the 1-to-1 line. Based on this comparison, using probabilistic model results from SDU 9 only, as opposed to modeling all 15 SDUs, provides a reasonable approximation of the results of the SDF system as a whole.

Figure B-5: Peak Doses to the MOP at the 100-Meter Well from 1,000 Realizations Using All SDUs Versus Using Only SDU 9

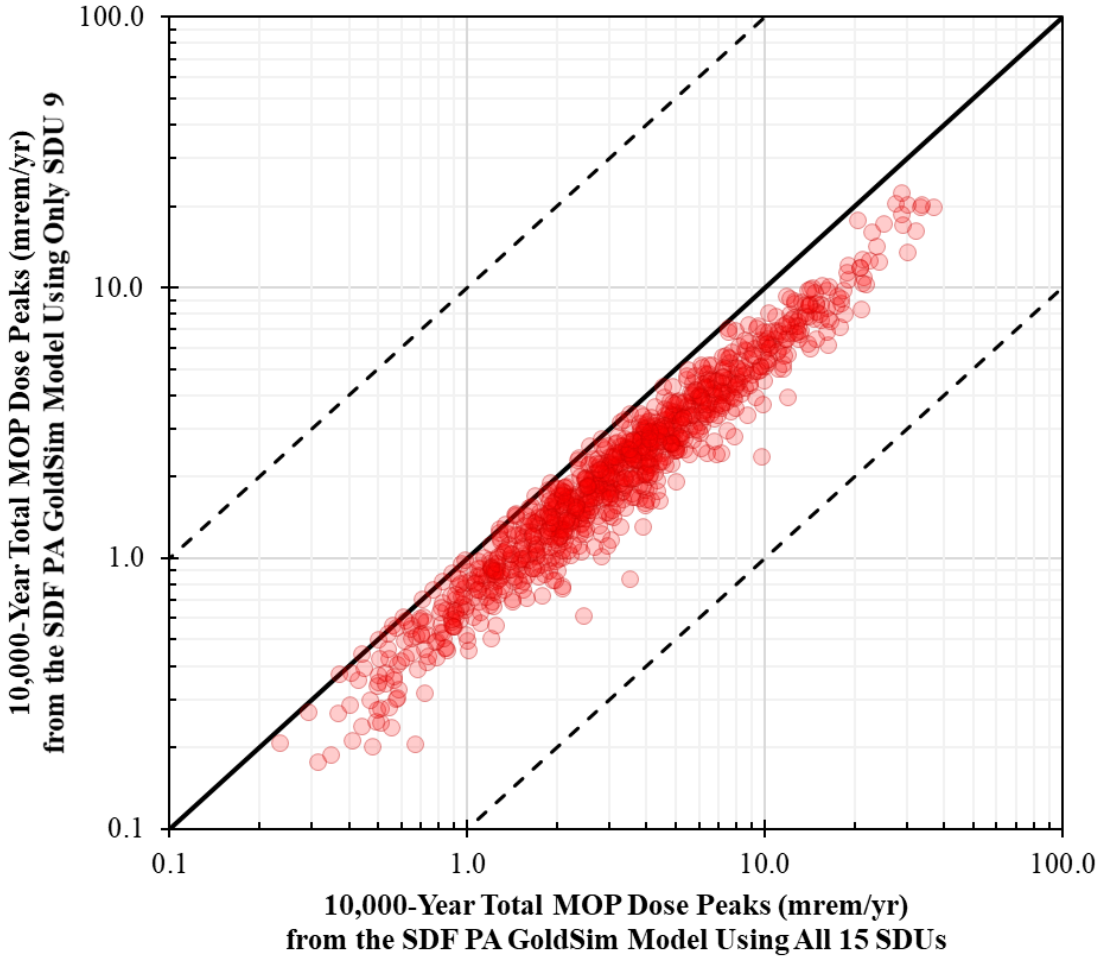

This page intentionally left blank.

APPENDIX C. INTRODUCTION TO PROBABILISTIC SENSITIVITY ANALYSES

Complex modeling, such as the probabilistic models, provides an effective tool for exploring the dynamics of systems where multiple variables interact in a nonlinear manner. The probabilistic simulation approach used in the SDF GoldSim Model propagates uncertainty regarding the independent variables (e.g., inputs such as physical soil properties or inventory) through the model to the dependent variables or predicted response (e.g., dose or concentration). One of the goals of this sensitivity analysis is to identify which independent variables have distributions that exert the greatest influence on the response.

The primary sensitivity analysis procedures used herein involve the determination and presentation of partially ranked correlation coefficients (PRCCs) and stepwise rank regression coefficients (SRRCs).

C.1 Partially Ranked Correlation Coefficients

PRCCs provide a measure of the strength of the monotonic relationships between an independent variable and a specific model result after a correction has been made to remove the monotonic effects of the other independent variables in the analysis (i.e., one independent variable is analyzed at a time by isolating and ignoring the combined effects of the other independent variables). Many of the independent variables have varying effects on the results as a function of time. For such variables, the presentation of PRCCs as functions of time provides an informative display of sensitivity analysis results.

As indicated by the name, PRCCs involve the analysis of rank-transformed data. With this approach, the values for variables are replaced with their ranks and then the PRCCs are calculated with these ranks rather than with the original values for the variables. Specifically, the smallest value of a variable is given a rank of 1, the next largest value is given a rank of 2, equal observations are assigned the average of what their ranks would have been if they had not been equal, and so on up to the largest value, which is given a rank equal to the number of sample elements in use. The effect of the rank transformation is to transform monotonic relationships into linear relationships. Further, the rank transformation tends to reduce the skewing effects of outliers, which permits the regression analysis to represent the general relationships between the inputs and the specific result. Although no variable transformation is universally successful in improving the resolution of a sensitivity analysis in the presence of nonlinear relationships, the rank transformation has been found to be a broadly effective and useful means of enhancing the insights in sensitivity analyses based on partial correlation and sensitivity analyses based on stepwise regression.

Figure 4.2-1 in Section 4.2 shows the PRCCs over time, as determined using the sampling results from 1,000 realizations. Thus, at each modeled time step, there are 1,000 values for each result for which a PRCC is calculated.

Because most results are not influenced by every variable, these PRCC calculations were performed using a sub-set of the variables. For example, while the GoldSim Model described in Section 3.0 includes 28 stochastic elements (i.e., elements used to implement probabilistic

distributions), not all of them influence the saltstone degradation rates. Some of these elements are included as part of the copy of the Probabilistic Infiltration Model and provide information on things like runoff and evapotranspiration.

Elements which have no influence on the degradation of saltstone were screened out (i.e., not considered in the specific analyses).

The analysis only examined variables whose PRCCs exceed 0.10 in absolute value at some point in time. Variables with PRCCs with an absolute value less than 0.10 have only a limited monotonic effect on the results under consideration.

Values of PRCCs fall in the interval [−1, 1], where:

- positive PRCCs indicate that two variables tend to increase and decrease together (i.e., the independent variable has a positive effect on the dependent variable),
- negative PRCCs indicate that two variables tend to move in opposite directions (i.e., the independent variable has a negative effect on the dependent variable), and
- the absolute value of a PRCC indicates the strength of the relationship between two variables (i.e., a PRCC close to 1 in absolute value indicates a strong monotonic relationship between two variables after the removal of the monotonic effects associated with the other independent variables under consideration).

C.2 Stepwise Rank Regression Coefficients

An alternative to the use of PRCCs is to carry out stepwise rank regressions to determine the effects of uncertain inputs on analysis results of interest. In analyses of this type, the regressions are carried out with rank-transformed variables as previously discussed rather than with the original values.

In a stepwise rank regression, the single independent variable that makes the largest contribution to the uncertainty in the dependent variable (model result) is selected in the first step. Then, at the second step, the single independent variable that, in conjunction with the first independent variable, makes the largest contribution to the uncertainty in the dependent variable is selected. This process then continues until no additional variables are found that make identifiable contributions to the uncertainty in the dependent variable; at this point, the stepwise selection process terminates. For these analyses, a significance level of $\alpha_{in} = 0.10$ is used as the criterion for entering variables into the stepwise regression and $\alpha_{out} = 0.10$ was used for dropping variables from the stepwise regression analysis. Selection of these significance levels was based on preliminary sensitivity analyses, in which it was observed that a greater value tended to introduce obviously spurious variables into the regression models. In the context of stepwise regression analysis, variable importance is indicated by the order of selection in the stepwise selection process, incremental changes in R^2 values with the successive entry of individual variables into the regression model, and the sign and size of the ranked regression coefficients in the final regression model. Because rank-transformed values were used, the regression coefficients are more correctly identified as stepwise rank regression coefficients (SRRCs) in the SRRC result tables.

The R^2 values correspond to the fraction of the uncertainty in the dependent variable that is accounted for by a regression model. Thus, R^2 values monotonically increase as additional variables are added to the regression model and, for a very successful regression analysis, approach 1 as additional variables are added to the model. The SRRCs provide a measure of the fractional contribution of individual independent variables to the uncertainty in the dependent variable under consideration. As with the PRCCs, a positive SRRC indicates that the independent variable and dependent variable tend to increase and decrease together, and a negative SRRC indicates that the independent variable and dependent variable tend to move in opposite directions.

As discussed above, the PRCCs are computed as a function of time. In contrast, SRRCs are computed at fixed times (i.e., for each dependent variable, the time of the peak of the means is used). These times for SRRC computation were chosen to illustrate the changes in importance of uncertain parameters over time. The same analysis times are generally used for analysis of all SDF model output variables to facilitate comparisons between the sensitivity analysis results across output variables.

Related, but not identical, information is provided by PRCCs and SRRCs. Specifically, PRCCs measure the strength of the monotonic relationship between an independent variable and a dependent variable after correcting for the effects of other independent variables, and SRRCs provide a measure of the fractional contribution of an individual independent variable to the uncertainty in the dependent variable under consideration. Except in rare situations involving SRRCs from a regression model involving multiple correlated variables, PRCCs and SRRCs have the same sign, which indicates either a positive or a negative correlation between an input variable and an output variable. Because PRCCs are selected for display based on the maximum absolute value over time and SRRCs are computed at specific times, the selection and order of important variables indicated by PRCCs and SRRCs may be different between the two analyses.

As described in the PRCC discussion above, subsets of the variables were used as inputs in these analyses. No-impact variables were excluded from these analyses in response to computational limitations and to reduce the occurrence of spurious correlations in the PRCC calculation results.

C.3 PRCC and SRRC Analysis Tool

The PRCC and SRRC analyses were both performed using the software tool mView Version 4.00. This software was developed by Intera, Inc. to support the performance assessments for the U.S. Department of Energy (DOE) Office of Civilian Radioactive Waste Management (i.e., the Yucca Mountain Project) (B-SQP-C-00005).

Because this is the same software as used for developing the SDF PA (SRR-CWDA-2019-00001), the same software QA applies. Section 6.0 of the *Performance Assessment for the Saltstone Disposal Facility at the Savannah River Site: Quality Assurance Report* (SRR-CWDA-2018-00068) provides a summary of the software QA, which includes mView.